JAERI-M
87-051

EVALUATION REPORT ON CCTF CORE-II REFLOOD TEST C2-16 (RUN 76)

—EFFECT OF ASYMMETRIC UPPER PLENUM INJECTION ON REFLOOD PHENOMENA—

(Work done under Contract with the Government)

March 1987

Tadashi IGUCHI, Jun SUGIMOTO*, Hajime AKIMOTO
Tsutomu OKUBO, Tsuneyuki HOJO and Yoshio MURAO

日本原子力研究所
Japan Atomic Energy Research Institute

JAERI-Mレポートは，日本原子力研究所が不定期に公刊している研究報告書です。
入手の問合わせは，日本原子力研究所技術情報部情報資料課（〒319－11茨城県那珂郡東海村）あて，お申しこしください。なお，このほかに財団法人原子力弘済会資料センター（〒319-11茨城県那珂郡東海村日本原子力研究所内）で複写による実費頒布をおこなっております。

JAERI-M reports are issued irregularly.
Inquiries about availability of the reports should be addressed to Information Division, Department of Technical Information, Japan Atomic Energy Research Institute, Tokai-mura, Naka-gun, Ibaraki-ken 319-11, Japan.

編集兼発行　日本原子力研究所
印　　刷　日立高速印刷株式会社

Evaluation Report on CCTF Core-II Reflood Test C2-16 (Run 76)
—— Effect of asymmetric upper plenum injection on reflood phenomena ——

Tadashi IGUCHI, Jun SUGIMOTO*, Hajime AKIMOTO,
Tsutomu OKUBO, Tsuneyuki HOJO and Yoshio MURAO

Department of Reactor Safety Research,
Tokai Research Establishment
Japan Atomic Energy Research Institute
Tokai-mura, Naka-gun, Ibaraki-ken

(Received February 28, 1987)

This report presents the result of the upper plenum injection (UPI) test C2-16 (Run 76), which was conducted on October 23, 1984, with the Cylindrical Core Test Facility (CCTF) at Japan Atomic Energy Research Institute (JAERI). The CCTF is a 1/21.4 scale model of a 1,100 MWe PWR with four loop active components to provide information on the system and core thermo-hydrodynamics during reflood.

The objectives of the test are to investigate the reflood phenomena with single failure UPI condition and to investigate the effect of the asymmetry of UPI on the reflood phenomena. The test was performed with an asymmetric UPI condition at the injection rate simulating single failure of LPCI pumps.

It was observed that

(1) a UPI test simulating no LPCI pump failure gave the slightly lower peak clad temperature than a UPI test simulating single LPCI pump failure, indicating that single LPCI pump failure assumption is conserrative for UPI condition, and

(2) an asymmetric UPI lead to a higher core water accumulation and then a higher heat transfer coefficient, resultantly a lower peak clad

---

The work was performed under the contract with the Atomic Energy Bureau of Science and Technology Agency of Japan.

* Science and Technology Agency

temperature than a symmetric UPI, indicating that asymmetric UPI does not lead to a poorer core cooling than symmetric UPI.

Keyword: Cylindrical Core Test Facility, Upper Plenum Injection, Core-II Reflood, Thermo-hydrodynamics

大型再冠水円筒第二次炉心試験 C2－16（Run76）評価報告書

日本原子力研究所東海研究所原子炉安全工学部
井口　正・杉本　純*・秋本　肇
大久保　努・北條　恒行・村尾　良夫

（1987年2月28日受理）

本報告書は，原研で実施中の大型再冠水効果実証試験計画の中の円筒炉心試験装置による上部プレナム注水試験C2－16（Run76）の評価結果である。本試験は，1984年10月23日に実施された。円筒炉心試験装置は，1100MWe級PWRを約1／21，4で縮少した装置で，再冠水過程の熱水力挙動をよく模擬するように設計されている。

本試験の目的は，低圧注入系ポンプ単一故障を仮定した上部プレナム注水条件における再冠水現象を調べることおよび冷却水を非対称に注入した時の再冠水現象への影響を調べることである。

本上部プレナム注水試験の結果，次のことが見いだされた。

(1) 低圧注入系ポンプ無故障を模擬した試験では，単一故障を模擬した本試験より低い被覆管最高温度が得られた。これは，上部プレナム注水条件では，低圧注入系ポンプの単一故障仮定が保守的な仮定であることを示す。

(2) 非対称注入をしたところ，対称注入の場合に比べて炉心内蓄水量は増加し，熱伝達率は大きくなり，その結果，被覆管最高温度は低下した。これは，非対称注水による局所的な炉心冷却の悪化はないことを示す。

東海研究所：〒319-11 茨城県那珂郡東海村白字白根2-4
本報告書は，電源開発促進対策特別会計法に基づき，科学技術庁からの受託によって行った研究の成果である。
* 科学技術庁

Contents

目　　次

Table List

Figure list

1. Introduction

A reflood test program[1] for a large-break loss-of-coolant accident (LOCA) of pressurized water reactor (PWR) has been conducted at Japan Atomic Energy Research Institute (JAERI), using large scale test facilities. The facilities are the Cylindrical Core Test Facility (CCTF)[2] and the Slab Core Test Facility (SCTF)[3]. Since 1979, a lot of reflood tests have been performed with CCTF[2] and SCTF[4]. This report presents the evaluation for an asymmetric upper plenum injection (UPI) test C2-16 (Run 76), which was performed with CCTF on October 23, 1984.

The CCTF is an experimental facility designed to model a four-loop 1100 MWe class PWR with the flow scaling ratio of 1/21.4 and to simulate the thermo-hydraulic behavior in the primary system during the refill and the reflood phases of a PWR-LOCA as well as possible. The CCTF has a scaled pressure vessel with a non-nuclear full-length core and four loops with passive and active components. The core consists of 1,824 electrically heated rods and 224 non-heated rods arranged in a cylindrical configuration, and is subdivided into thirty two 8 x 8 rod bundles which model typical 15 x 15 fuel bundles of a PWR.

The basic objective of the test program using the CCTF is to investigate the core thermo-hydraulic behavior coupled with the system behavior in the primary loops for the refill and the reflood phases of a PWR-LOCA, especially :

(1) to demonstrate capability of emergency core cooling system (ECCS) during refill and reflood periods,

(2) to verify reflood analysis codes, and

(3) to collect information to improve the thermo-hydrodynamic models in the reflood analysis codes.

One of the objectives of the test program is to study the effectiveness of upper plenum injection (UPI) system, which is used in several two-loop plants of Japan at present. For UPI system, the ECC water of low pressure coolant injection (LPCI) is injected into the upper plenum through two injection pipes located diagonally on the side wall of the upper plenum. If assuming no failure of LPCI pumps, the ECC water is injected relatively symmetrically through two injection pipes. On one hand, if assuming single failure of LPCI pumps, the ECC water is injected asymmetrically through one injection pipe. The UPI rate at single failure

of LPCI pumps is half of one at no failure of LPCI pumps.

For the investigation of the reflood phenomena under UPI condition, three UPI tests, Test C2-AA1 (Run 57), Rest C2-AS1 (Run 59) and C2-13 (Run 72), were performed with CCTF by February, 1984. From these tests, the reflood phenomena under UPI condition was analysed, and the qualitative characteristics were understood[(5),(6)]. However, in these tests the UPI water was injected relatively symmetrically through two injection pipes located in diagonally-opposite peripheral regions with each other. The effect of the asymmetric UPI on the reflood phenomena, which is expected to be realized in an actual PWR with single failure of LPCI pumps, has not been studied.

In order to study the effect of the asymmetric UPI on the reflood phenomena, the asymmetric UPI test C2-16 (Run 76) has been performed with CCTF. In this test, the UPI water has been injected through one injection pipe located in one peripheral region. The result of the test has been compared with those of the previous UPI tests.

The present report describes the effect of the asymmetric UPI on the reflood phenomena observed in the above UPI tests.

1.1 Identification of the present test

asymmetric UPI test

1.2 Test number of the present test

C2-16 (Run 76)

1.3 Objectives of the present test

(1) To investigate the reflood phenomena with single failure UPI condition

(2) To investigate the effect of the asymmetry of UPI on the reflood phenomena

1.4 Type of the present test

(1) Reflood test with single failure UPI condition

2. Test description

2.1 Test facility

The CCTF Core-II was designed in consideration of the following objectives and criteria:

a. Design objectives

(1) The facility should provide the capability to reasonably simulate the flow conditions in the primary system of a PWR during the refill and reflood phases of a LOCA.

(2) The downcomer design should provide ECC flow behavior throughout the test which is reasonably representative of that of the PWR downcomer.

b. Design criteria

(1) The reference reactors are the Trojan reactor in USA and certain aspects of the Ohi reactor in Japan.

(2) The vertical dimensions and locations of system components are kept as close to those of the reference reactors as possible.

(3) The flow areas of the system components are scaled down in proportion to the scaling factor of core flow area.

(4) The facility is equipped with four loops which are composed of three intact loops and a broken loop.

(5) A cold leg break is simulated.

(6) The ECCS consists of an accumulator (Acc) and a low pressure coolant injection (LPCI) system, and the injection locations are the upper plenum and the downcomer as well as the lower plenum and the cold legs.

(7) The maximum allowable pressure of the facility is 588 kPa (6 kg/cm^2 absolute).

(8) The maximum allowable temperature of the simulated fuel rods is 1173 K (900°C).

(9) The maximum allowable temperature of the components in the primary system except the simulated fuel rod assembly is 623 K (350°C).

(10) The reactor vessel contains approximately 2,000 electrically heated rods simulating the fuel rods.

(11) The design of upper plenum internals is based on that of a new 17×17 type fuel assembly.

(12) The flow resistance of each loop is adjusted by an orifice in the pump simulator.

(13) The containment system consists of two tanks.

A bird's-eye view and a schematic diagram of the CCTF are shown in Figs. 2.1 and 2.2, respectively. The scaled dimensions of the components are given in Tables 2.1 and 2.2.

The differences in the design of the Core-II facility from the Core-I are:

(1) Axial peaking factor of heater rods.

(2) Local peaking factor of heater rods in a bundle.

(3) Core structure (Grid spacers)

(4) Upper plenum structures (upper plenum internals, plugging devices in top nozzle region and a upper ring).

(5) Vent valves.

(6) Alternative ECCS (downcomer injection and upper plenum injection).

(7) Instruments.

2.1.1 Pressure vessel and internals

The pressure vessel is of a cylindrical type as shown in Fig. 2.3. The height is the same as the reference reactor pressure vessel. The radial direction is scaled down in proportion to the core flow area scaling, that is, 1/21.44. The upper ring was newly installed for the installation of the upper plenum ECC water injection lines and the instruments. Four vent valves and two downcomer ECC water injection nozzles, which are called Core Flooding Nozzle (CFN), are also newly equipped in the Core-II facility as shown in Figs. 2.3 and 2.4. Vent valves and CFNs are for the simulation of a Babcock & Wilcox (B & W) type PWR. The vent valves and CFNs are forcedly closed in this test.

The cross section of the pressure vessel is shown in Fig. 2.4 and the dimensions are given in Fig. 2.5. The core consists of thirty-two 8×8 electrically heated rod bundles arranged in a cylindrical configuration and simulates Westinghouse 15×15 type fuel assemblies.

The downcomer is an annulus of 61.5 mm gap. In determining the gap size, the flow area of the core baffle region was added to that of the downcomer region. Thus, the core baffle flow area is included in the downcomer simulation and is not simulated separately in this vessel.

The vessel wall is constructed of carbon steel which is cladded with stainless steel lining. The wall is 90 mm thick and simulates the stored energy as reasonably as possible during ECC water injection.

The design of upper plenum internals is based on that of the new Westinghouse 17×17 type fuel assemblies instead of the old type simulated in the Core-I facility. The internals consists of ten control rod guide tubes, ten support columns and twelve open holes as shown in Fig. 2.6. The radius of each internals is scaled down by factor of 8/15 from that of an actual reactor. They are illustrated in Fig. 2.7. Flow resistance baffles are inserted into the guide tubes. The baffles consist of kinds of baffle plates and a shaft. The baffle plates are shown in Fig. 2.8.

The end box and the upper core support plate (UCSP) are installed between the core and the upper plenum. The structure for one heater rod bundle is shown in Fig. 2.9. The tie plate is a 10 mm thick perforated plate with round flow holes. Plugging devices are installed newly in the Core-II facility as shown in Figs. 2.9 and 2.10 to simulate the flow resistance more correctly. The UCSP is a 60 mm thick perforated plate. The geometry of the perforation is analogous to that of an actual reactor.

2.1.2 Heater rod assembly

The heater rod assembly simulating the fuel assembly consists of thirty-two 8×8 array rod bundles. Each bundle consists of fifty-seven electrically heated rods and seven non-heated rods as shown in Fig. 2.11. The core is usually subdivided into three regions to achieve a desired radial power distribution. This is shown in Fig. 2.5. The high, medium and low power regions are named as A, B and C regions, respectively. The local peaking factor of heated rods in a bundle is unity, that is, all heated rods in a bundle have the same power density in the Core-II facility.

A heater rod consists of a nichrome heating element, magnesium oxide (MgO) and boron nitride (BN) insulators, and Inconel-600 sheath. BN is used for only central part of the heated region and MgO for the other part as shown in Fig. 2.12. The heated length and the outer diameter of the heater rods are 3.66 m and 10.7 mm, respectively, which are identical to the corresponding dimensions of actual PWR fuel rods. The sheath wall thickness is 1.0 mm and is thicker than the actual fuel cladding, because of the requirements for thermocouple installation. The heating element

is a helical coil with a varying pitch to generate a 17 steps chopped consine axial power profile as shown in Fig. 2.13. The peaking factor is 1.40, instead of 1.489 for a Core-I rod.

Non-heated rods are either stainless steel pipes or solid bars of 13.8 mm O.D. All the pipes are utilized for installation of instruments such as steam superheat probes and thermocouples. All the bars are used for carrying the assembly loads.

The heater rods and non-heated rods are held in radial position by grid spacers which are located at six elevations along the axial length as shown in Fig. 2.13. A grid spacer is a lattice structure composed of stainless steel plates of 0.4 mm and 0.8 mm thick and 40 mm high. The top and the bottom edges of the stainless steel plates are sharpened in CCTF Core-II. The rod pitch is 14.3 mm which is same as that of the reference PWR.

The heater rods penetrate through the bottom plate of the vessel to facilitate lead out of the power cables from the bottom of the vessel. The outer diameter of the rods in the lower plenum is reduced to 8.6 mm. Three phase electric current is used for heating the heater rods and the electrical neutral point is at the top of the rods where they are interconnected to each other.

2.1.3 Primary loops and ECCS

Primary loop consists of three intact loops and a broken loop. Each loop consists of hot leg and cold leg pipings, a steam generator simulator and a pump simulator. The cold leg break is simulated for the broken loop. The broken cold leg is connected to two containment tanks through blowdown valves. The primary loop arrangement is shown in Figs. 2.14 and 2.15.

The inner diameter of the pipings is scaled down in proportion to the core flow area scaling. The length of each piping section is almost the same as the corresponding sections of the reference PWR.

The steam generator simulators are of U-tube and shell type as shown in Fig. 2.16. The tube length is about 5 m shorter than the reference PWR. The vertical height of the steam generator simulators is also about 5 m lower than the reference PWR. The primary coolant passes through the tube side and the secondary coolant is stagnant in the shell side. The steam generator simulators of two loops are housed in a single shell assembly which has two sets of separated inlet and outlet headers for

two loops. The wall thickness of the U-tube is 2.9 mm instead of 1.27 mm for the reference PWR, because of a higher pressure difference between the primary and secondary sides in the steam generator simulator.

The pump simulator consists of the casing and vane simulators and an orifice plate as shown in Fig. 2.17. The each loop resistance is simulated wth the orifice plate. Each orifice plate has a hole with diameter and thickness of 95 mm and 10 mm, respectively.

ECC water can be injected into each cold leg, lower plenum and upper plenum, as shown in Fig. 2.14.

Figure 2.18 shows the upper plenum injection devices. ECC water from Alternative tank 1 flows into a header installed in upper ring. The header has two water injection pipes, which inside diameters are 49.5 mm. Each water injection pipe has a flow hole of 3 mm diameter at the elevation of the hot leg center line. The ECC water is injected horizontally into upper plenum through the flow holes. In order to keep the same flow rates between the flow holes, orifices with 33 mm diameter are installed between the header and the water injection pipes.

The radial location of the water injecion pipes is shown in Fig. 2.19. The arrows in the figure show the injection direction of the ECC water.

2.1.4 Instrumentation

The instrumentation is divided into two groups. One of them is JAERI-supplied instruments measuring the temperatures, absolute pressures, differential pressures, water levels and flow rates. Thermocouples measure the temperatures of the rod surface, fluid and structure. The absolute pressures are measured in the upper and lower plena, steam generator plena and containment tanks. The differential pressure measurements are carried out at many locations covering the whole system almost completely. In the ECC water supply tanks and the containment tank 1, the liquid levels are measured. The flow meters measure the ECC water flow rate. Furthermore, flow rates in the downcomer, loop seal pipings and vent line from the containment tank 2 to the atmosphere are measured with the drag disk flow meter, pitot tubes and ventulli tube, respectively. The total number of the JAERI-supplied instruments are 1316 channels and the signals from these instruments are recorded on magnetic tapes.

The other group of the instrumentation is the USNRC-supplied instruments. They are the advanced instrumentation for the two-phase flow measurement. The names and quantities of those are tabulated in Table 2.3. The total number is 536 channels.

Table 2.1 CCTF Component scaled dimensions

Component		PWR	JAERI	Ratio
Pressure vessel				
Vessel inside diameter	(mm)	4394 (173")	1084	
Vessel thickness	(mm)	216 (8 1/2")	90	
Core barrel outside diameter	(mm)	3874	961	
Core barrel inside diameter	(mm)	3760	929	
Thermal shield outside diameter	(mm)	4170		
Thermal shield inside diameter	(mm)	4030		
Downcomer length	(mm)	4849	4849	1/1
Downcomer gap	(mm)	114.3	61.5	
Downcomer flow area	(m^2)	4.23	0.197	1/21.44
Lower plenum volume	(m^3)	29.6	1.38	1/21.44
Upper plenum volume	(m^3)	43.6	2.76	1/15.8
Fuel (heater rod) assembly				
Number of bundles	(—)	193	32	
Rod array	(—)	15×15	8×8	
Rod heated length	(mm)	3660	3660	1/1
Rod pitch	(mm)	14.3	14.3	1/1
Fuel rod outside diameter	(mm)	10.72	10.7	1/1
Thimble tube diameter	(mm)	13.87	13.8	1/1
Instrument tube diameter	(mm)	13.87	13.8	1/1
Number of heater rods	(—)	39372	1824	1/21.58
Number of non-heated rods	(—)	4053	244	1/18.09
Core flow area	(m^2)	5.29	0.25	1/21.2
Core fluid volume	(m^3)	17.95	0.915	1/19.6
Primary loop				
Hot leg inside diameter	(mm)	736.6 (29")	155.2	1/4.75
Hot leg flow area	(m^2)	0.426	0.019	1/22.54
Hot leg length	(mm)	3940	3940	1/1
Pump suction inside diameter	(mm)	787.4 (31")	155.2	1/5.07
Pump suction flow area	(m^2)	0.487	0.019	1/25.77
Pump suction length	(mm)	9750	7950	1/1

Table 2.1 (cont'd)

Component		PWR	JAERI	Ratio
Cold leg inside diameter	(mm)	698.5 (27.5")	155.2	1/4.50
Cold leg flow area	(m^2)	0.383	0.019	1/20.26
Cold leg length	(mm)	5600	5600	1/1
Steam generator simulator				
Number of tubes/loop	(—)	3388	158	1/21.44
Tube length (average)	(m)	20.5	15.2	1/1.35
Tube outside diameter	(mm)	22.225 (0.875")	25.4	
Tube inside diameter	(mm)	19.7 (0.05")	19.6	1/1
Tube wall thickness	(mm)	1.27	2.9	
Heat transfer area/loop	(m^3)	4784 (51500 ft^2)	192	1/24.92
Tube flow area/loop	(m^2)	1.03	0.048	1/21.44
Inlet plenum volume/loop	(m^3)	4.25	0.198	1/21.44
Outlet plenum volume/loop	(m^3)	4.25	0.198	1/21.44
Primary side volume/loop	(m^3)	30.50 (1077 ft^3)	1.2	1/25.4
Secondary side volume/loop	(m^3)	157.33 (5556 ft^3)	2.5	1/62.9
Containment tank 1	(m^3)		30	
Containment tank 2	(m^3)		50	
Storage tank	(m^3)		25	
Acc. tank	(m^3)		5	
Saturated water tank	(m^3)		3.5	

Table 2.2 Component elevations of Cylindrical Core Test Facility

COMPONENT		PWR	CCTF	DISCREPANCY
BOTTOM OF HEATED REGION IN CORE	(mm)	0	0	0
TOP OF HEATED REGION IN CORE	(mm)	3660	3660	0
TOP OF DOWNCOMER	(mm)	4849	4849	0
BOTTOM OF DOWNCOMER	(mm)	0	0	0
CENTERLINE OF COLD LEG	(mm)	5198	4927	-271
BOTTOM OF COLD LEG (INSIDE)	(mm)	4849	4849	0
CENTERLINE OF LOOP SEAL LOWER END	(mm)	2056	2047	- 9
BOTTOM OF LOOP SEAL LOWER END	(mm)	1662	1959	+297
CENTER OF HOT LEG	(mm)	5198	4927	-271
BOTTOM OF HOT LEG (INSIDE)	(mm)	4830	4849	+ 19
BOTTOM OF UPPER CORE PLATE	(mm)	3957	3957	0
TOP OF LOWER CORE PLATE	(mm)	- 108	- 50	+ 58
BOTTOM OF TUBE SHEET OF STEAM GENERATOR SIMULATOR	(mm)	7308	7307	- 1
LOWER END OF STEAM GENERATOR SIMULATOR PLENUM	(mm)	5713	5712	- 1
TOP OF TUBES OF STEAM GENERATOR SIMULATOR (avg)	(mm)	17952.7	14820	

Table 2.3 Instruments provided by USNRC

Instrument	Number of sets	Number of sensors
DC FDG	18	162
DC VOP	1	1
DC drag disk	4	4
Core velocimeter	4	4
Core impedance probe	12	24
Core LLD	6	96
LP LLD	3	15
End box turbine meter	8	8
UP turbine meter	4	4
UP FDG	11	110
UP film probe	2	4
UP prong probe	2	4
UP VOP	1	1
VV turbine meter	2	2
VV string probe	2	2
HL film probe	2	4
HL VOP	1	1
Reference probe	1	1
Spool piece	8	89
Total	92	536

Note :

DC : Downcomer, FDG: Fluid distribution grid,
VOP: Video optical probe, LLD: Liquid level detector,
LP : Lower plenum, UP : Upper plenum,
VV : Vent valve

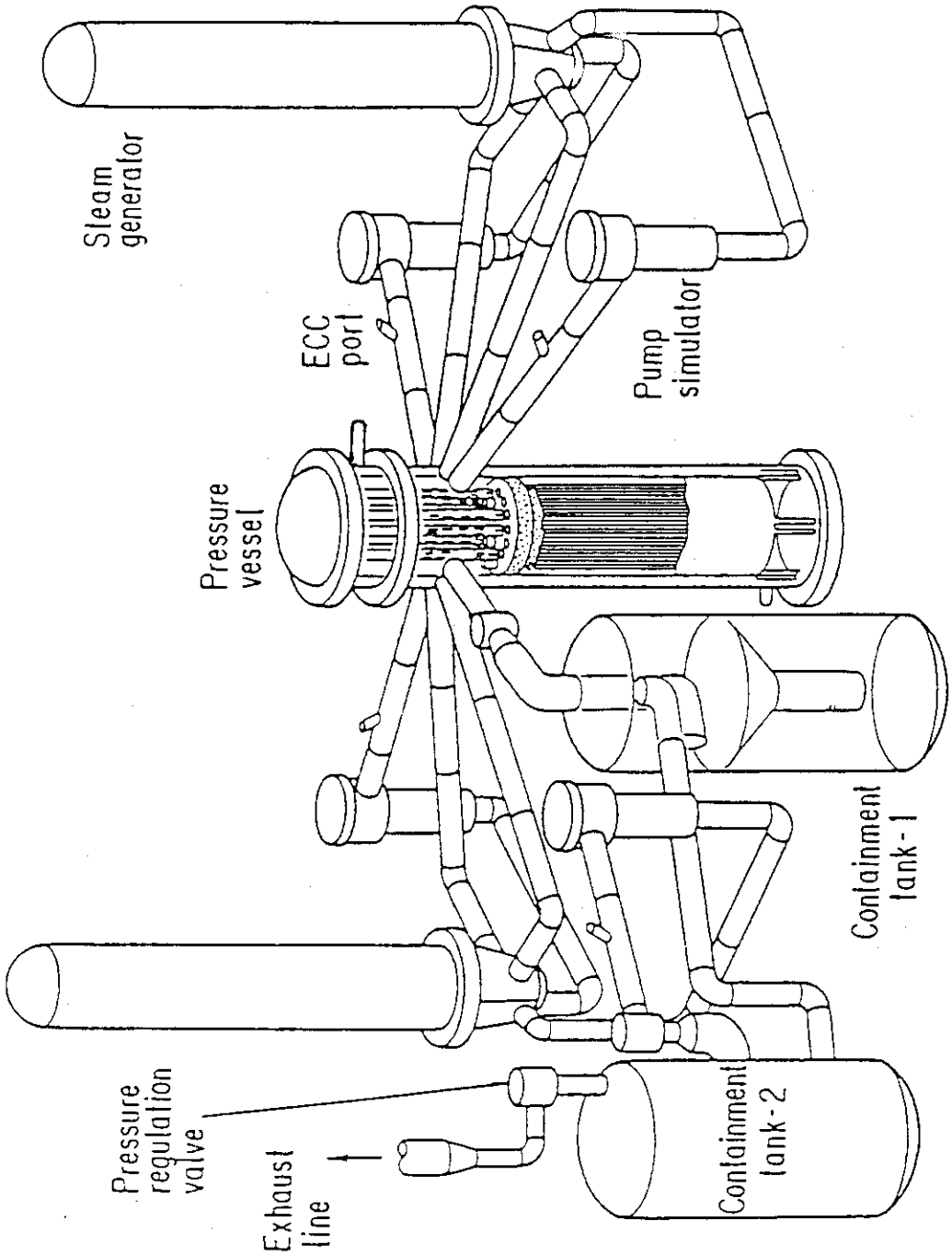

Fig. 2.1 Bird's-eye view of CCTF

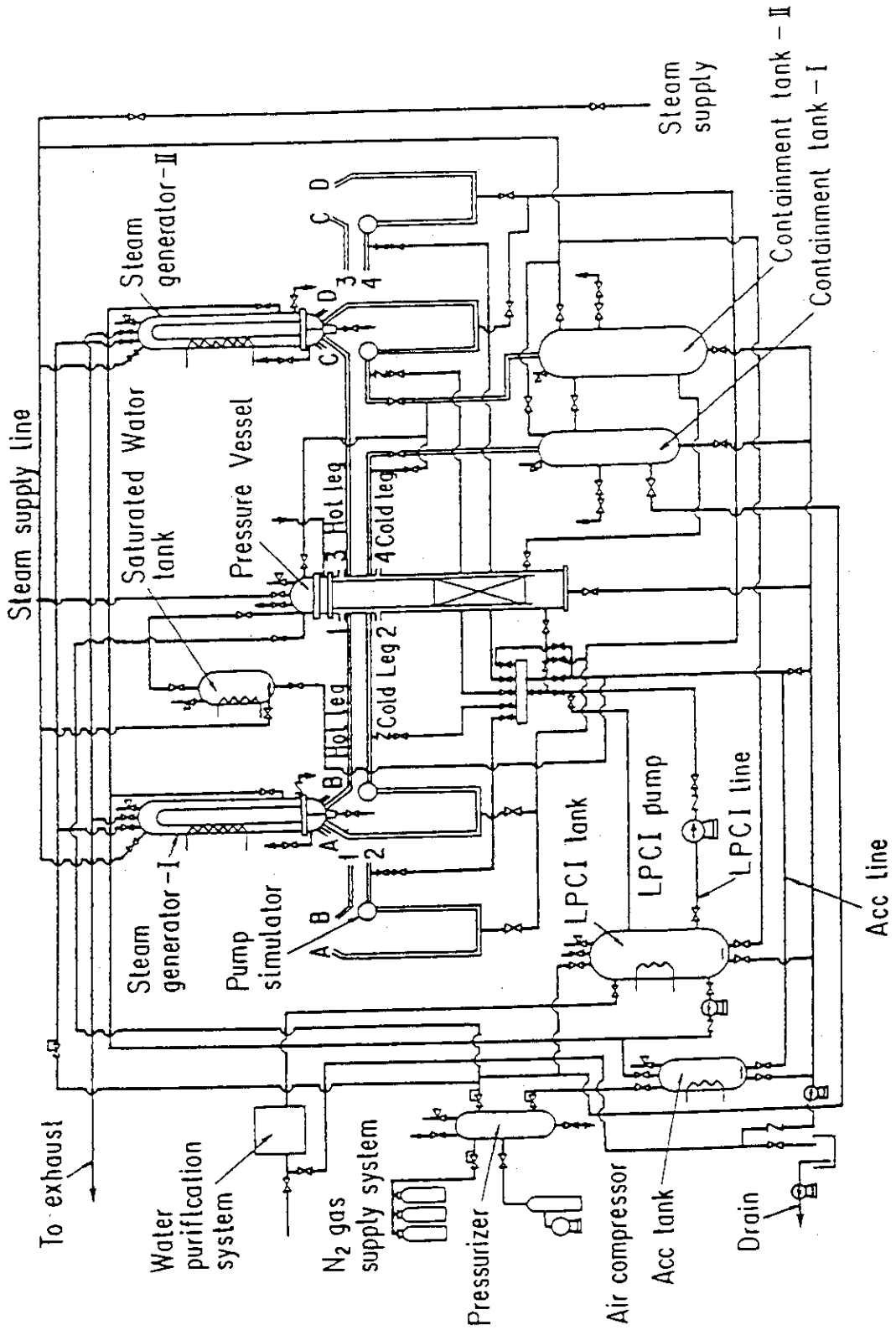

Fig. 2.2 Schematic diagram of CCTF

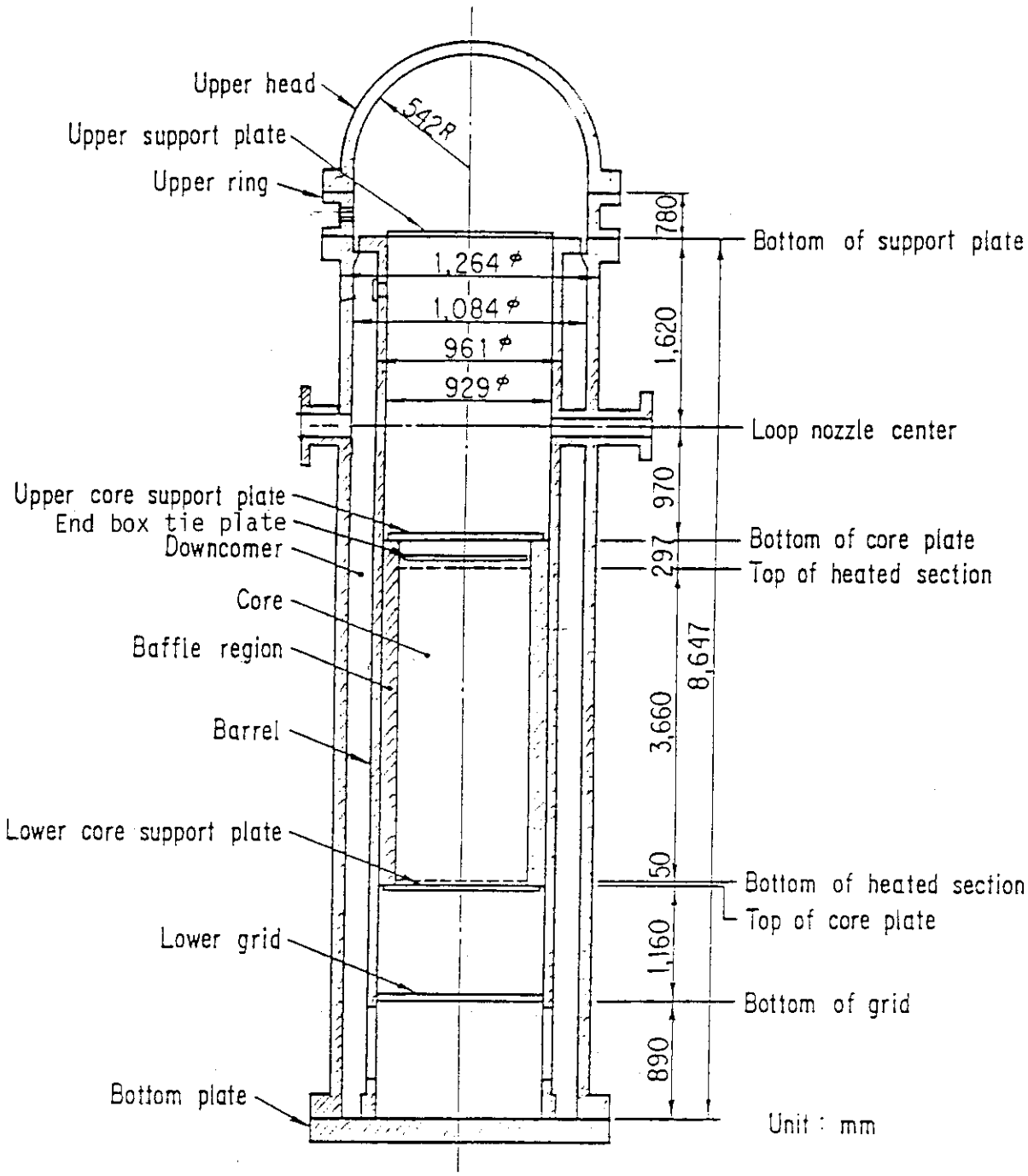

Fig. 2.3 CCTF Core-II pressure vessel

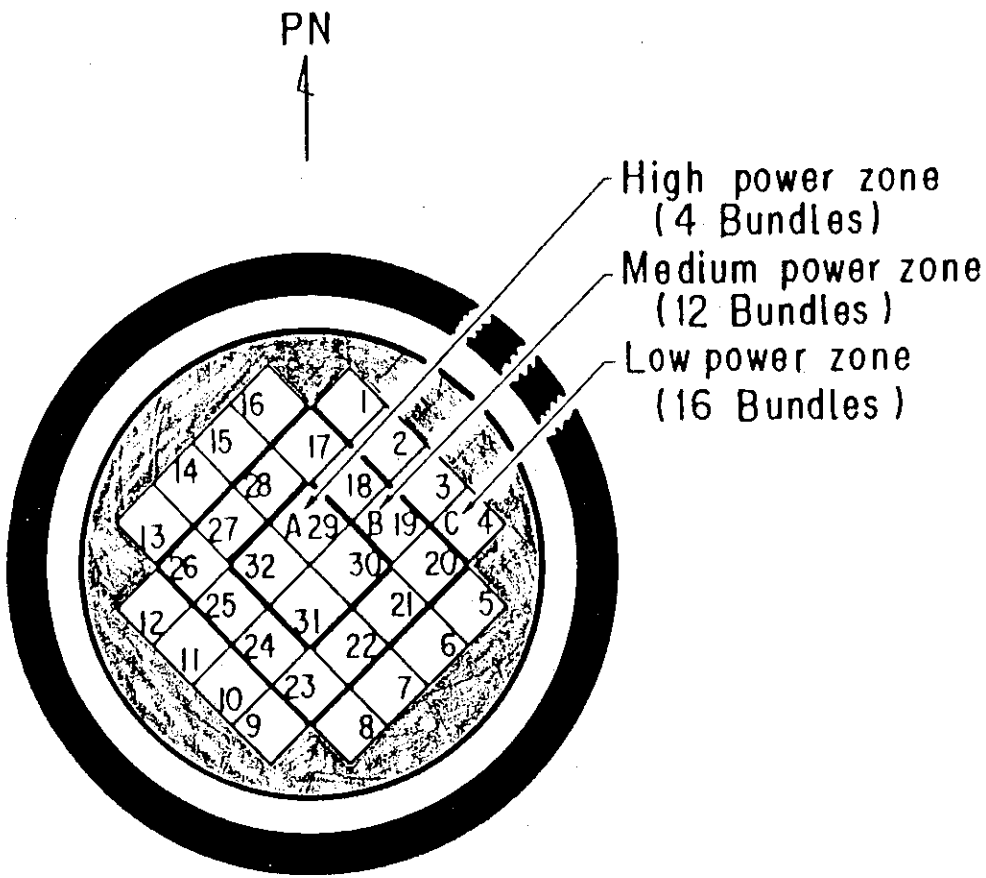

Fig. 2.4 Cross section of CCTF Core-II

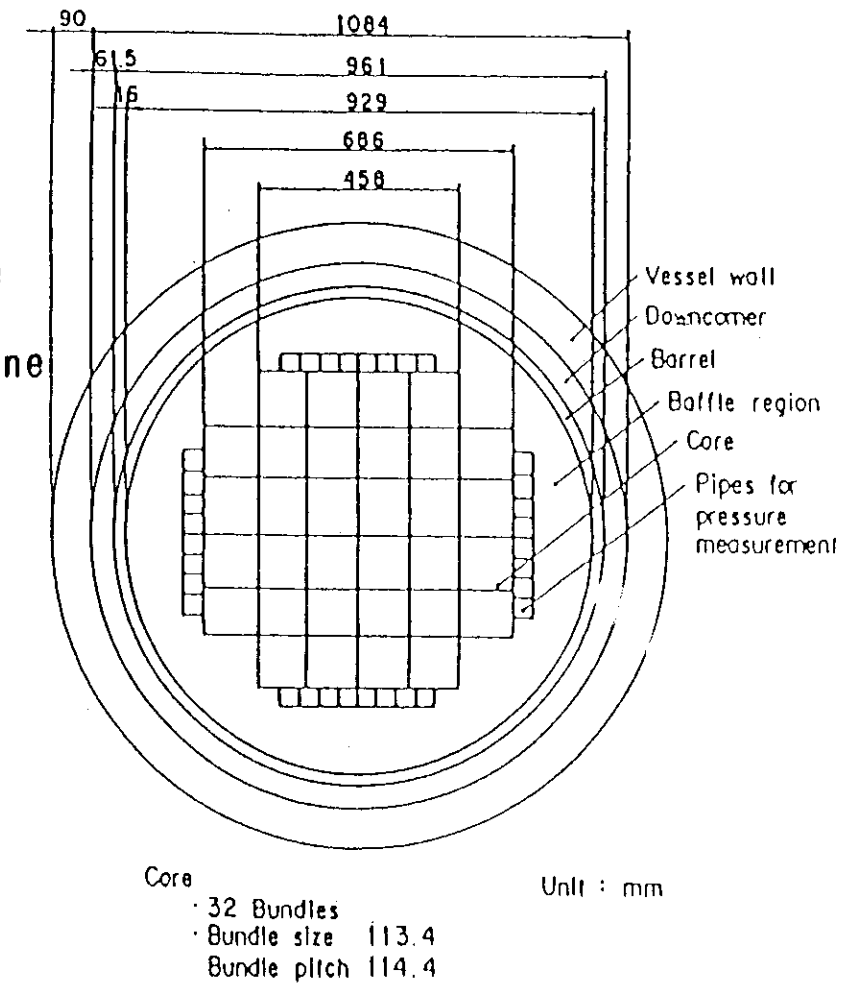

Fig. 2.5 Dimension of CCTF Core-II pressure vessel cross section

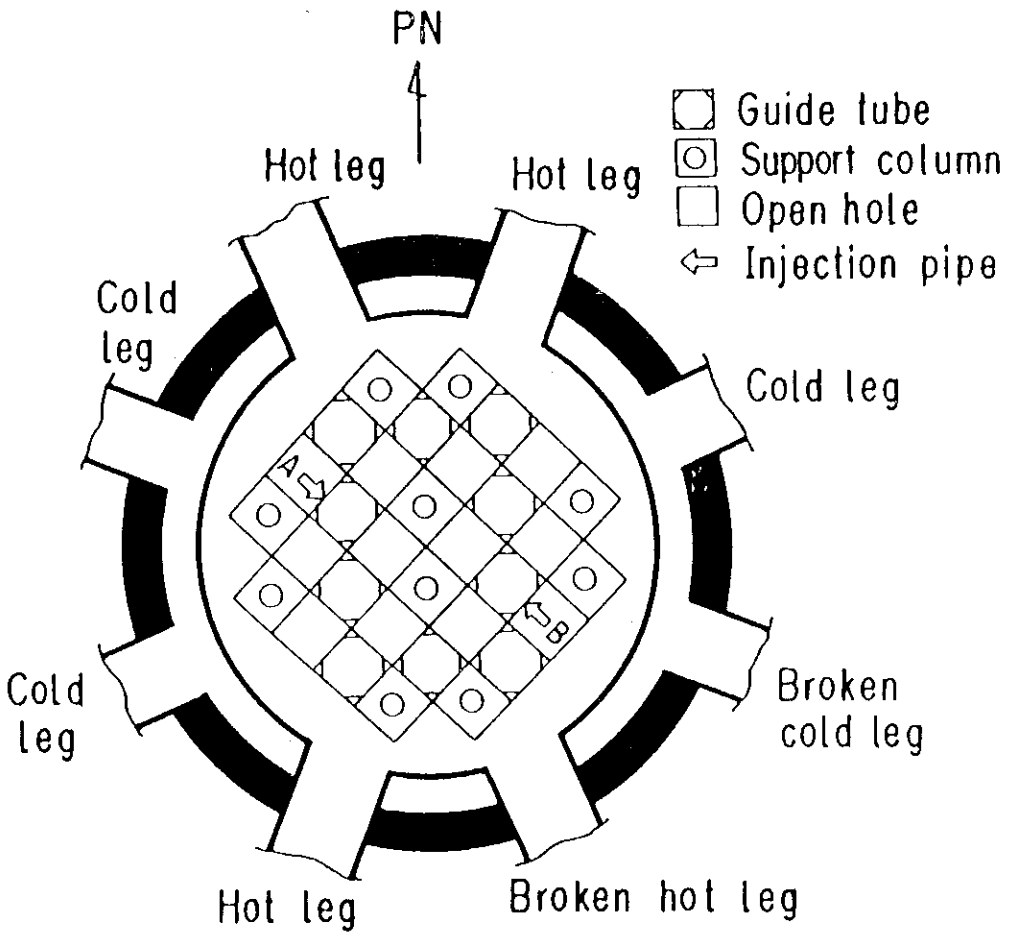

Fig. 2.6 Arrangement of upper plenum internals

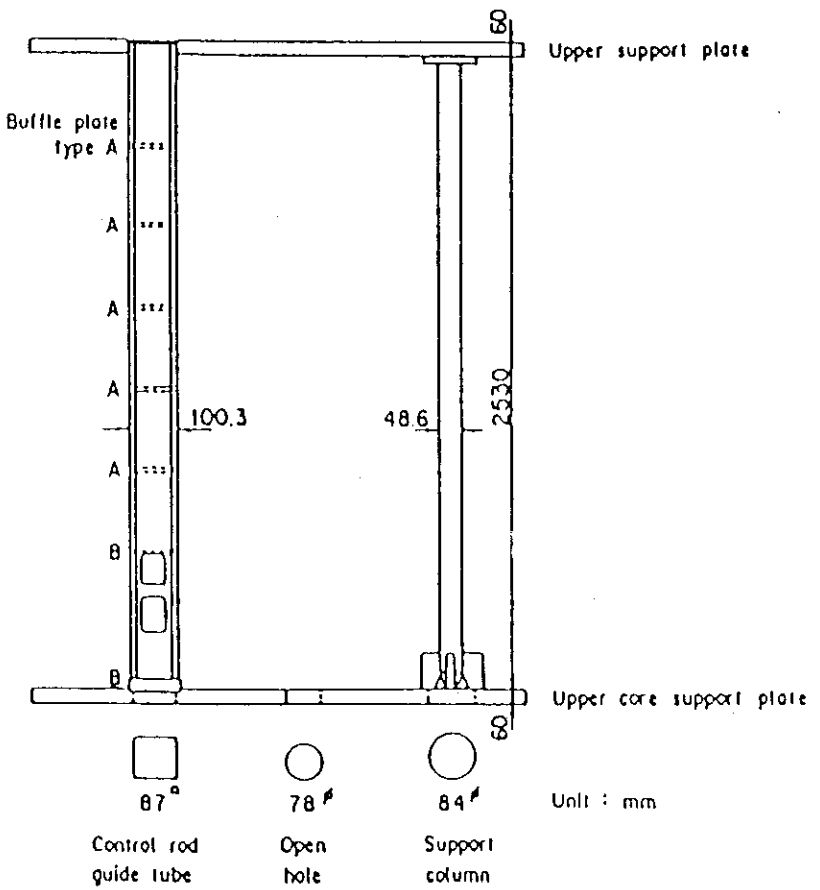

Fig. 2.7 Upper plenum internals

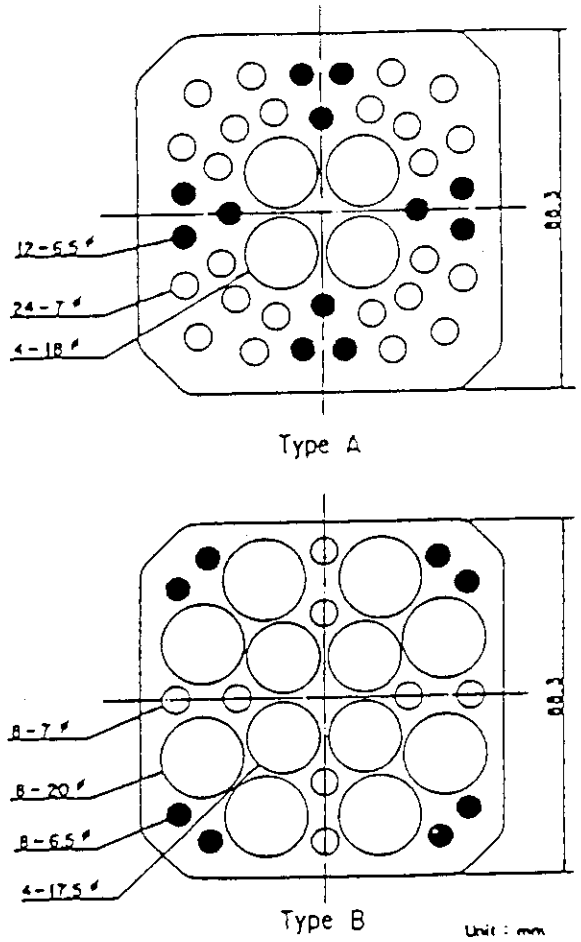

Fig. 2.8 Buffle plates in controd rod guide tube

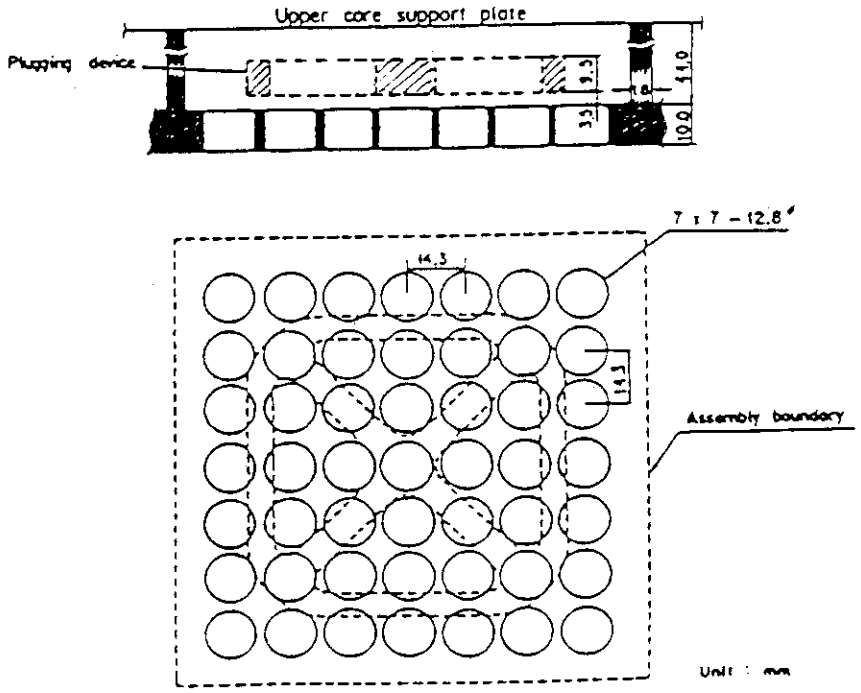

Fig. 2.9 Dimensions of holes of end box tie plate

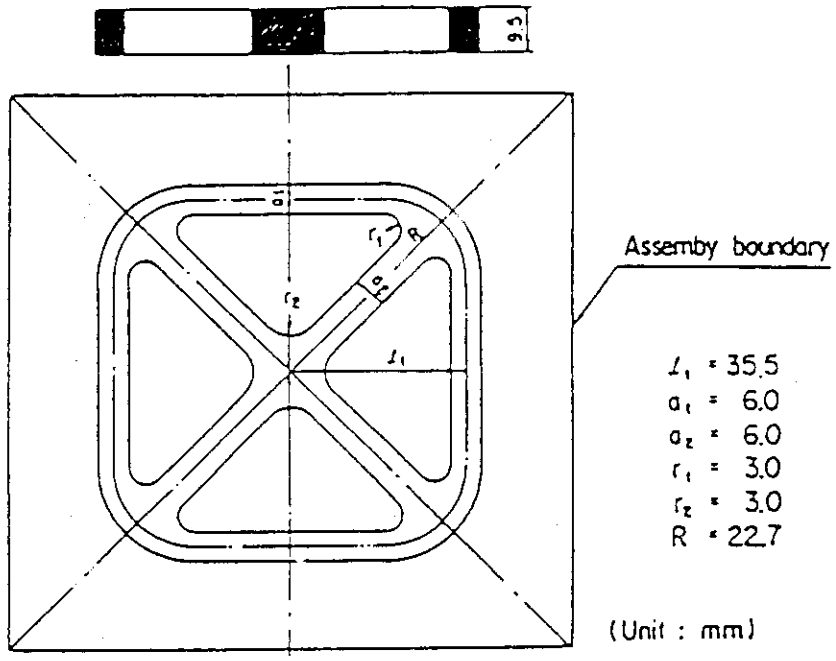

Fig. 2.10 Dimensions of plugging device

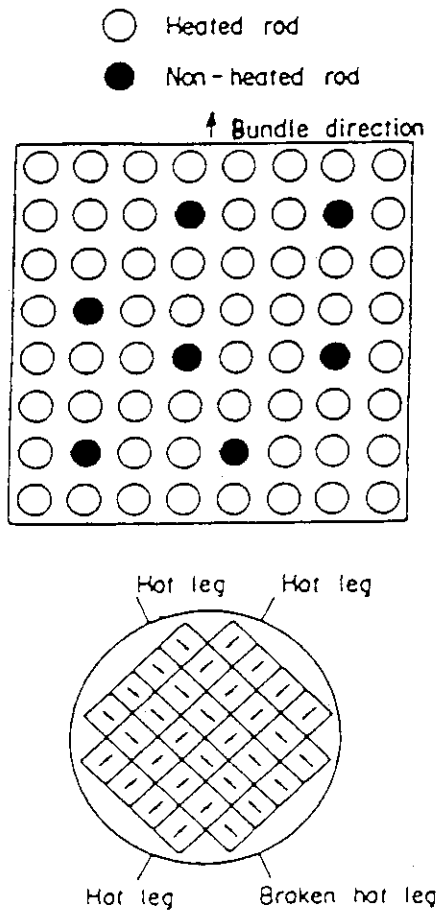

Fig. 2.11 Arrangement of non-heated rods bundle direction

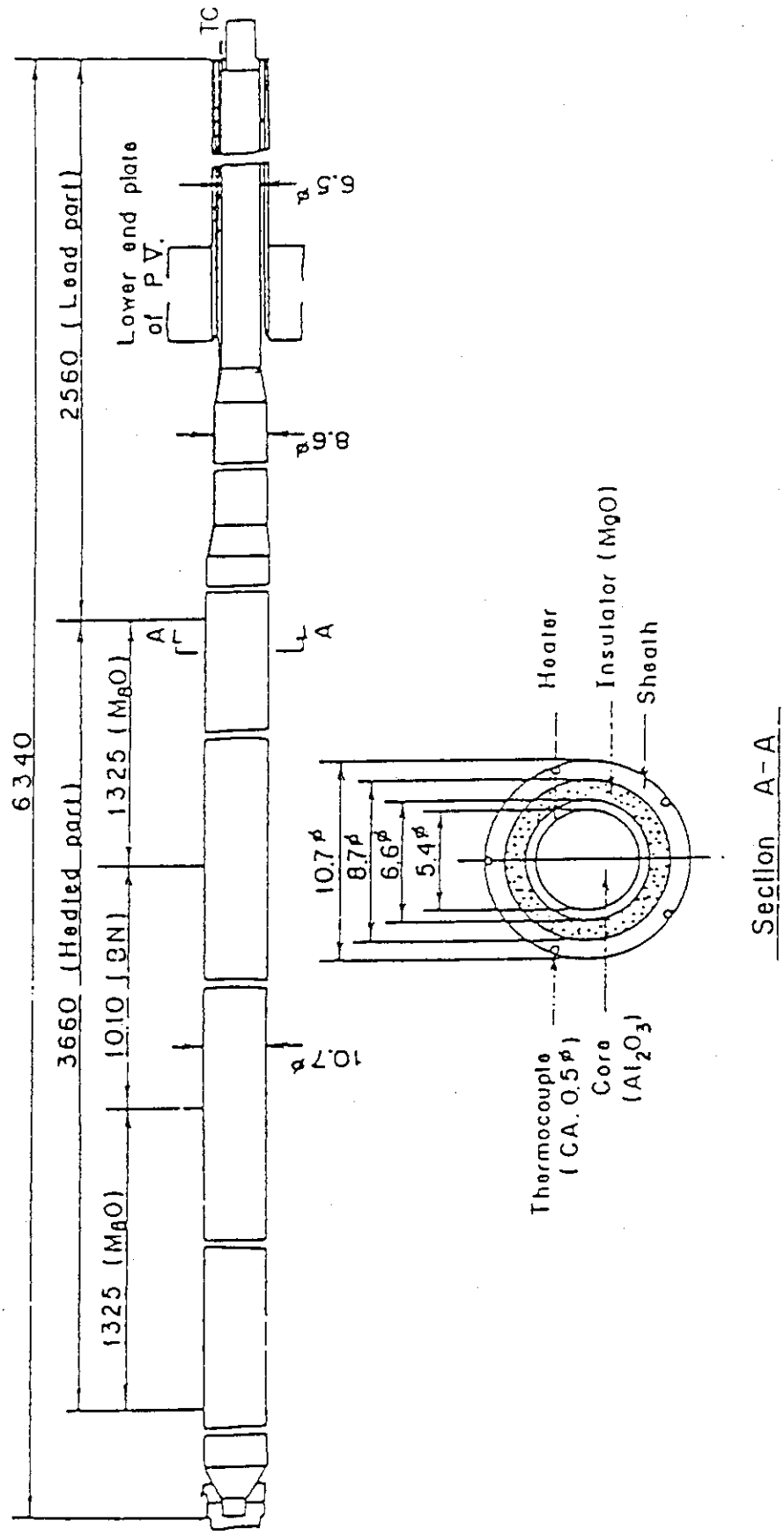

Fig. 2.12 Heater rod

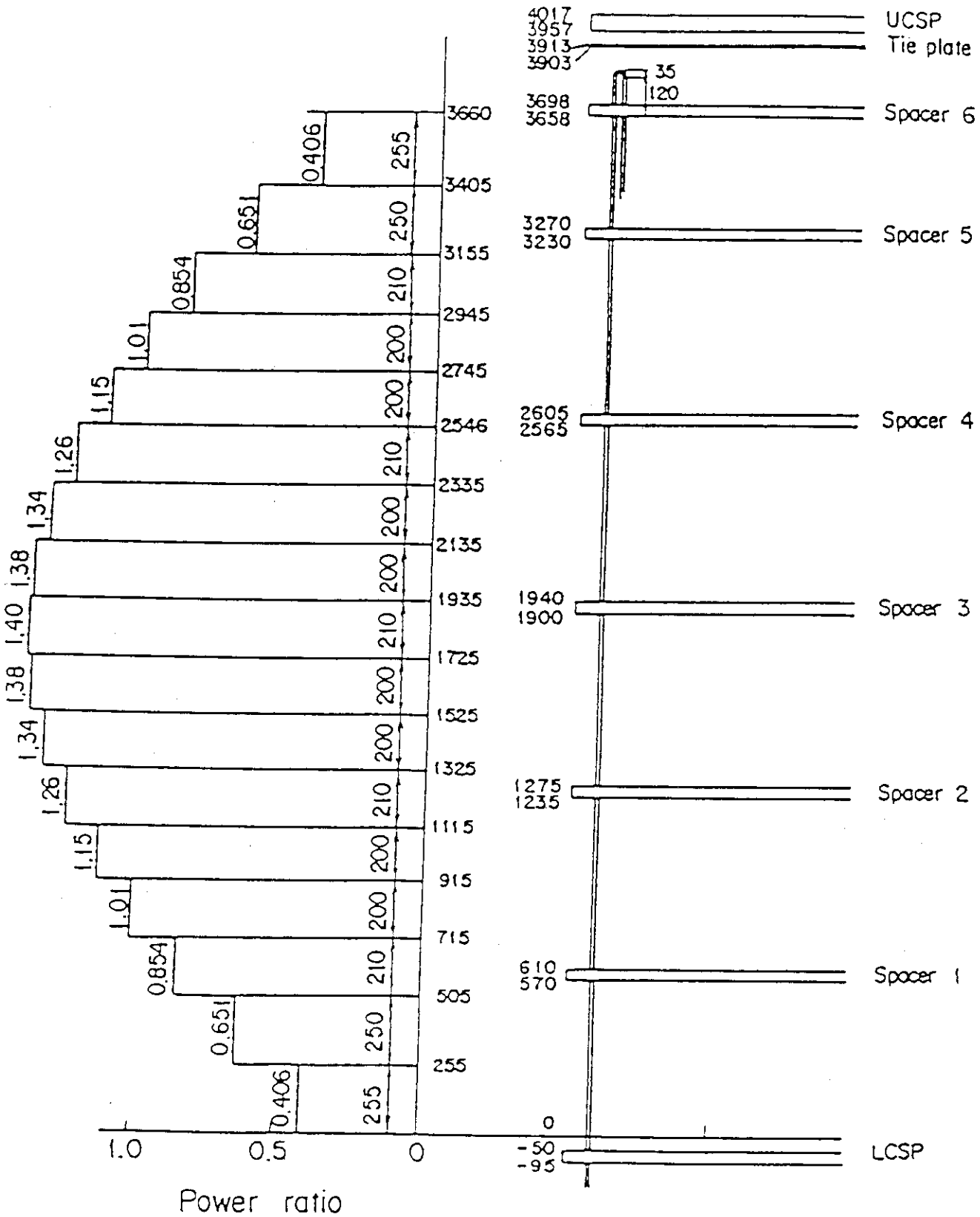

Fig. 2.13 Axial power profile of CCTF Core-II heater rod

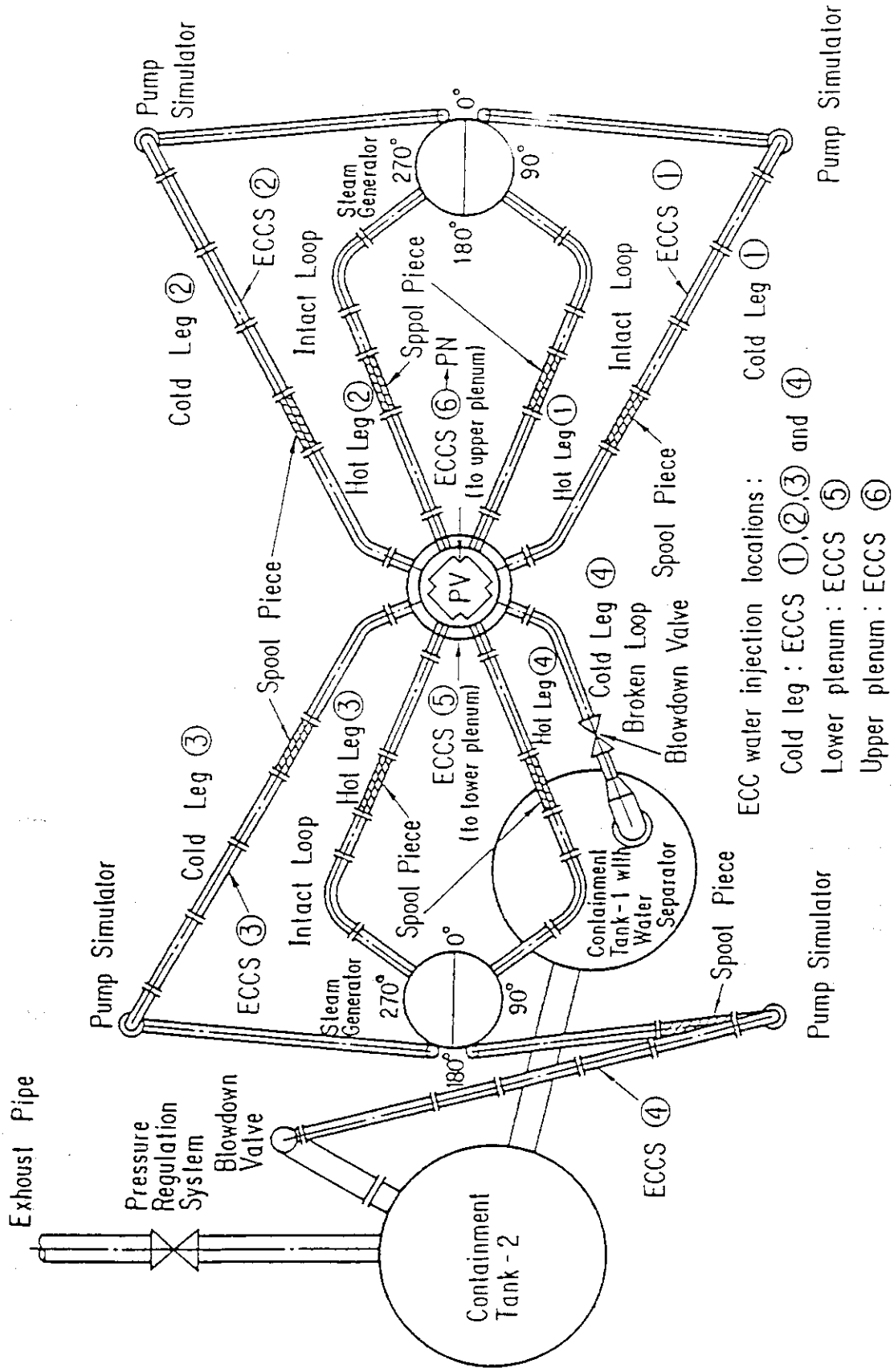

Fig. 2.14 Top view of primary loop pipings

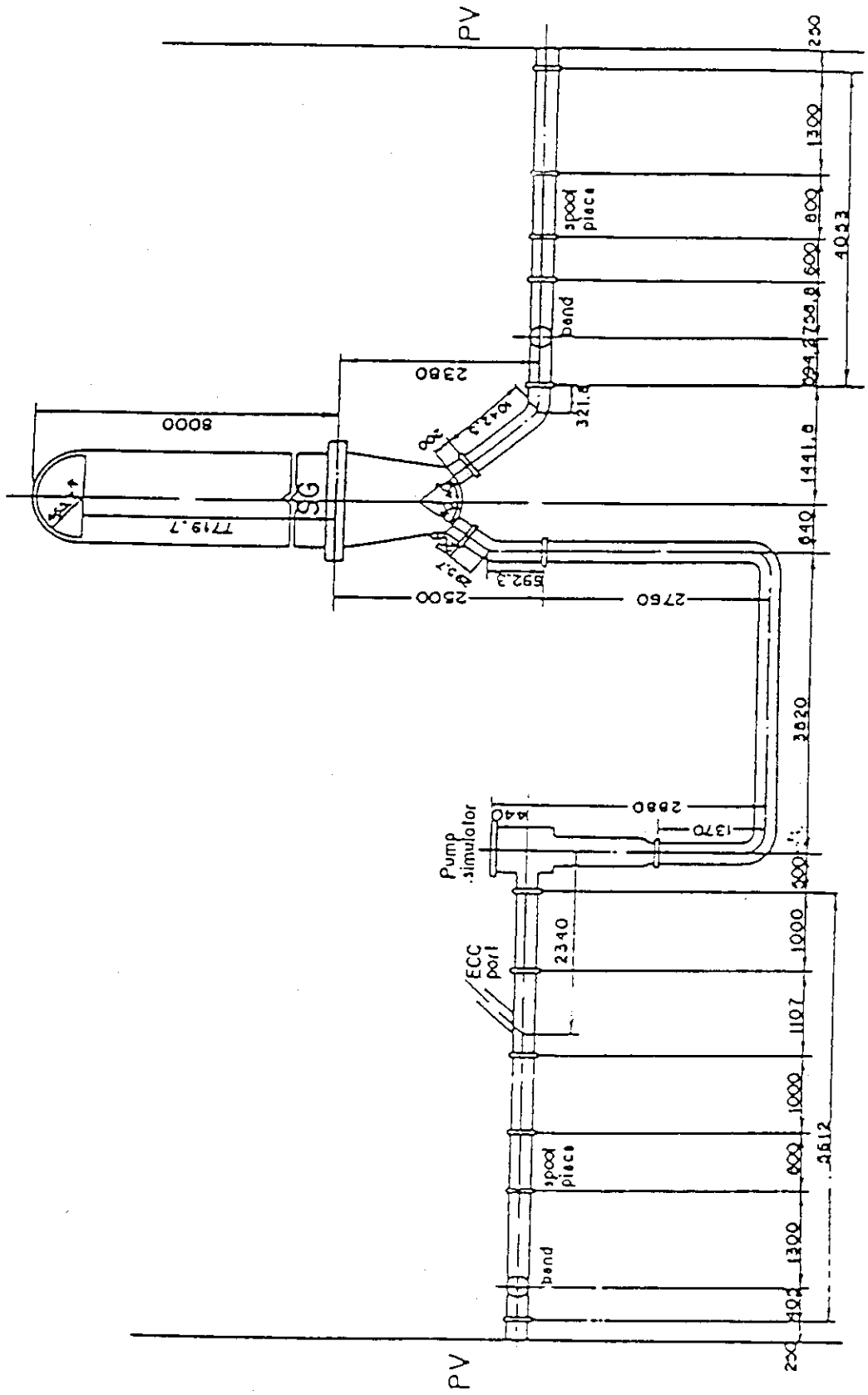

Fig. 2.15 Dimensions of primary loop

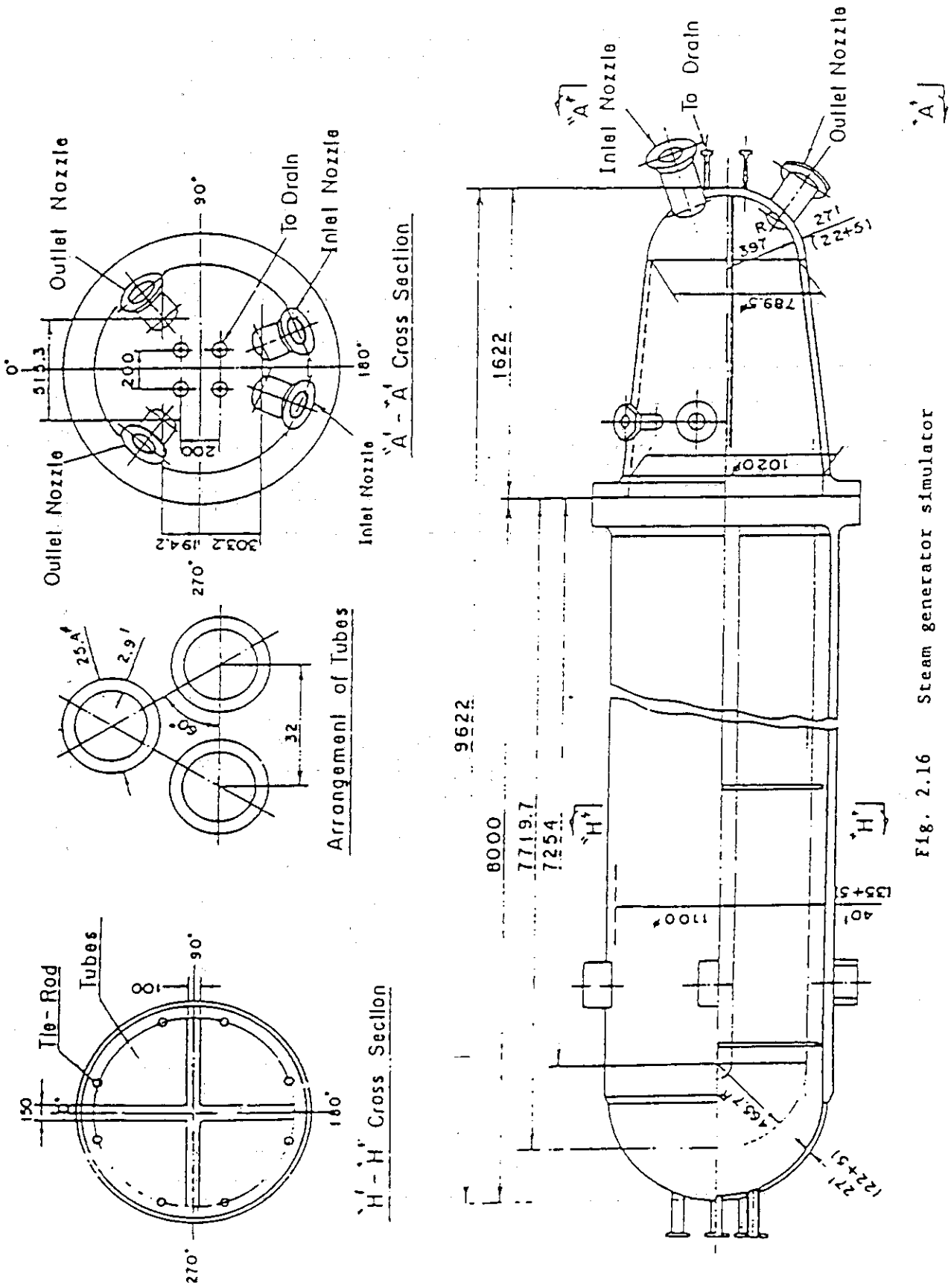
Outlet Nozzle
Inlet Nozzle
To Drain
"A' - A' Cross Section
Arrangement of Tubes
Tie-Rod
Tubes
"H' - H' Cross Section
1622
9622
8000
7719.7
7254
1020
1100
789.5
397
Steam generator simulator

Fig. 2.16

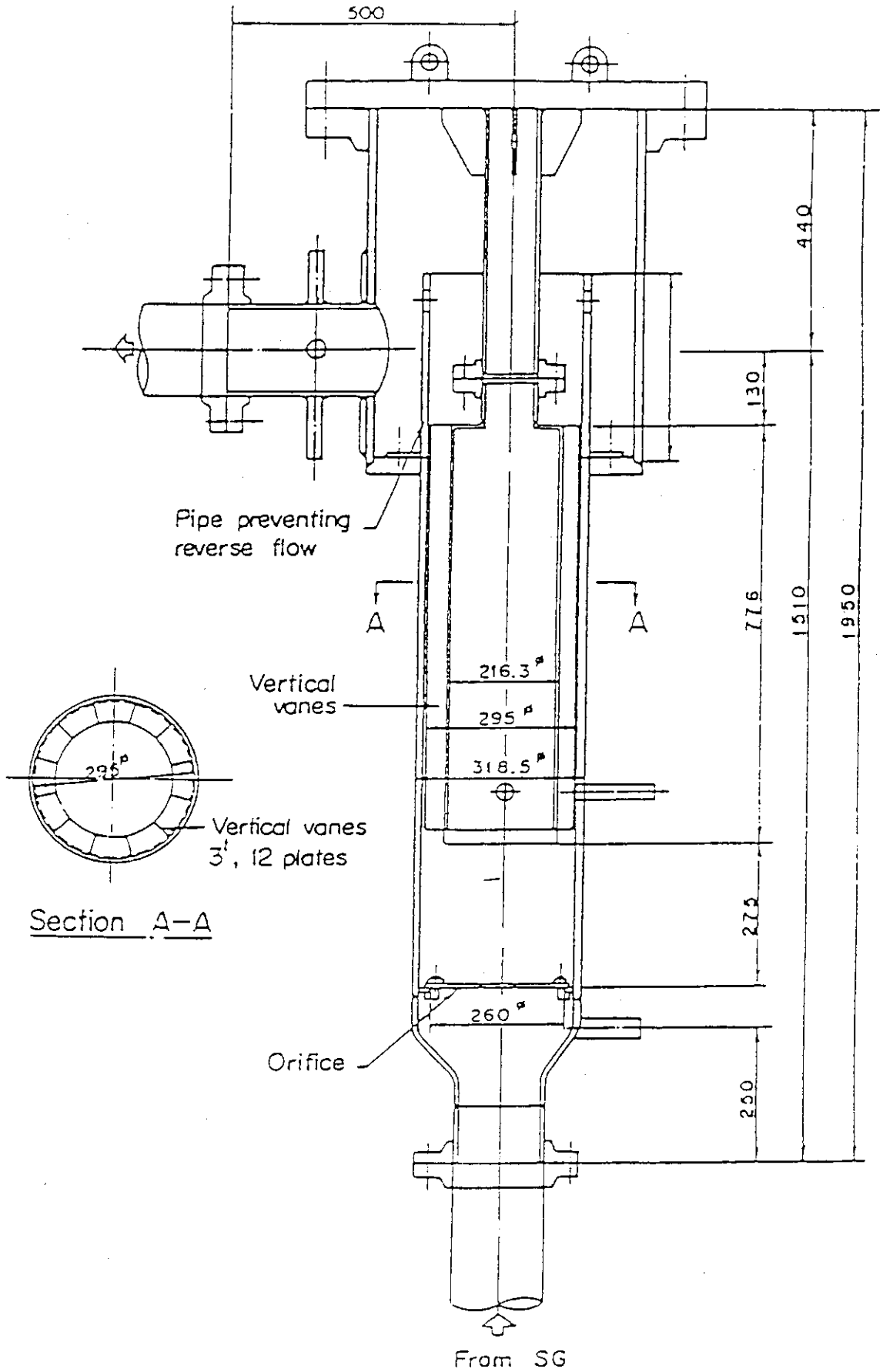

Fig. 2.17 Pump Simulator

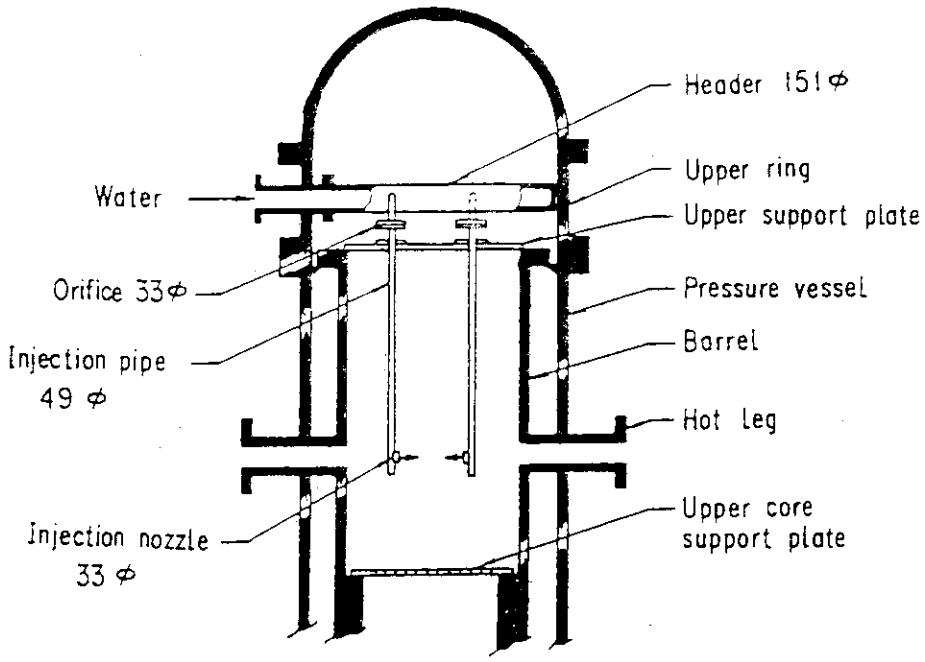

Fig. 2.18 Configuration of upper plenum injection pipe

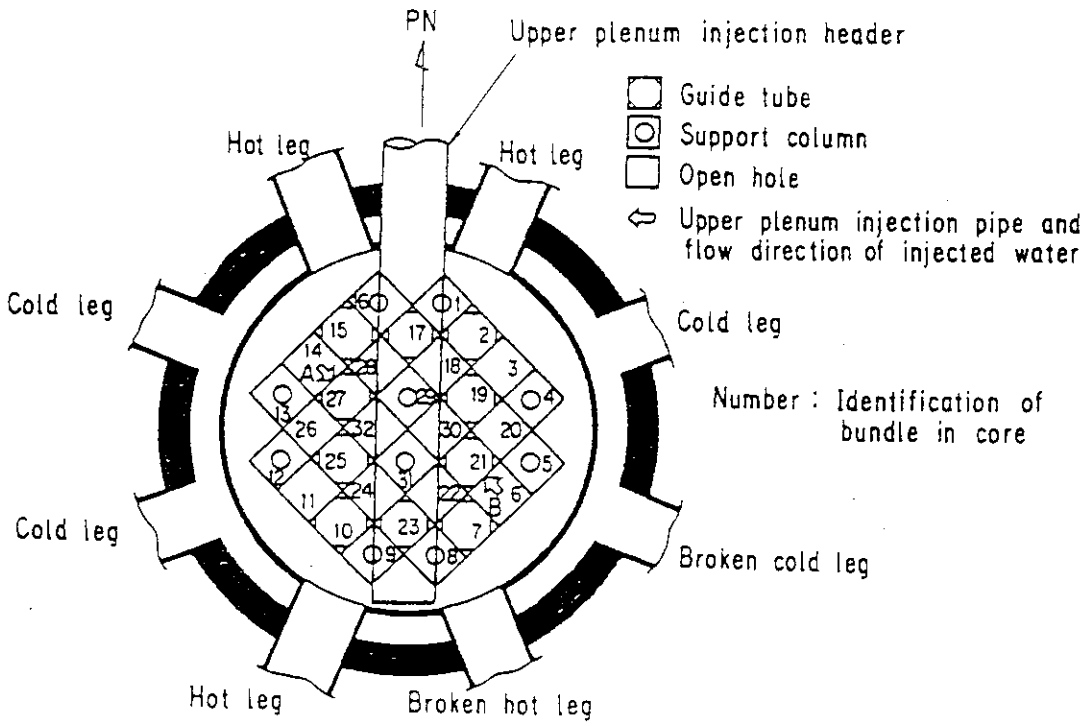

Fig. 2.19 Arrangement and location of upper plenum injection pipe

3. Test procedure and test conditions

3.1 Test procedure of Test C2-16 (Run 76)

In this section, the test procedure of the asymmetric UPI test C2-16 (Run 76) is described.

In preparation for the test, the Acc tank, the LPCI tank, the saturated water tank, Alternative tank 1 and the secondary sides of the steam generator simulators were filled with water which was purified with ion exchange resin. After all the components and instruments were inspected for mechanical and electrical leakages, the instruments were checked for their zero points and sensitivity.

After these preparatory operations, the primary system was heated with the preheaters to its specified temperatures (downcomer wall: 470 K, core internals: 393 K, and primary loop piping wall: 401 K) and pressurized to a specified pressure (0.2 MPa) by substituting steam for nitrogen gas in the system. The water in the Acc tank was electrically heated to its specified temperature (308 K) and pressurized with nitrogen gas to provide sufficient head to drive the injection flow required. The water in the LPCI tank was also heated to its specified temperature (308 K) and was circulated through the circulation line including the LPCI line to preheat the line to the same temperature as the water. The water in the saturated water tank was heated to near the saturation temperature (394 K) of the expected primary system pressure (0.2 MPa). The water in the Alternative tank 1 was heated to its specified temperature (308 K) and pressurized with nitrogen gas to provide sufficient head to drive the injection flow required. The water in the secondary side of each steam generator simulator was also heated and pressurized to the specified temperature (539 K) and pressure (5.3 MPa).

After establishing the initial conditions of the test, the electric power for preheating was turned off and the lower plenum was filled to 0.9 m directly from the satruated water tank. When the water level in the lower plenum reached the specified level and other initial conditions of the test stabilized at the allowable tolerance, electric power was applied to the heater rods in the core and the data recording was started. The temperature rises of the rods were monitored by using a computer. When a specified initial clad temperature (989 K) was

reached, direct injection (0.097 m^3/s) of the Acc water into the lower plenum and injection (0.01 m^3/s) of the ECC water into the upper plenum were initiated. The system pressure was maintained at the specified initial pressure (0.2 MPa) throughout the test by controlling the outlet valve of containment tank-II. Decay of power input to the rods was programmed to begin when the water reached the bottom of the heated region of the core. The specified initial clad temperature (989 K) of the heater rods for initiation of coolant injection was predetermined by interpolation between the clad temperature (394 K) after preheating and the clad temperature (1073 K) assumed for the time of core bottom recovery. The specified power decay was obtained by normalizing the decay curve of the ANS standard × 1.0 + ^{238}U capture decay at 30 s after shutdown.

When the assumed water level reached the specified level (0.5 m) from the bottom of the heated region of the core, the injection port for the Acc water was changed from the lower plenum to the three intact cold leg ECC ports. This water level was assumed to be the level at which considerable steam generation occurs in the core to minimize the atypical oscillatory behavior due to the condensation at the ECC ports.

The Acc injection flow rate was then reduced to 0.082 m^3/s in the cold leg injection period. At a specified time (15.0 s) after the time of core bottom recovery, the velves in the Acc lines and LPCI circulation lines were closed and the valves in LPCI injection line were opened. These actions transferred the ECC injection from Acc injection mode to HPCI mode. A specified HPCI flow rate (0.0028 m^3/s) was maintained constantly until the ECC injection was turned off.

The generated steam and the entrained water flowed via broken and intact loops to the containment tanks. The steam was then vented to the atmosphere to maintain a constant pressure in the containment tanks. After all thermocouples on the surface of the heater rods indicated quenching of the rods, the power supply to the heater rods and the ECC water injection were turned off. Then, the recording system was stopped, thus terminating the test.

3.2 Test conditions of Test C2-16 (Run 76)

In this section, the test conditions of the asymmetric UPI test C2-16 (Run 76) is described. This test is a UPI test simulating a

single failure of LPCI pumps under evaluation model condition.

Figure 3.1 shows the sequence of C2-16 (Run 76) test. Table 3.1 gives the summary of the initial test conditions of C2-16 (Run 76) test. Table 3.2 gives the chronology of the events of C2-16 (Run 76) test.

The pressure in the containment tank II was determined based on an audit analysis[7] and set at 0.2 MPa. The power was determined based on an following equation.

$$1.02 \times (\mathrm{ANS} \times 1.0 + \mathrm{Actinide} \times 1.1) \times \mathrm{Fex}$$

Considering the CCTF scaling (1/21.4), the experimental margin Fex of 1.07 and assuming that the reflood initiates at 30 s after scram, the initial power was set at 7.9 MW (the initial average linear power density = 1.18 KW/m). The injection rates of Acc and HPCI were determined based on CCTF scaling ratio with no failure assumption of these systems and these ECC waters were injected into the intact cold legs shortly after the injection into the lower plenum. Also, the injection rate of LPCI was determined based on CCTF scaling ratio with single failure assumption of LPCI pumps and this ECC water was injected into the upper plenum.

3.3 Comparison of test conditions among the present asymmetric UPI test and the previous UPI tests

In this section the test conditions of the present asymmetric UPI test C2-16 (Run 76) and the previous UPI tests, which are a symmetric UPI test with the same LPCI rate C2-AS1 (Run 59) and a symmetric UPI test with the doubled LPCI rate C2-13 (Run 72) simulating no failure of LPCI pumps.

The major differences for UPI condition are listed as follows.

	C2-16 (Run 76)	C2-AS1 (Run 59)	C2-12 (Run 72)
Injection mode	asymmetric	symmetric	symmetric
Ratio of injection rate A : B	1 : 0	1 : 1.6	1 : 1
Total injection rate (m^3/hr)	40	40	80

Figure 3.2 shows the ECC injection condition.

Figure 3.3 shows the pressure transients in three UPI tests, indicating nearly identical transients among the tests. Figure 3.4 shows the power transients. The power in C2-AS1 (Run 59) test is slightly higher than others. This is because the power was determined based on the following equation in the test.

$$1.02 \times (\mathrm{ANS} \times 1.03 + \mathrm{Actinide} \times 1.1) \times \mathrm{Fex}$$

ANS × 1.03 is nearly equal to (new ANS + 2σ).

The ECC injection rates simulating (Acc + HPCI) and being injected into cold legs shortly after the injection into the lower plenum are shown in Figs. 3.5 and 3.6, indicating nearly identical transients among the tests.

Figure 3.7 shows the ECC flow rate simulating LPCI and being injected into the upper plenum. The flow rate in the asymmetric UPI test C2-16 (Run 76) is about 10 % lower during -10 s ∿ 200 s than that in the symmetric UPI test C2-AS1 (Run 59). After the period, it is nearly equal to that in C2-AS1 test (Run 59).

Table 3.1 Initial test condition of C2-16 (Run 76)

1. Test type: Upper plenum injection test (asymmetric)

2. Test No. : CCTF II main test No.16 C2-16 (Run 76)

3. Test Date: October 23, 1984

4. Power at 94s: A: Total; 7.88 MW; B: Linear; 1.18 kW/m

5. Relative radial power shape:

A: Zone:	A	B	C
B: Ratio:	1.38	1.20	0.76

6. Axial power shape: Chopped cosine

7. Pressure (MPa)

   A: System; 0.20
   B: Containment; 0.20
   C: Steam generator secondary; 5.3

8. Temperature (Deg. K)

   A: Downcomer wall; 470
   B: Vessel internals; 393
   C: Primary piping wall; 401
   D: Lower plenum liquid; 395
   E: ECC liquid; 308
   F: Steam generator secondary; 539
   G: Peak clad temperature at ECC initiation; 989

9. ECC injection type; Cold leg + Upper plenum

10. Pump K-factor: 15

11. ECC flow rates and duration:
    A: Acc+HPCI 350 m^3/hr from 81.0 to 91.5 seconds into lower plenum
    294 m^3/hr from 91.5 to 106.0 seconds into cold legs
    B: HPCI 10 m^3/hr from 106.0 to 950.0 seconds into cold legs
    C: LPCI 36 m^3/hr from 80.5 to 300 seconds and 43 m^3/hr from 300 to 570 seconds into upper plenum

12. Initial water level in lower plenum: 0.9 m

13. Powre control: ANS * 1.0 + Actinide (30 sec after scram)

14. BOCREC time: 91.0 sec

15. Peak temperature at BOCREC: 1038 K

* Note: Time in this table is defined as time after test initiation

Table 3.2 Chronology of events for test C2-16 (Run 76)

Event	Time after test initia' on(s)	Time after reflood initiation(s)
Test Initiated (Heater Rods Power on) (Data Recording Initiated)	0(15.30.09)	-91.0
LPCI to Upper plenum Initiated	80.5	-10.5
(Acc+HPCI) to Lower Plenum Initiated	81.0	-10.0
Power Decay Initiated (Bottom of Core Recovery) (Reflood Initiation)	91.0	0.0
(Acc+HPCI) Switched from Lower Plenum to Cold Legs	91.5	0.5
Acc Injection to Cold Legs Ended and HPCI to Cold Legs Continued	106.0	15.0
LPCI to Upper Plenum Ended	770.0	679.0
Power Off	950.0	859.0
HPCI to Cold Legs Ended	1004.0	913.0
Test Ended (Data Recording Ended)	1034.0	943.0

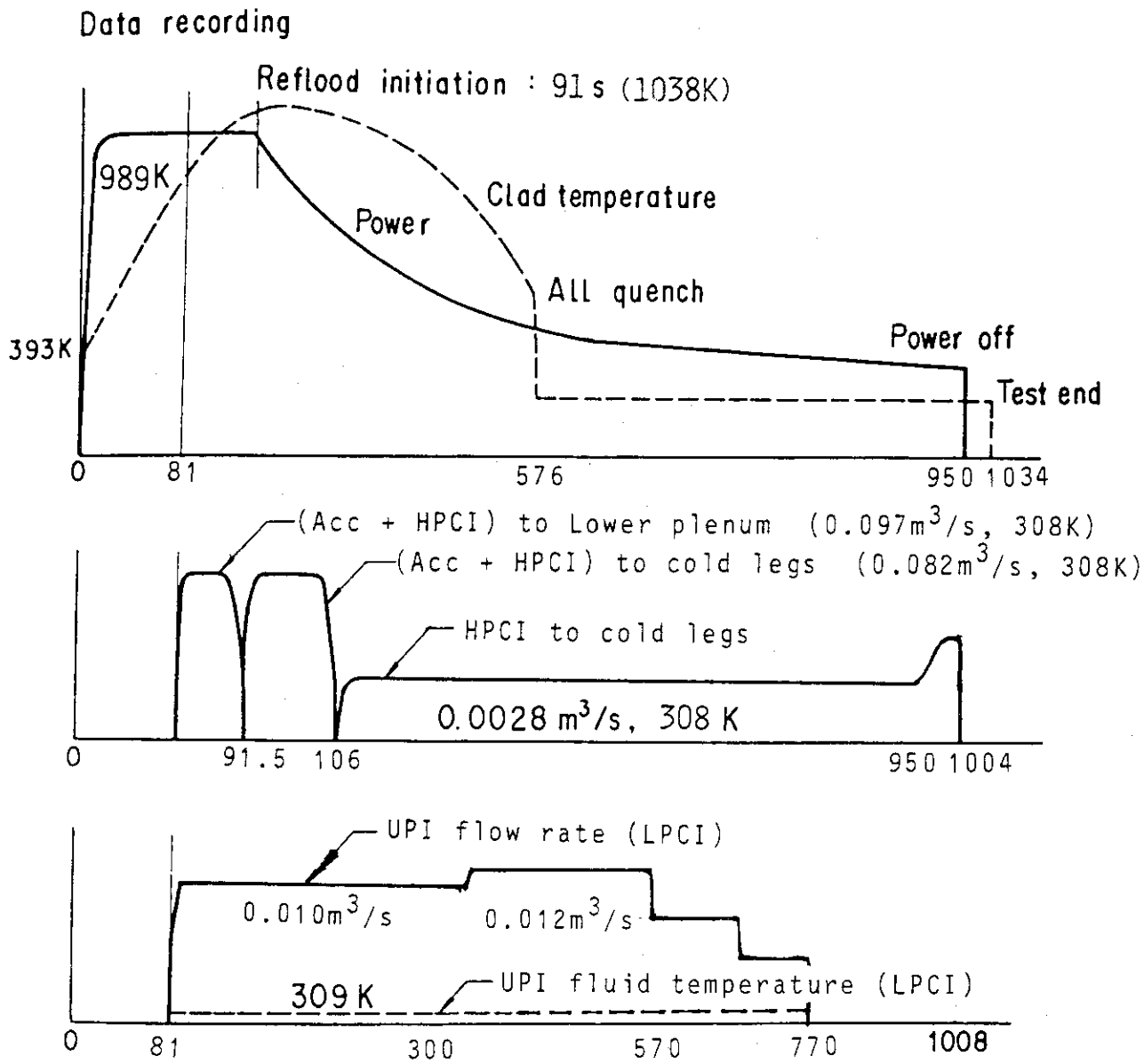

Fig. 3.1 Test sequence of C2-16 (Run 76)

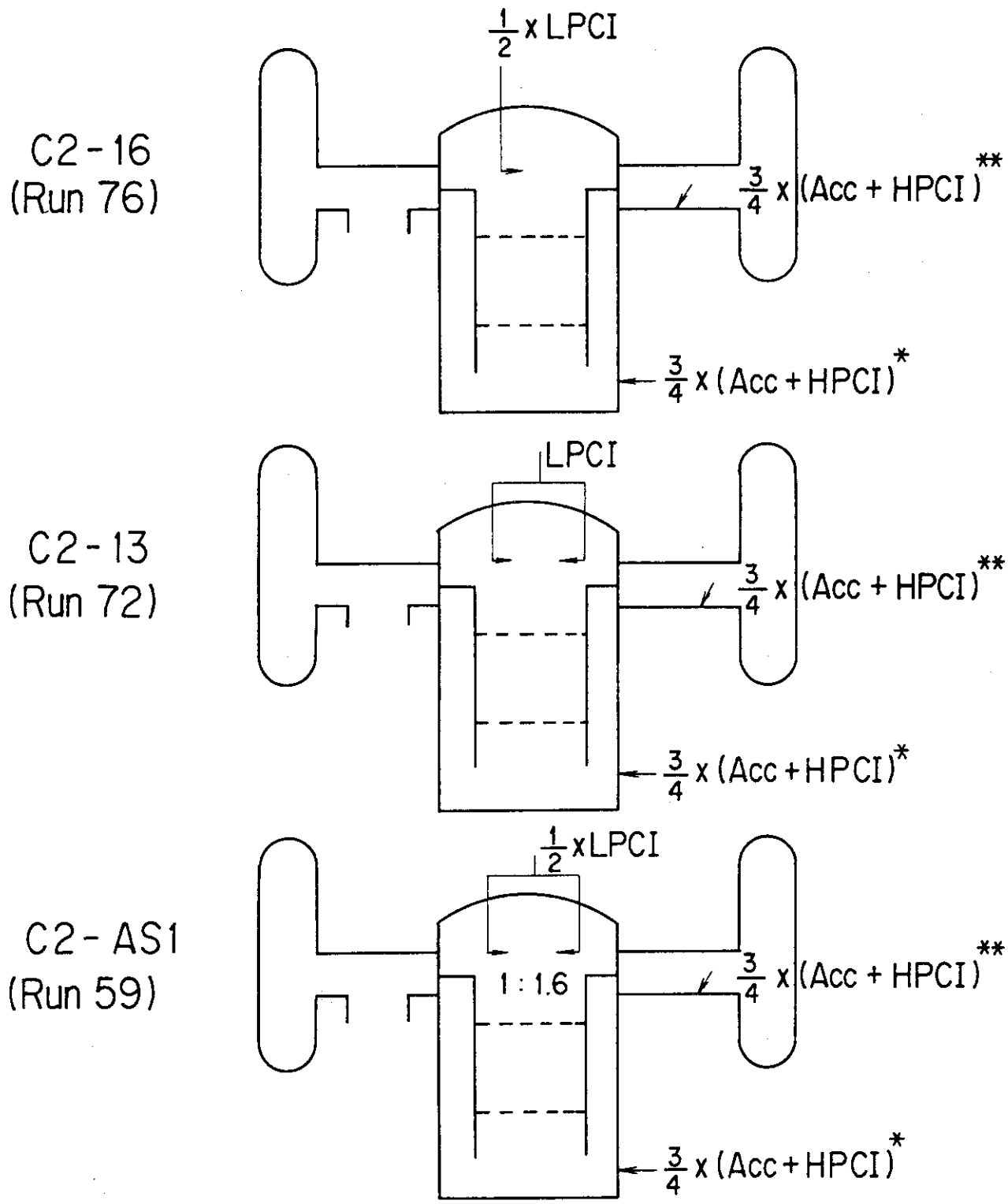

* For early period only

** Except for early period

Fig. 3.2 ECC injection condition

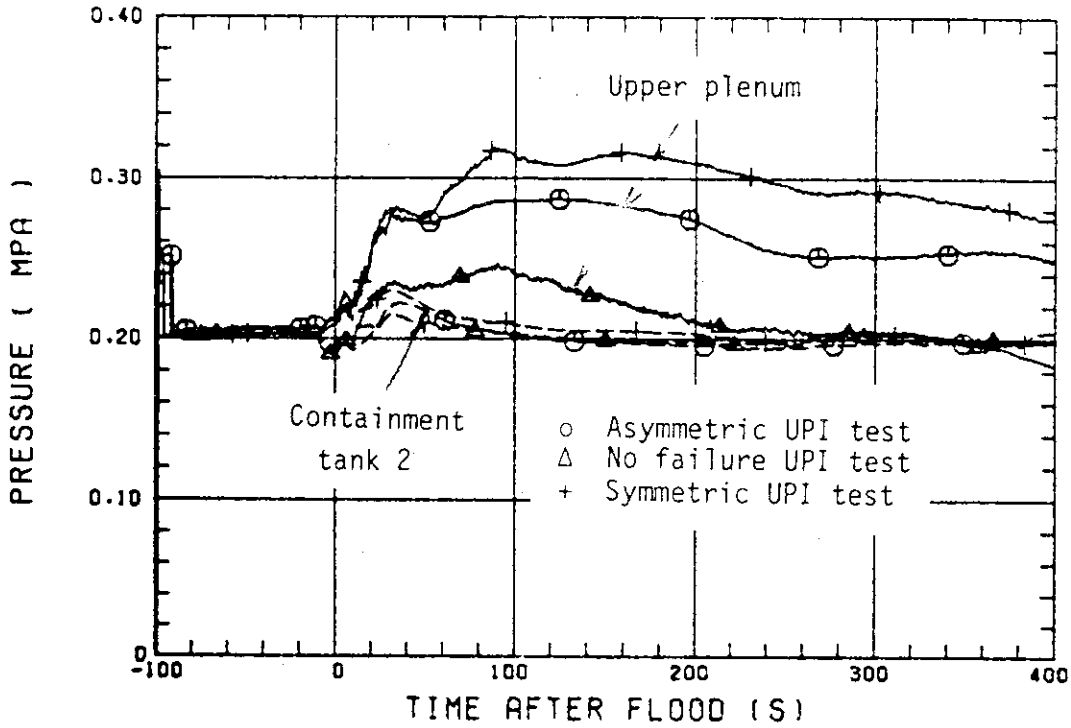

Fig. 3.3 Comparison of pressure

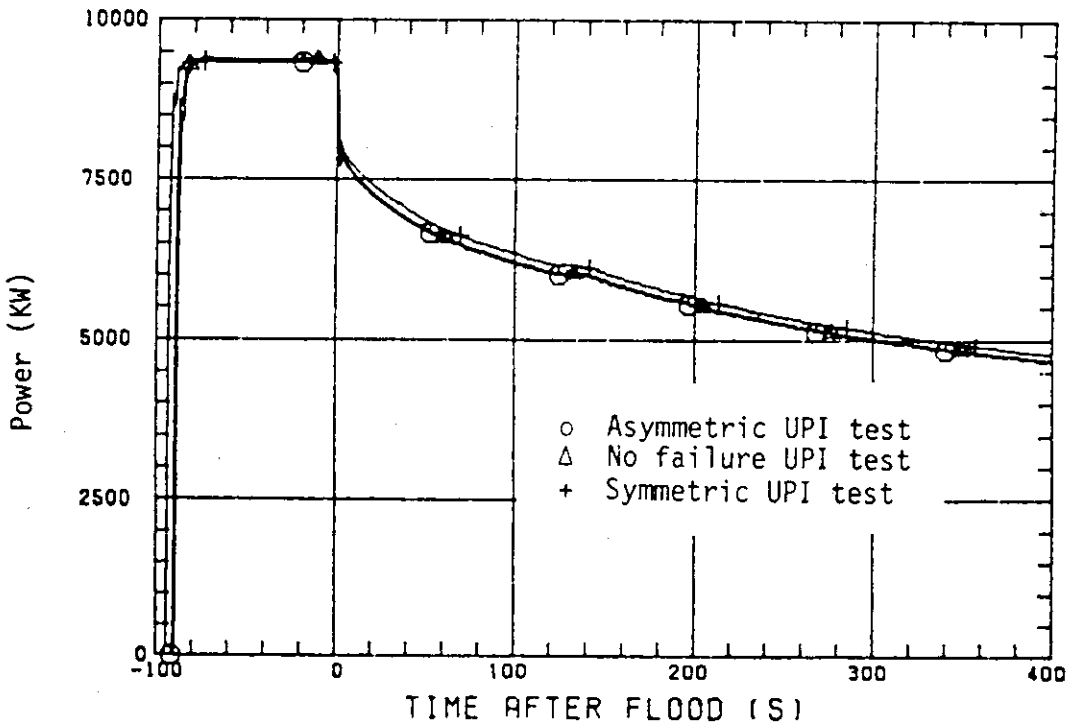

Fig. 3.4 Comparison of power

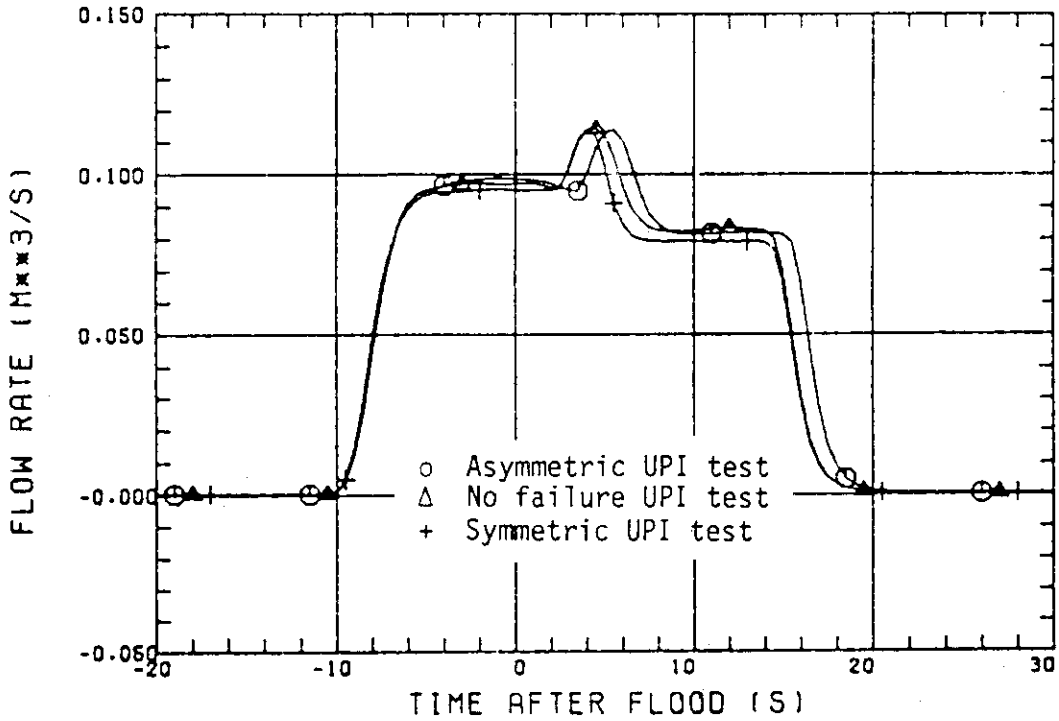

Fig. 3.5 Comparison of ECC (Acc + HPCI) injection from Acc tank

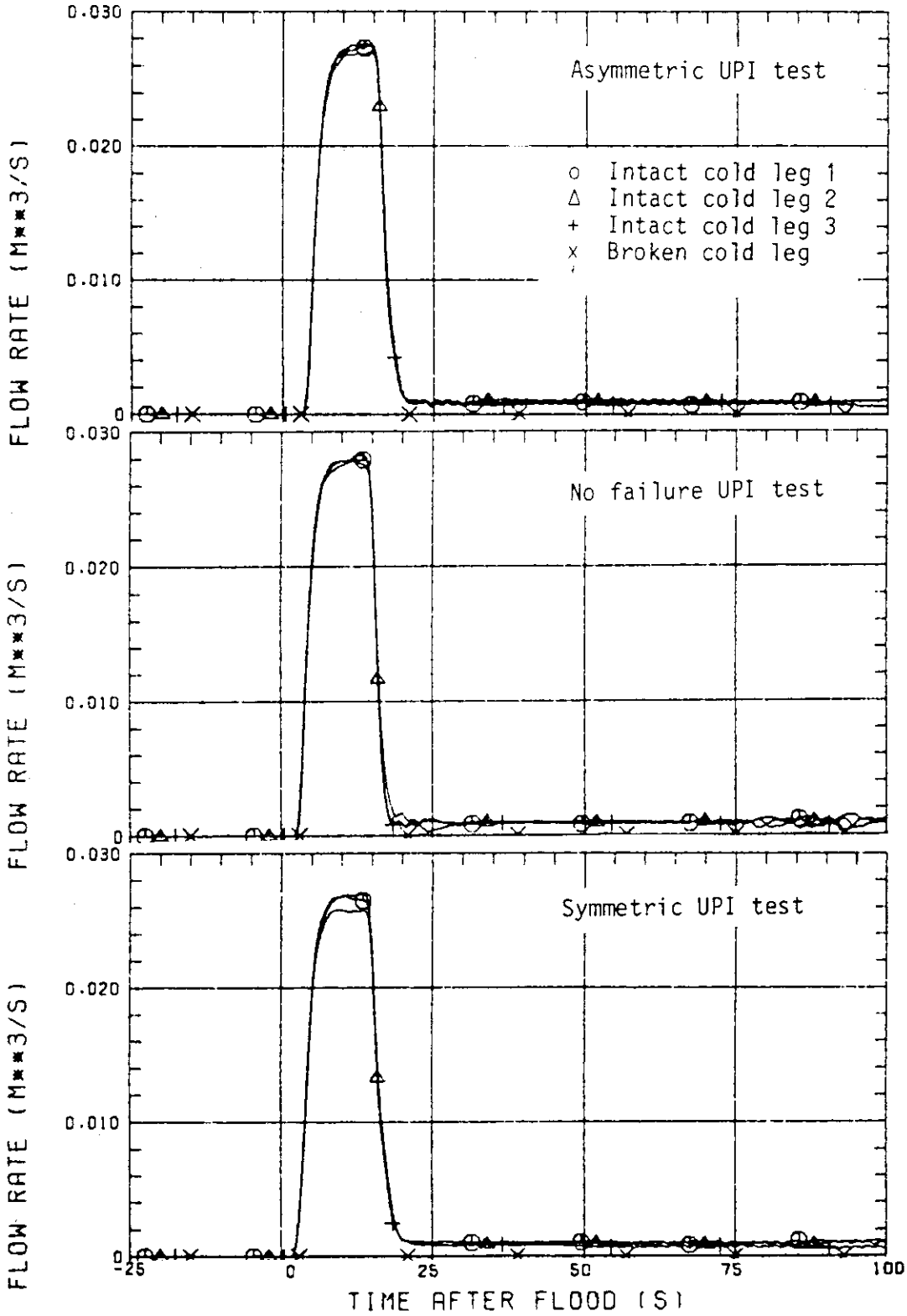

Fig. 3.6 Comparison of ECC (Acc + HPCI) injection to cold legs

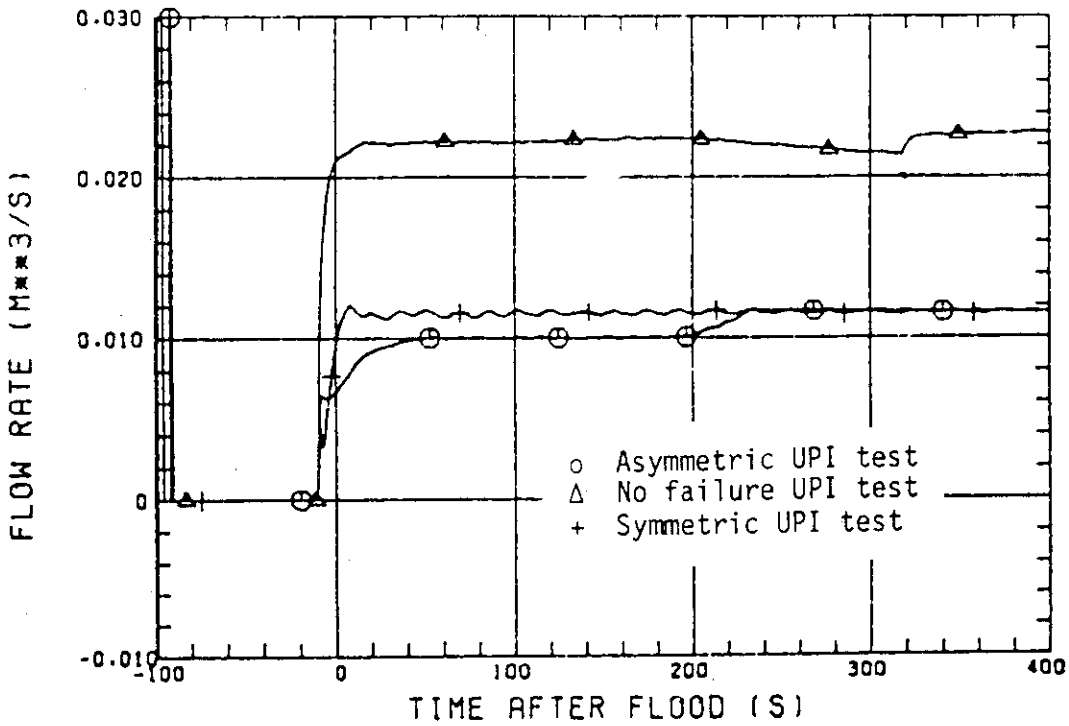

Fig. 3.7 Comparison of ECC (LPCI) injection to upper plenum

4. Results and discussion

4.1 Fluid behavior in upper plenum

4.1.1 Transient of water accumulation

Figure 4.1 shows the differential pressure across the bottom and the top of the upper plenum. Since the gravity term is a dominant factor for the differential pressure in the upper plneum because of the low water mass flow rate, the differential pressure means the static head of the accumulated water on the upper core support plate (UCSP), or in the upper plenum. The result of the present test C2-16 (Run 76) shows the following transient. Before the reflood initiation, the differential pressure is zero even if the UPI water is injected into the upper plenum. After the reflood initiation, the differential pressure increases with the rate of almost 100 % accumulation. Eventualy, the increase of the differential pressure terminates at 50 s and then the differential pressure keeps constant value.

The difference of the upper plenum differential pressure between the present test and C2-SH1 (Run 59) test is observed only during 0 s ~ 50 s. The upper plenum differential pressure in the present test is lower than in C2-SH1 test. One of the reasons for this is considered to be a lower UPI rate in the present test, as shown in Fig. 3.6. The effect of the asymmetric UPI is negligibly small at least both before BOCREC (< 0 s) and after the upper plenum filling with two phase mixture (> 50 s), since for those periods the upper plenum differential pressure is equal with each other between both tests.

4.1.2 Azimuthal distribution of water accumulation

Figure 4.2 shows the azimuthal histributions of the upper plenum differential pressure ΔP_U and the end box differential pressure ΔP_{EB} which is defined to be a differential pressure between the top of the heated core and the top of UCSP. From the figure it can be recognized as:

(1) For the early period (< 50 s for C2-16 (Run 76), < 30 s for C2-13

(Run 72), < 50 s for C2-SH1 (Run 59)), ΔP_U and ΔP_{EB} are azimuthally uniform for all UPI tests.

(2) For the later period (Except for the above early period), ΔP_U and ΔP_{EB} are azimuthally ununiform for all UPI tests. The larger ΔP_U region corresponds to the smaller ΔP_{EB} region.

(3) For both periods, (ΔP_u + ΔP_{EB}) are always azimuthally uniform for all UPI tests.

Even when the upper plenum injection is uniform (C2-13 (Run 72)), the unevenly distributed ΔP_U is attained, indicating that the asymmetric UPI is not only the cause of the ununiform ΔP_U. In addition, when the upper plenum injection is not uniform, the region of the higher upper plenum injection rate tends to be a higher ΔP_U region. Thus, the asymmetric UPI affects on the locations of higher ΔP_U and ΔP_{EB} distributions.

The quantitative difference of ΔP_U between both regions (i.e. the higher ΔP_U region and the lower ΔP_U region) is ~ 15 % at 100 s for the present test and ~ 15 % at 100 s for C2-SH1 (Run 59). This difference is beyond the uncertainty of the measurement system.

Although the quantitative difference of ΔP_U in the azimuthal direction is observed, the degree is independent of the degree of the asymmetric UPI, since nearly the same ununiformity of ΔP_U is observed between the present test and C2-SH1 (Run 59) which is relatively symmetric UPI condition.

4.1.3 Transient of fluid temperature

Figure 4.3 shows the examples of fluid temperatures in the upper plenum and in the end box. They show the saturation temperature during the entire transient. According to the inspection of all fiuid temperatures measured in the upper plenum, the subcooled temperature was detected only in the limited region close to the UPI nozzle, as shown in Fig. 4.4.

Hence, the region of the steam condensing due to the subcooled ECC water into the upper plenum is very limited and the level is at least near or above the hot leg nozzle elevation. In most region between the UCSP level and the hot leg nozzle level, the thermal equilibrium is attained. Thus, the asymmetric UPI condition affects on the location

of the subcooled region in the upper plenum. However, the thermal equilibrium which was attained in C2-SH1 (Run 59) was preserved at UCSP level and the end box level even in the present asymmetric UPI test.

4.2 Fluid behavior in lower plenum and core

Figure 4.5 shows the azimuthal distribution of the lower plenum differential pressure in the present UPI test. No different transient is observed among the lower plenum differential pressures measured in four azimuthally different directions, indicating the uniform lower plenum differential pressure.

Figure 4.6 shows the lower plenum differential pressure, indicating the water inventory in the lower plenum. No different transient is observed among three UPI tests, indicating no effect of asymmetric UPI on the lower plenum water inventory.

Figure 4.7 shows the azimuthal distribution of the core sectional differential pressure ΔP_{ci} (i = 1, 2, ··, 6) at various elevations.

The ununiform ΔP_c is observed during the later period (> 50 s) in both the upper and lower core for the present test and in the upper core for C2-AS1 (Run 59).

Figure 4.8 shows the comparison of the core sectional differential pressure ΔP_{ci} among the UPI tests.

(1) For the early period (< 50 s), ΔP_{ciS} (i = 1 ~ 6) in the present UPI test are equal to those in C2-SH1 (Run 59) test, indicating no effect of asymmetric UPI on the core sectional water inventory during the early period.

(2) For the later period (> 50 s), ΔP_{ciS} (i = 2, 3) in the present UPI test are equal to those in C2-SH1 (Run 59) test, indicating no effect of asymmetric UPI on the core sectional water inventory in the lower core during the later period.

(3) For the later period (> 50 s), ΔP_{ciS} (i = 4 ~ 6) in the present UPI test are higher than those in C2-SH1 (Run 59) test, indicating the higher water accumulation in the upper core during the later period due to asymmetric UPI.

The summary is as bollows. The effect of asymmetric UPI on the upper plenum inventory, the core inventory and the lower plenum

inventory concerning the uniformity and the quantity was not observed during the early period (< 50 s). This effect was observed during the later period (> 50 s). The asymmetric UPI gave the higher average ΔP_{ci} in the upper part of the core as well as the ununiformity of ΔP_{ci}.

Figure 4.9 shows the overall azimuthal distribution of the differential pressures in the upper plenum, the upper core, the lower core and the lower plenum. This figure shows the situation during the later period (> 50 s). The higher core sectional differential pressure than the average at the same elevation is observed in the upper core for asymmetric UPI test. The higher core sectional differential pressure region is corresponding to the higher upper plenum differential pressure region, indicating the effect of asymmetric UPI on the location of the higher water accumulation region.

4.3 Fluid behavior in downcomer

Figure 4.10 shows the azimuthal distribution of the downcomer sectional differential pressure ΔP_{Di} (i = 1, 2, ··, 5) at various elevations in the present UPI test. No different transient is observed among ΔP_{DiS} measured in four azimuthally different directions, indicating the uniform downcomer differential pressure.

Figure 4.11 shows the downcomer differential pressure, indicating the water inventory in the downcomer. No different transient is recognized between the present UPI test and C2-SH1 (Run 59) test, indicating no effect of asymmetric UPI on the downcomer water inventory.

4.4 Fall back characteristics from upper plenum into core

The UPI water fell down from upper plenum into core and the negative net flow was established in both previous UPI tests (C2-SH1/ Run 59 and C2-13/Run 72). The core inlet mass flow rate shown in Fig. 4.12 was estimated with the following equation.

$$\dot{m}_F = - \dot{m}_{ECC/up} + (\dot{m}_{loop1} + \dot{m}_{loop2} + \dot{m}_{loop3} + \dot{m}_{loop4})$$

The regative net flow at core inlet and the falling-down UPI water are preserved in the present asymmetric UPI test as well as previous UPI tests.

Figure 4.13 shows the measured result of the fluid upflow with turbine meters located at end box. The ununiform measured results is indicated, suggesting the ununiform steam upflow and water downflow. The water downflow is dominant in the UPI region. This indicates that the asymmetric UPI affects on the location of the water downflow region.

Even when the UPI is uniform (C2-13 (Run 72)), the unevenly distributed steam upflow is attained, indicating that the asymmetric UPI is not only the cause of the ununiform steam upflow. In addition, the relation between the distribution of the steam upflow and the distributions of the core power and/or the clad temperature is not recognized, indicating that the latter distributions are neither only the cause of the ununiform steam upflow. The previous UPI test results have suggested that (i) the steam flows up from the core in nearly half cross section and (ii) separately the water downflow region is formed.

The above characteristics (i) and (ii) are preserved in asymmetric UPI test.

4.5 Fluid behavior in loops

4.5.1 Intact loops

Figure 4.14 shows the differential pressures through various parts of intact loops. The differential pressure DT14H between riser part and SG inlet plenum shows the increase with time, indicating the water accumulation in those volumes. The differential pressure across pump simulator DT13L shows the decrease with time, indicating the decrease of loop mass flow rate.

Figure 4.15 shows the comparison of the differential pressure between three UPI tests. The differential pressure DT14H between riser part and SG inlet plenum is lower in the asymmetric UPI test up to 50 s than in C2-SH1 test and it is equal each other in both tests later than 50 s, indicating no effect of asymmetric UPI on water accumulation at riser part and SG inlet plenum. The differential pressure DT11G across SG is equal with each other in both tests, indicating no effect of asymmetric UPI on fluid flow rate through SG. The differential pressure DT13L across pump simulator is equal with each other in both tests up to 100 s, and it is lower in asymmetric UPI test than in

C2-SH1 test, indicating the lower mass flow rate through the primary pump simulater in intact loop. This is because of the less steam generation in SG for the present UPI test, which can be judged from the slower decreasing of the fluid temperature of the secondary side in SG for the present test.

However, it cannot be explained enough only by the less steam generation in steam generators. The further investigation is necessary.

4.5.2 Broken loop of SG side

Figure 4.16 shows the comparison of the differential pressure across the broken loop SG side. Up to 50 s, the differential pressure in asymmetric UPI test is equal to that in C2-SH1 test, indicating no effect of asymmetric UPI on the differential pressure. Later than 50 s, it is lower in asymmetric UPI test than that in C2-SH1 test. For example, it is ~ 20 % lower at 100 s. The main factors of the reduced ΔP (- 20 KPa) through broken loop are a reduced ΔP (- 12 KPa) across the primary pump simulator and a reduced ΔP (- 5 KPa) across the part downstream the primary pump simulator. This suggests that the lower mass flow rate through broken loop plays the major role in the reduced differential pressure across the broken loop.

The fluid temperature in secondary side of SGs shows the slower decreasing in asymmetric UPI test than in C2-SH1 test, indicating the less steam generation in asymmetric UPI test. This is consistent with the lower mass flow rate in asymmetric UPI test. However, the quantitative explanation is not enough and the further investigation is necessary.

4.5.3 Broken loop of downcomer side

Figure 4.17 shows the comparison of the differential pressure across the broken loop downcomer side. Similarly to the transient of the differential pressure across the broken loop SG side, the differential pressure across the broken loop downcomer side in asymmetric UPI test is equal to that in C2-AS1 (Run 59) upto 50 s, and it is lower than that in C2-AS1 (Run 59) later than 50 s. The reason of lower differential pressure across the broken loop downcomer side in asymmetric UPI test than in C2-AS1 (Run 59) later than 50 s is not clear.

4.6 Fluid behavior around break point

Figure 4.18 shows the water mass flow rate through broken loop downcomer side. This result was obtained by the differential of the measured static head of the water accumulated in containment tank I.

The water mass flow rate increases at 50 s in both of asymmetric UPI test and C2-SH1 test. This time is corresponding to the initiation of overflowing of the water from the downcomer to break point.

4.7 Core cooling behavior

4.7.1 Clad temperature

Figure 4.19 shows the clad temperature transient at the various elevations in the high power region. In both asymmetric UPI test and C2-SH1 test, the lower part of the core (0.38 m and 1.02 m elevations) is cooled uniformly, and the upper part of the core (1.83 m, 2.44 m and 3.05 m elevations) is cooled uniformly during the early period (< 50 s) and is cooled ununiformly during the later period (> 50 s).

Figure 4.20 shows the clad temperature transient at the various elevations in the low power region. Similarly to the case of the high power region, in both asymmetric UPI test and C2-SH1 (Run 59) test the lower part of the core is cooled uniformly, and the upper part of the core is cooled uniformly during the early period and is cooled ununiformly during the later period.

The uniform core cooling in the lower core and the upper core for the early period is also recognized from the heat transfer coefficient shown in Fig. 4.21. Besides, the ununiform core cooling in the upper core for the later period is recognized from Fig. 4.21.

The ununiform core cooling region is correspondent to the ununiform core sectional differential pressure mentioned in 4.2. Besides, the better core cooling region is correspondent to the higher ΔPci region. The ununiformity of the core cooling is caused not only by the asymmetric UPI, since this ununiformity has been observed in C2-AS1 (Run 59).

As shown in Fig. 4.19, the highest clad temperature in the high power region for asymmetric UPI test is lower at any time than that for C2-SH1 test. Also as shown in Fig. 4.20, the clad temperature in the

low power region for asymmetric UPI test is lower in ununiform core cooling region (≧ 1.83 m) than that for C2-SH1 test, and it is nearly equal to each other in uniform core cooling region between both UPI tests. The higher heat transfer coefficient of asymmetric UPI test than that of C2-AS1 (Run 59) in ununiform core cooling region is also shown in Fig. 4.22. Thus, at least the asymmetric UPI did not give a poorer core cooling than the symmetric UPI, even in the ununiform core cooling region. It is consistent with the higher averaged ΔP_{ci} in the upper part of the core for asymmetric UPI test than that for C2-AS1 (Run 59) test, based on Murao-Sugimoto's heat transfer coefficient correlation which shows that the higher ΔP_{ci} gives the higher heat transfer coefficient.

It is necessary to study further if the better core cooling in asymmetric UPI test can be explained only by the higher ΔP_{ci}.

4.7.2 Turnaround temperature and quench time

Figure 4.23 shows the comparison of the turnaround temperature. In the lower part of the core (< 1.1 m) the turnaround temperature is ~ 10 K lower in asymmetric UPI test than that in C2-SH1 test. In the upper part of the core (> 1.4 m) it is ~ 25 K lower in asymmetric UPI test than that in C2-SH1 test. The initial clad temperature is ~10 K lower in asymmetric UPI test than that in C2-SH1 test, as noticed from Figs. 4.19 and 4.20. Even taking into account the lower initial clad temperature in asymmetric UPI test, the smaller temperature rise in the upper core is attained in asymmetric UPI test than C2-SH1 test, indicating the better core cooling in the upper core due to the asymmetric UPI.

In summary, a UPI test simulating single LPCI pump failure with asymmetric UPI gave the lower peak clad temperature than a UPI test with the same LPCI injection rate but more symmetric UPI. It indicated that the asymmetric UPI condition did not give a locally poor core cooling.

Figure 4.24 shows the comparison of the quench time. The quench time is nearly equal between asymmetric UPI test and C2-SH1 test, indicating little effect of asymmetric UPI on bottom quenching.

Figure 4.25 shows the comparison of the turnaround temperature between aaymmetric UPI test and C2-13 (Run 72) test simulating no failure of LPCI pumps.

In the lower part of the core (< 1.1 m), the turnaround temperature of the asymmetric UPI test is nearly equal to that of C2-13 (Run 72) test. In the middle part of the core (1.1 m ∿ 2.4 m), the former is ∿ 15 K higher than the latter. In the upper part of the core (> 2.4 m), the former is ∿ 50 K higher than the latter.

In summary, a UPI test simulating no LPCI pump failure (Run 72) gave the lower peak clad temperature than a UPI test simulating single LPCI pump failure (Present test/Run 76). It indicated for UPI type PWRs that no LPCI pump failure assumption gave the more conservative core cooling than single LPCI pump failure assumption.

Figure 4.26 shows the comparison of the quench time. For both asymmetric UPI test and no failure UPI tests, top quenching occurrence is widely observed in comparison of the test result simulating cold-leg-injection-type PWR, where the top quenching is considered to occur only in the part above ∿ 3 m elevation.

4.8 Summary of asymmetric UPI effect

Asymmetric UPI effect on reflood phenomena, which is described in the former sections, is summarized in this section.

4.8.1 Qualitative effect of asymmetric UPI

Qualitative effect of asymmetric UPI is shown in Fig. 4.27.

For the early period (< 50 s), the following uniformities over the horizontal cross section were observed in asymmetric UPI test.

(1) uniformity of ΔP_u
(2) uniformity of ΔP_{ci}
(3) uniformity of ΔP_{LP}
(4) uniformity of ΔP_{Di}
(5) uniformity of T_{ci} (although there exists the dependency on radial power profile)
(6) uniformity of h_i (although there exists the dependency on radial power profile)
(7) uniformity of fluid flow between core and upper plenum

ΔP_u : Differential pressure across bottom and top of upper plenum
ΔP_{ci} : Core sectional differential pressure
ΔP_{LP} : Differential pressure across bottom and top of lower plenum
ΔP_{Di} : Downcomer sectional differential pressure
T_{ci} : Clad temperature at i'th elevation
h_i : Heat transfer coefficient at i'th elevation

These uniformities are observed also in symmetric UPI test, suggesting no effect of asymmetric UPI on thermo-hydraulic behavior for the early period.

For the later period (> 50 s), the following ununiformities over the horizontal cross section were observed in asymmetric UPI test, as shown in Fig. 4.27.

(1) ununiformity of ΔP_u
(2) ununiformity of ΔP_{ci} in upper core
(3) ununiformity of T_{ci} in upper core
(4) ununiformity of h_i in upper core

(5) ununiformity of fluid upflow between core and upper plenum including the separation of two-phase upflow region and water downflow region.

The UPI region corresponded to the higher ΔP_u, the higher ΔP_{ci}, the lower T_{ci}, the higher h_i, and the lower fluid upflow region (or water downflow region), suggesting that asymmetric UPI formed the water downflow region leading to the higher water accumulation regions in upper plenum and in core, and resultantly the higher heat transfer coefficient region and the lower clad temperature region.

Following uniformities were preserved for the later period even in asymmetric UPI test.

(1) uniformity of ΔP_{ci} in lower core
(2) uniformity of T_{ci} in lower core (although there exists the dependency on radial power profile)
(3) uniformity of ΔP_{LP}
(4) uniformity of ΔP_{Di}

Accordingly, it can be said that asymmetric UPI effect is limited in the upper part of core and upper plenum for the later period.

Symmetric UPI test also gave ununiformity of ΔP_U, ΔP_{ci} in upper core, T_{ci} in upper core, hi in upper core and fluid up-flow between core and upper plenum for later period, so that above ununiformities in asymmetric UPI test are derived not only by asymmetric UPI.

The possible reason for the ununiformity is considered to be due to ununiform arrangement of loop pipings (intact loops and a broken loop), ununiform arrangement of upper plenum structure, and so on. However, it has not been identified yet. Further study is needed for the identification.

4.8.2 Quantitative effect of asymmetric UPI

Quantitative effect of aaymmetric UPI is shown in Fig. 4.28.

For the early period, the following transients in asymmetric UPI test were narly equal to those in symmetric UPI test.

(1) transient of ΔP_u
(2) transient of ΔP_{ci}
(3) transient of ΔP_{LP}
(4) transient of ΔP_{Di}

(5) transient of m_F
(6) transient of P_I
(7) transient of P_B (SG side)
(8) transient of P_B (PV side)
(9) transient of h_i

m_F : mass flow rate at core inlet
ΔP_I : Differential pressure across intact loop
ΔP_B : Differential pressure across broken loop

For the later period, the following transients in asymmetric UPI test were different from those in symmetric UPI test, like:

(1) lower P_u
(2) higher ΔP_{ci} in upper core
(3) lower ΔP_B (SG side)
(4) lower ΔP_B (PV side)
(5) lower T_{ci} in upper core
(6) higher h_i in upper core

Item (2) is shown clearly in Fig. 4.29.

Items (2), (5) and (6) suggest that asymmetric UPI promoted the water accumulation in upper core, resultantly caused the higher heat transfer and the lower clad temperature.

The reason for items (1), (3) and (4) is not known and it is necessary to investigate further this.

On one hand, the following transients in asymmetric UPI test were nearly equal to those in symmetric UPI test for the later period.

(1) transient of ΔP_u
(2) transient of ΔP_{ci} in lower core
(3) transient of T_{ci} in lower core
(4) transient of ΔP_{LP}
(5) transient of ΔP_{Di}
(6) transient of m_F
(7) transient of ΔP_I

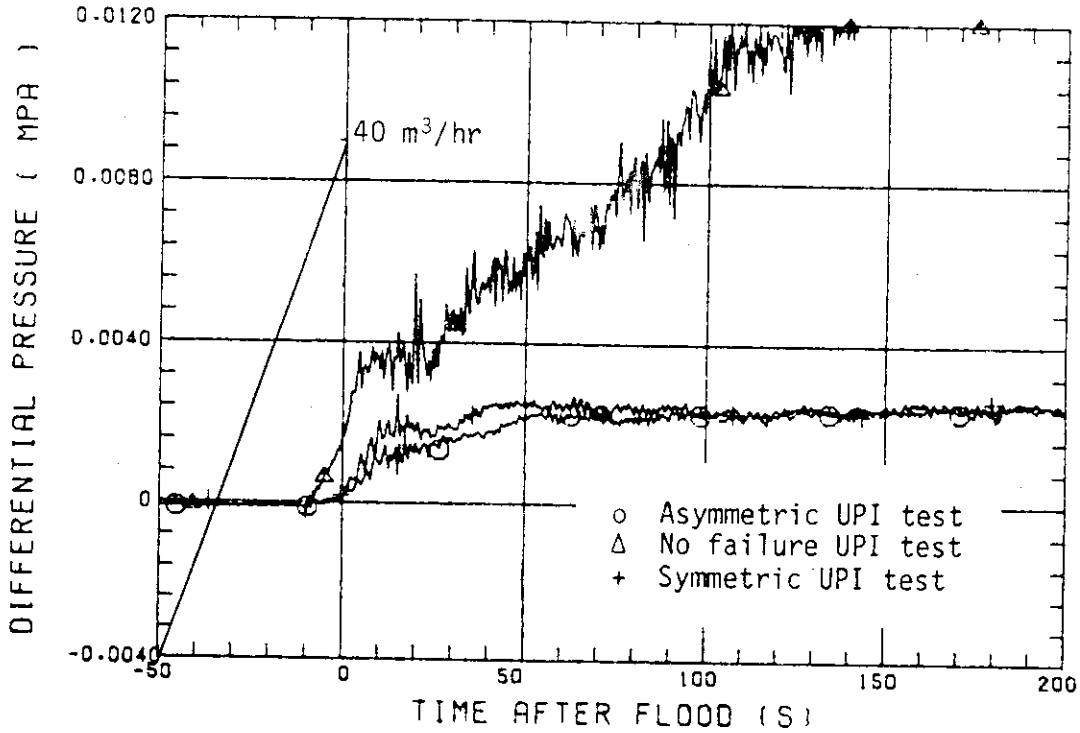

Fig. 4. 1 Differential pressure across the bottom and the top of upper plenum

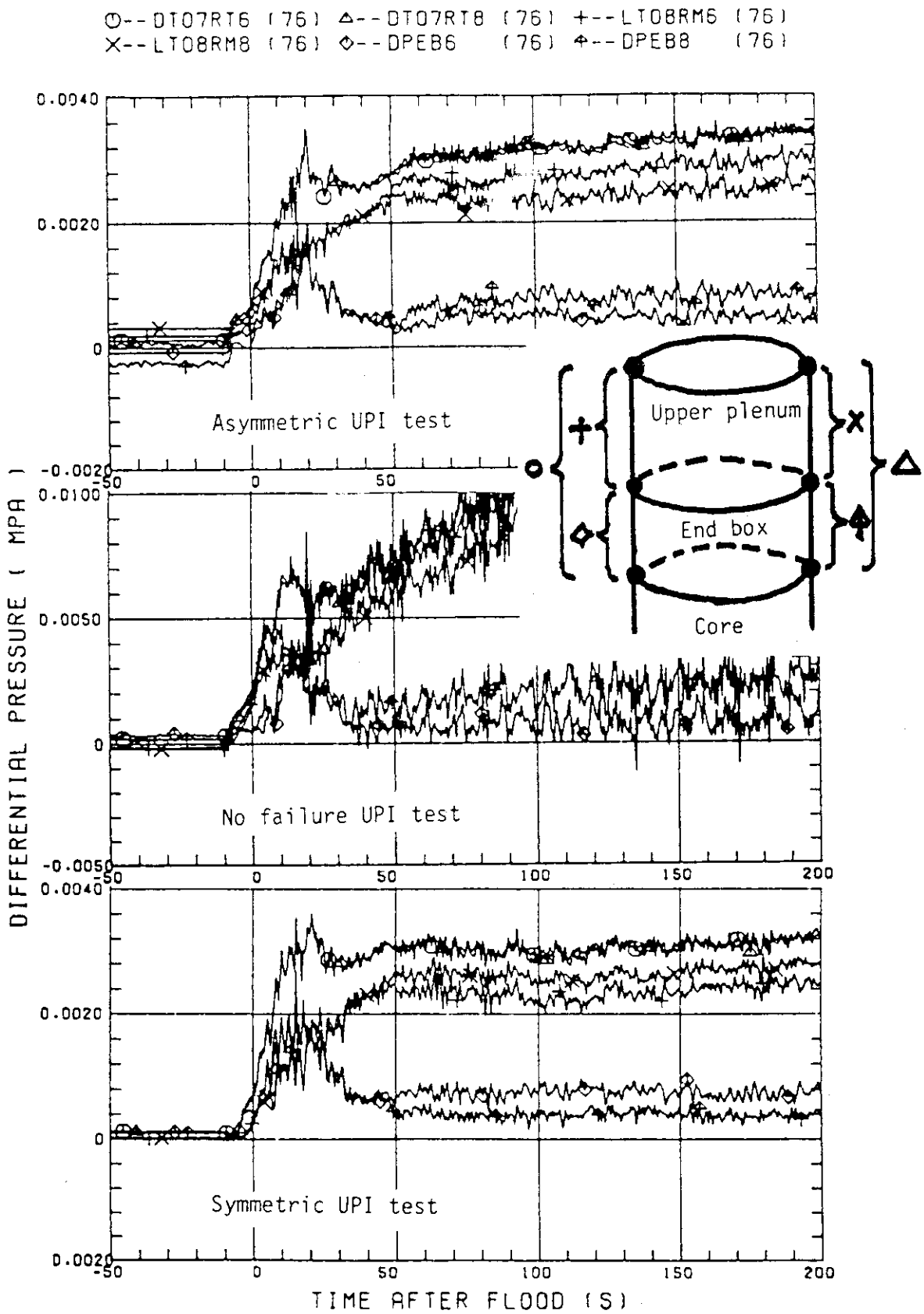

Fig. 4. 2 Azimuthal distribution of the upper plenum differential pressure and the end box differential pressure

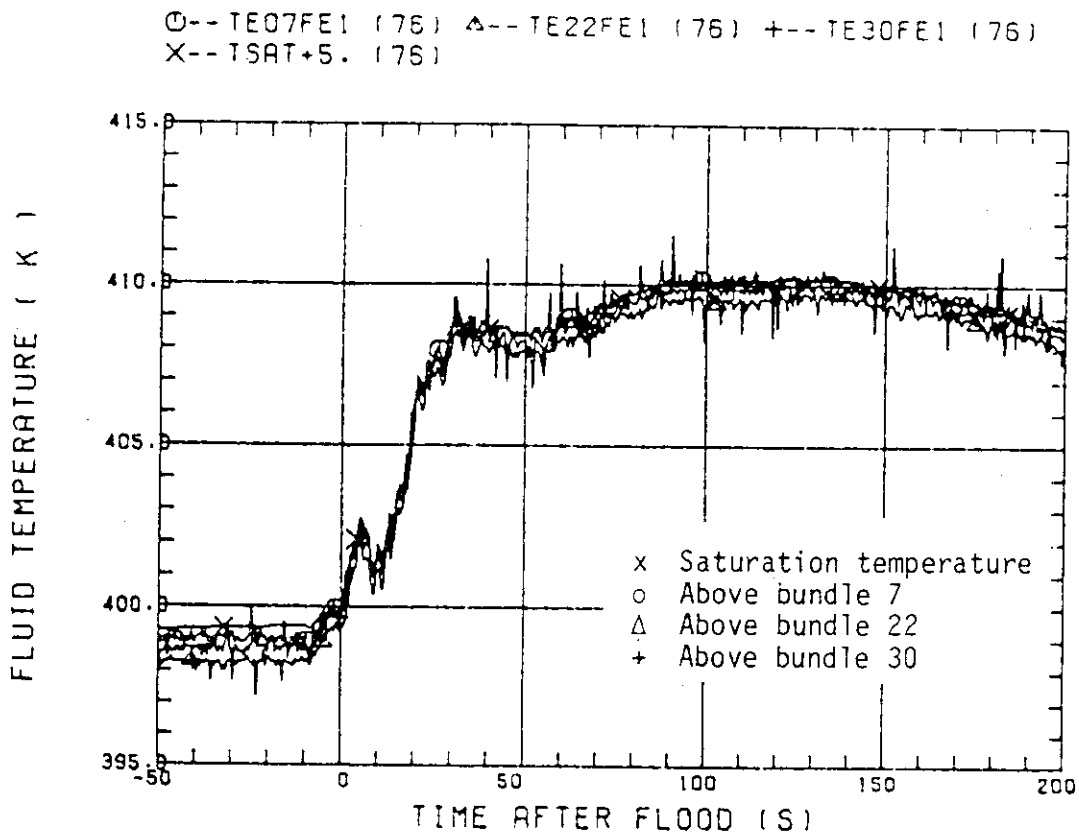

Fig. 4. 3 Fluid temperature in upper plenum

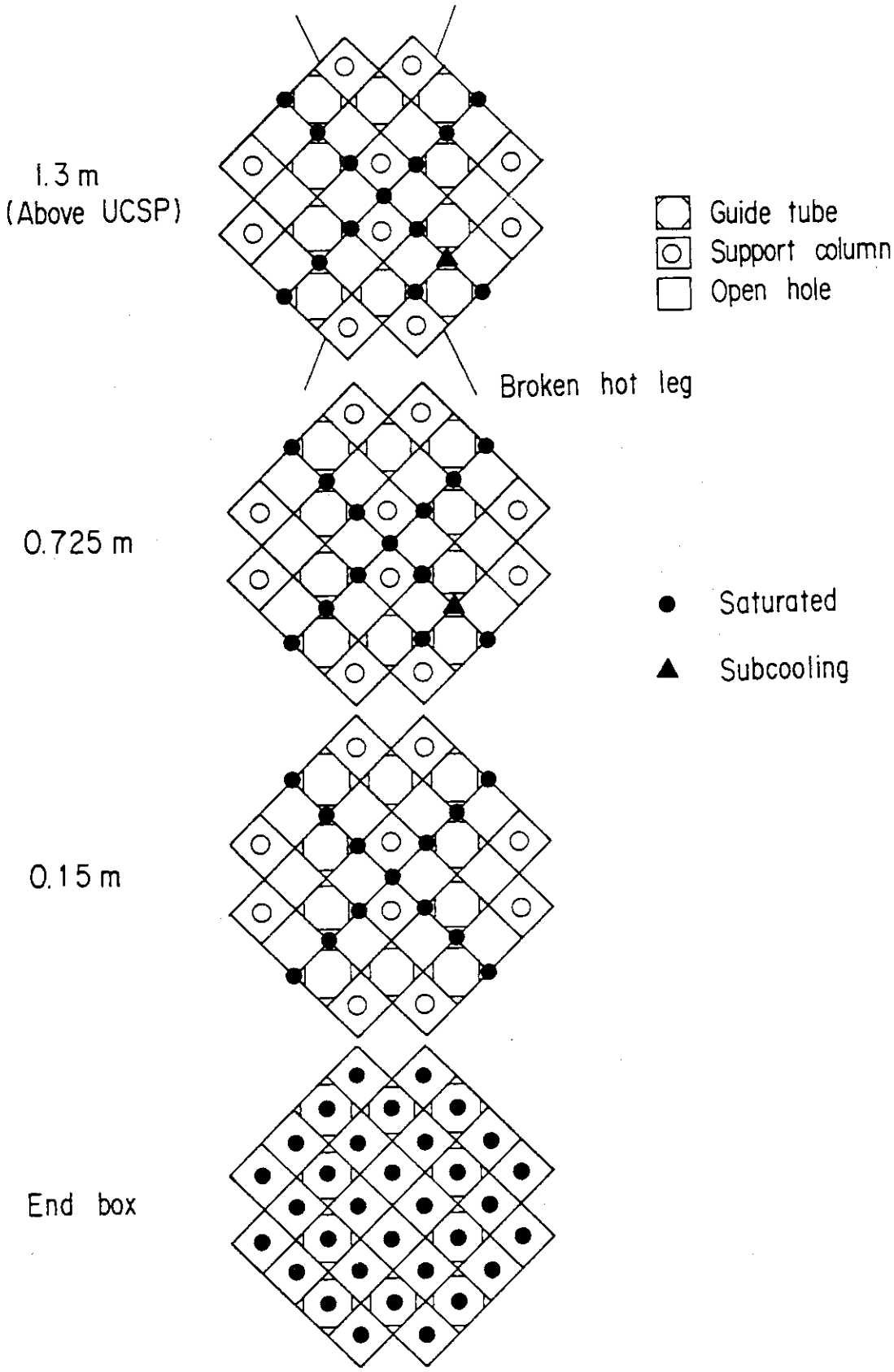

Fig. 4. 4 Subcooled region in upper plenum

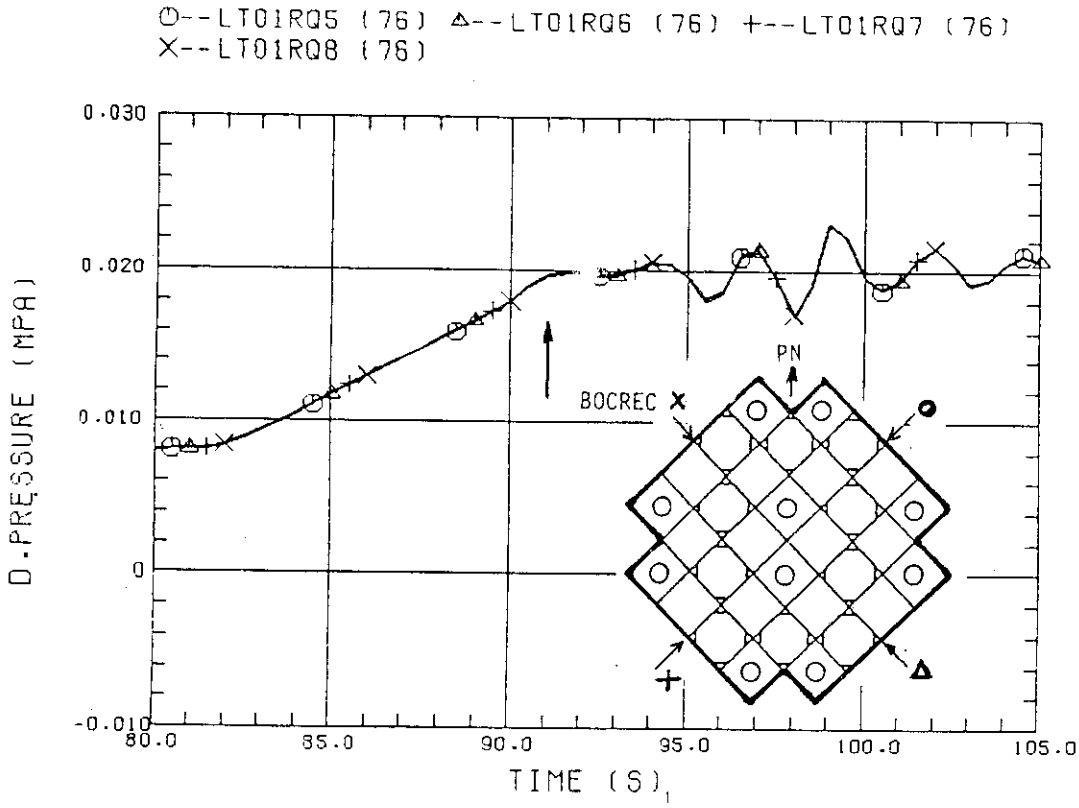

Fig. 4. 5 Azimuthal distribution of lower plenum differential pressure

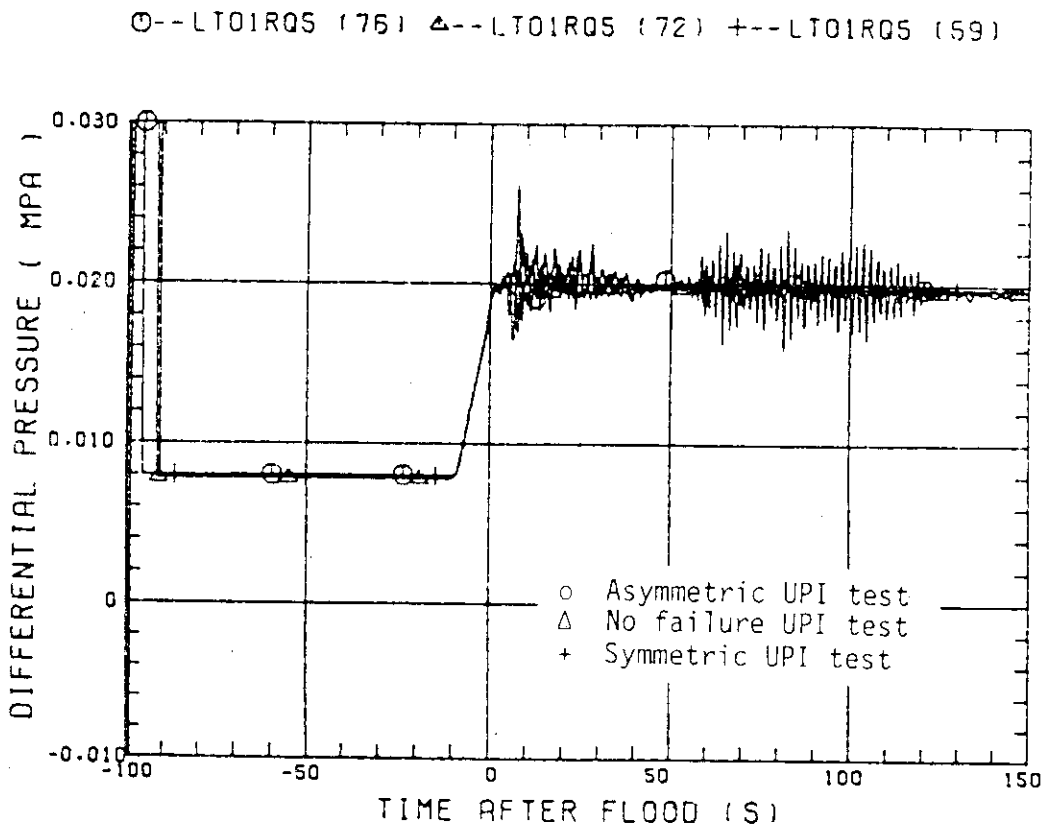

Fig. 4. 6 Comparison of lower plenum differential pressure

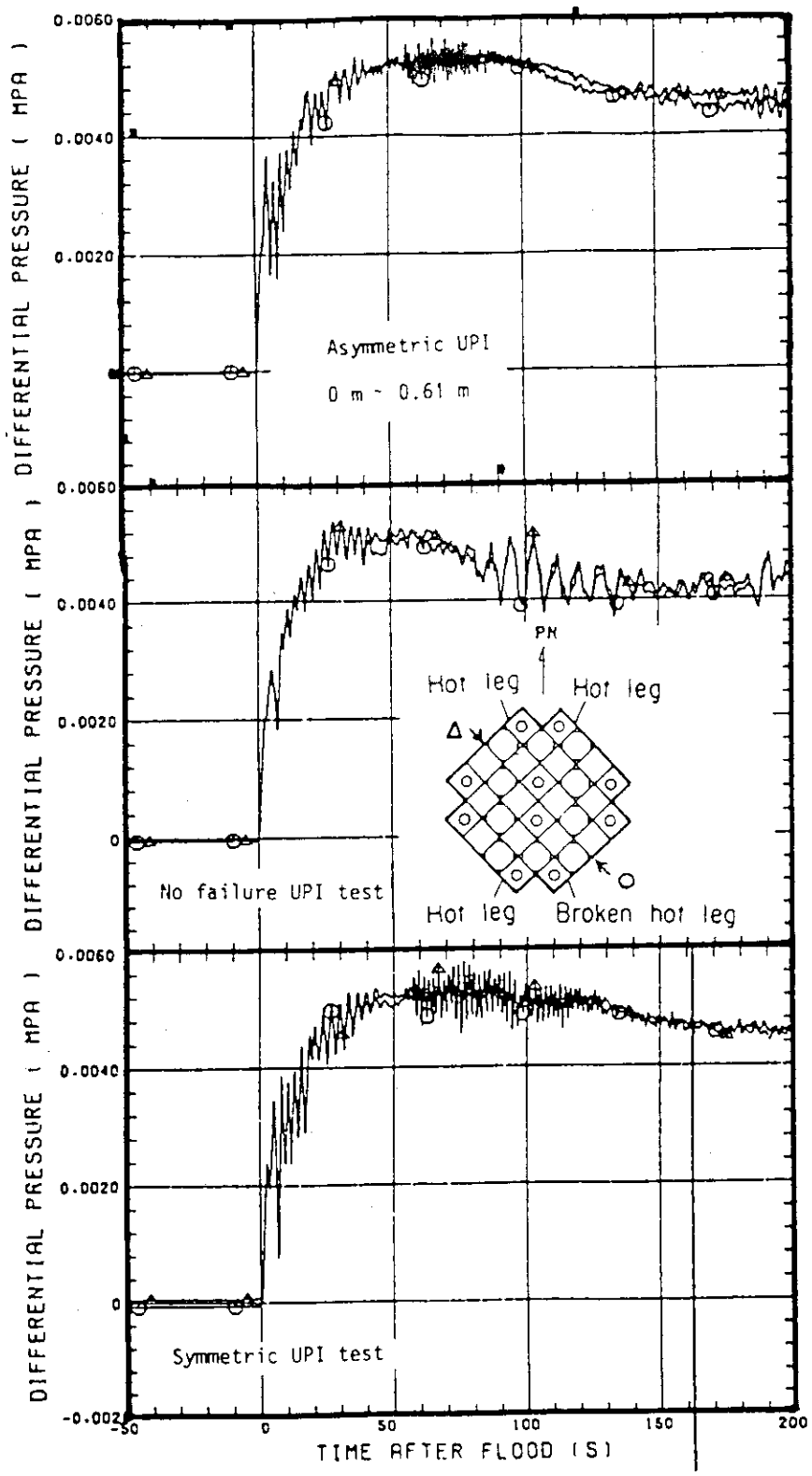

Fig. 4.7(1) Azimuthal distribution of core sectional differential pressure for lower core

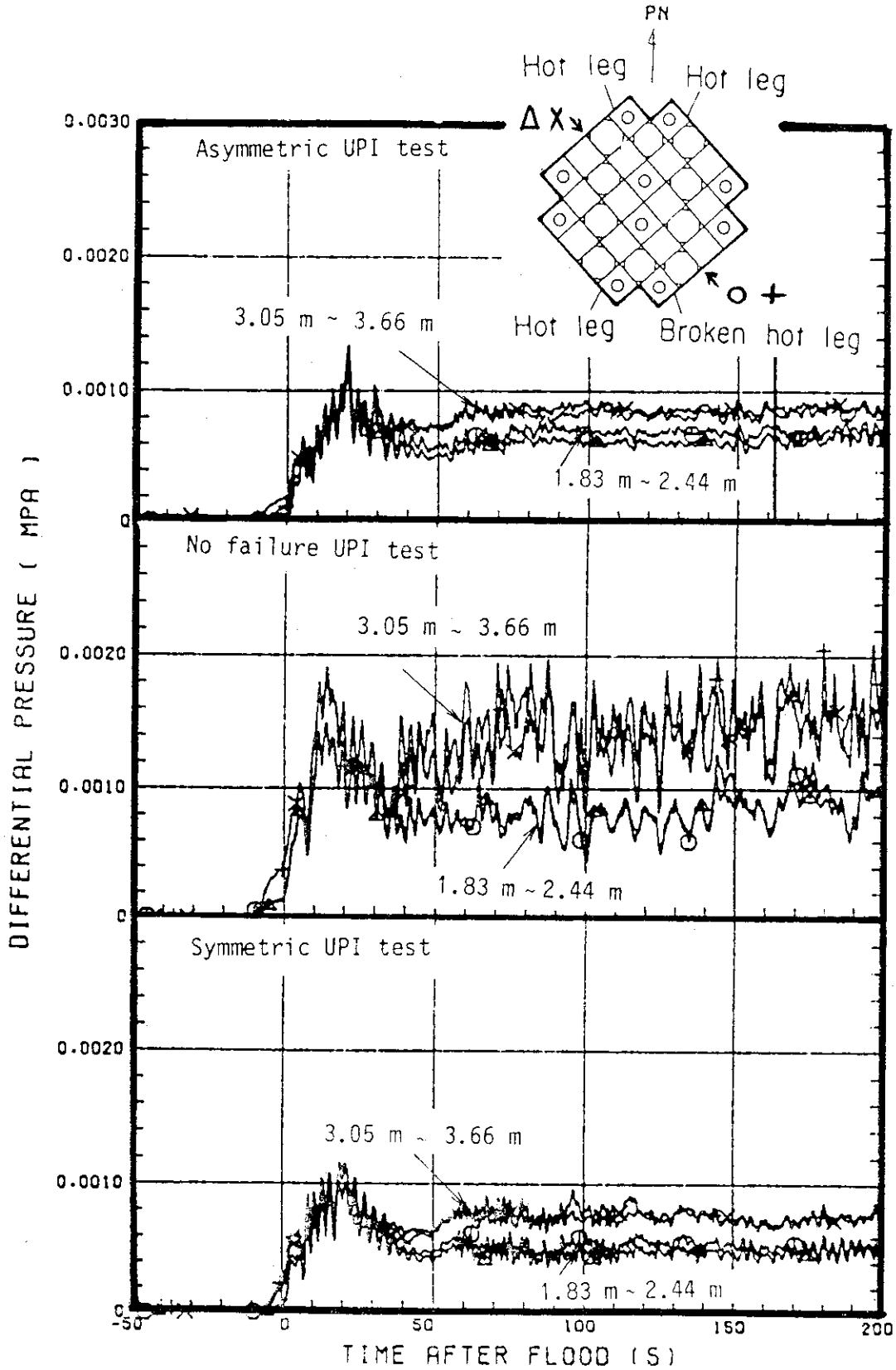

Fig. 4.7(2) Azimuthal distribution of core sectional differential pressure for upper core

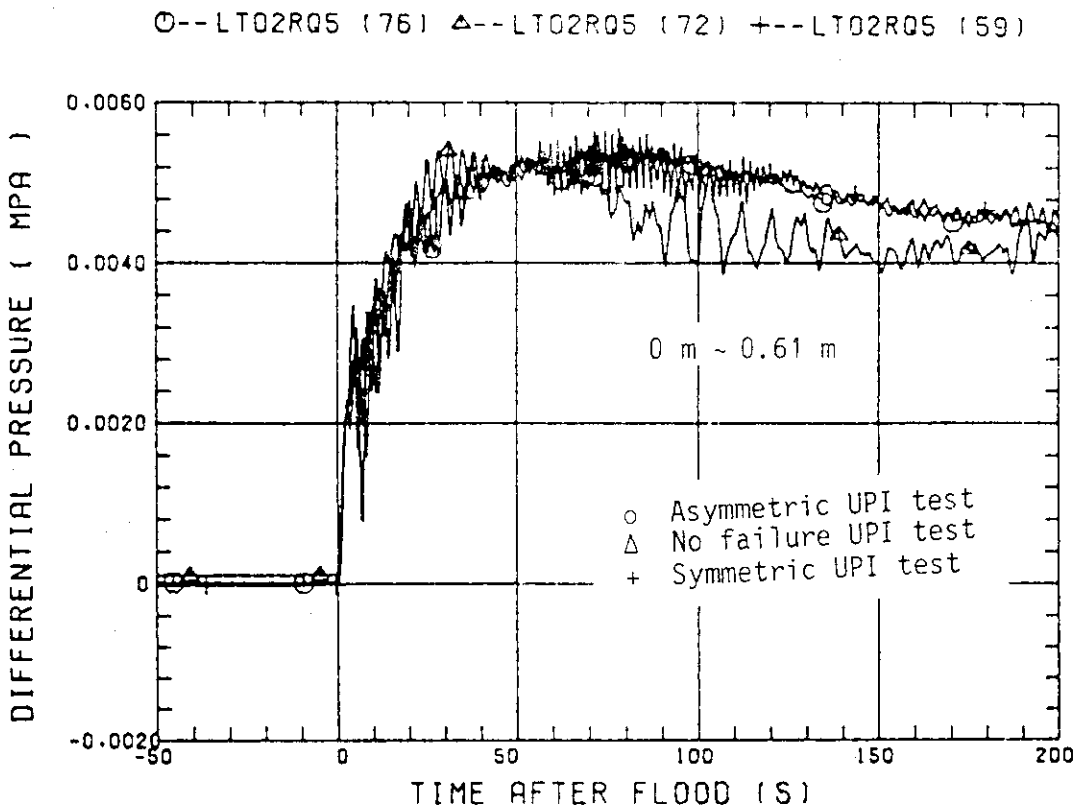

Fig. 4.8(1) Comparison of core sectional differential pressure (0 m ∿ 0.61 m)

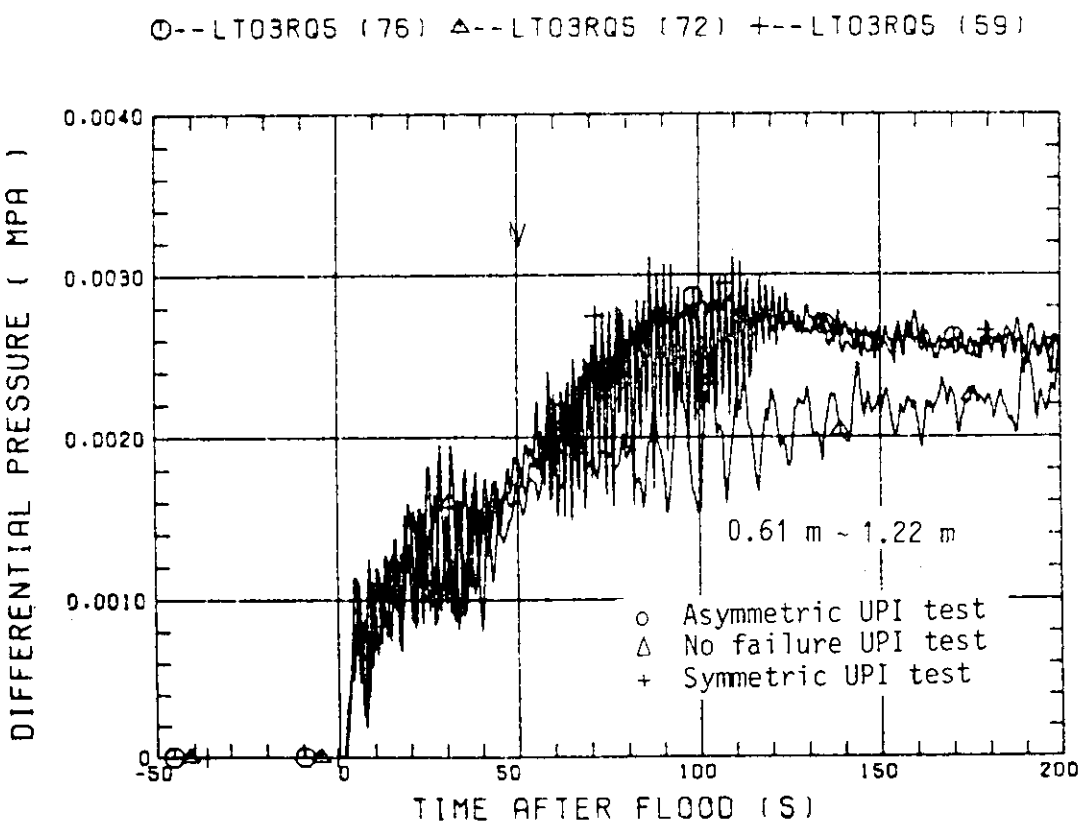

Fig. 4.8(2) Comparison of core sectional differential pressure (0.61 m ∿ 1.22 m)

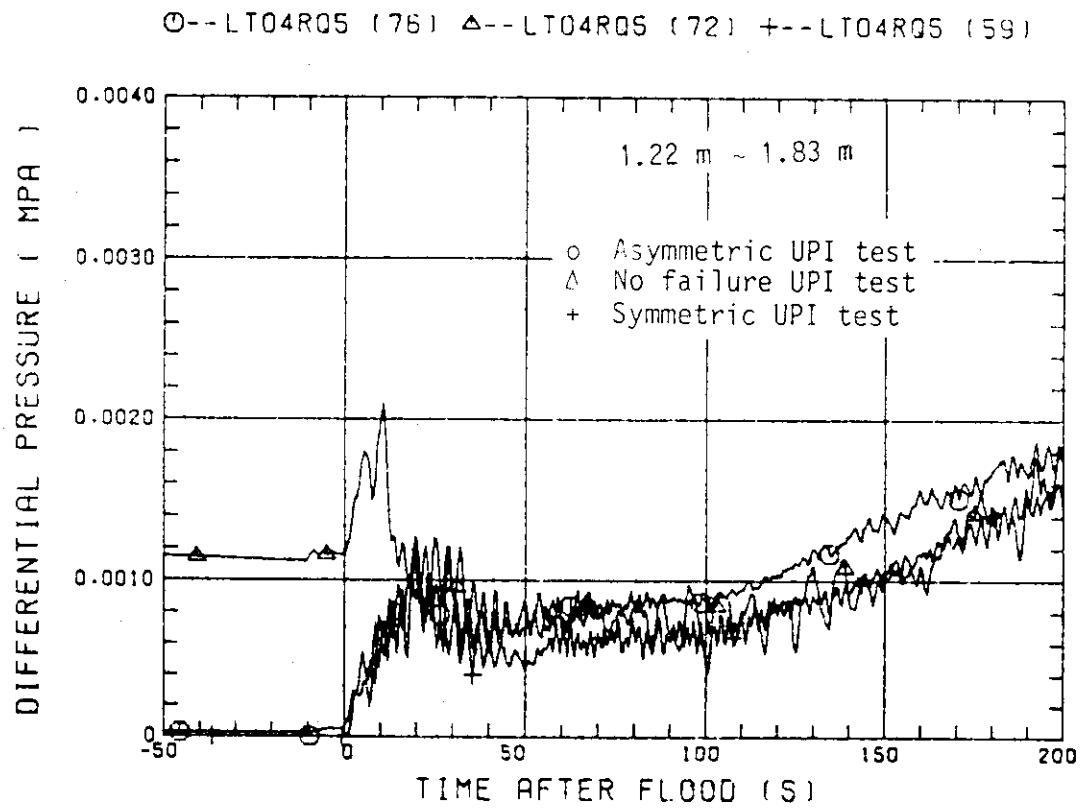

Fig. 4.8(3) Comparison of core sectional differential pressure (1.22 m∿1.83 m)

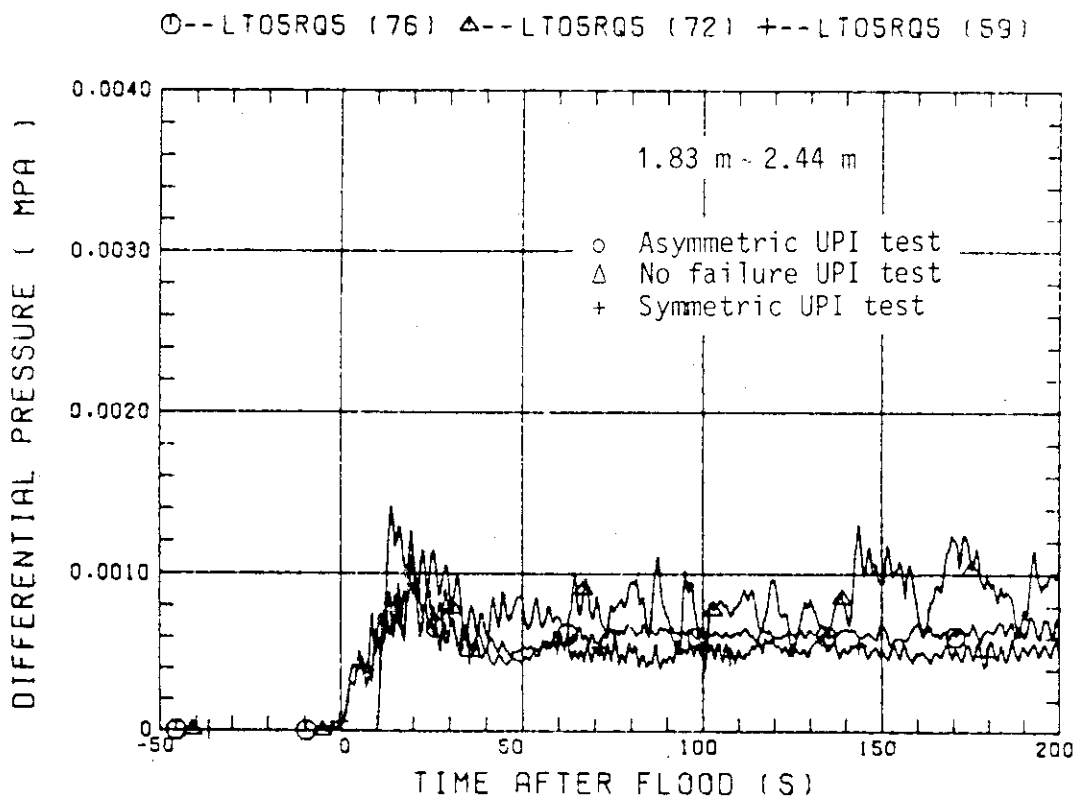

Fig. 4.8(4) Comparison of core sectional differential pressure (1.83 m∿2.44 m)

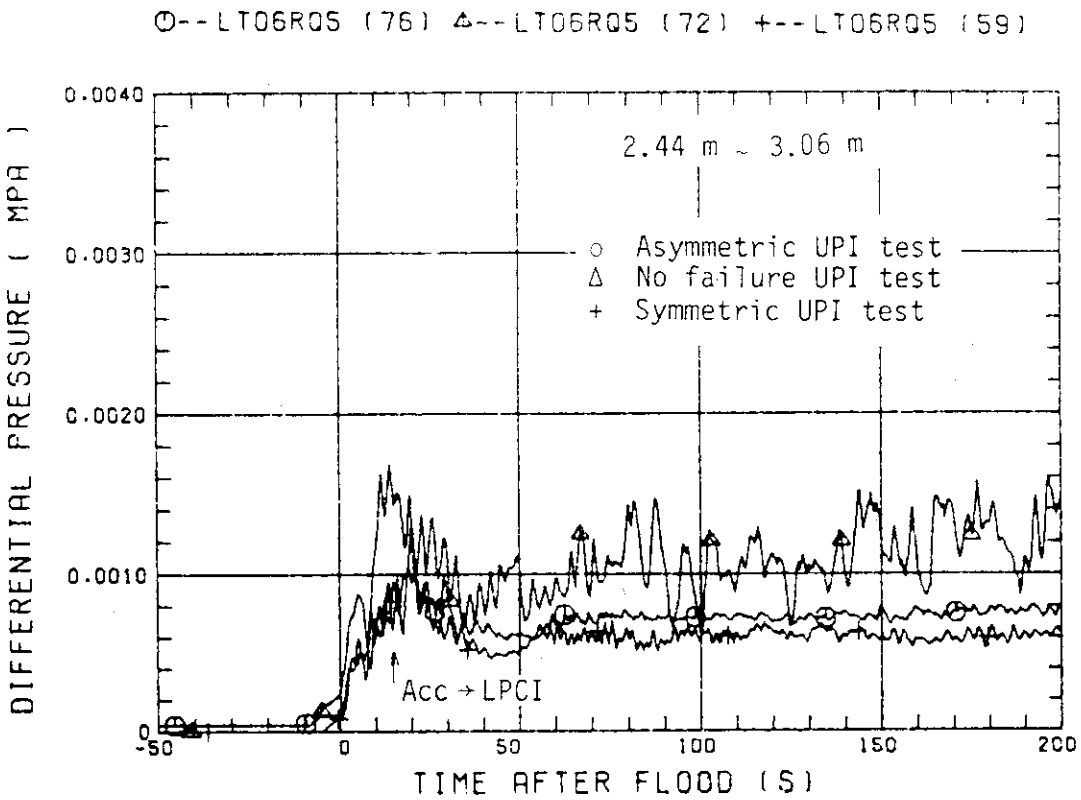

Fig. 4.8(5) Comparison of core sectional differential pressure (2.44 m ∿ 3.06 m)

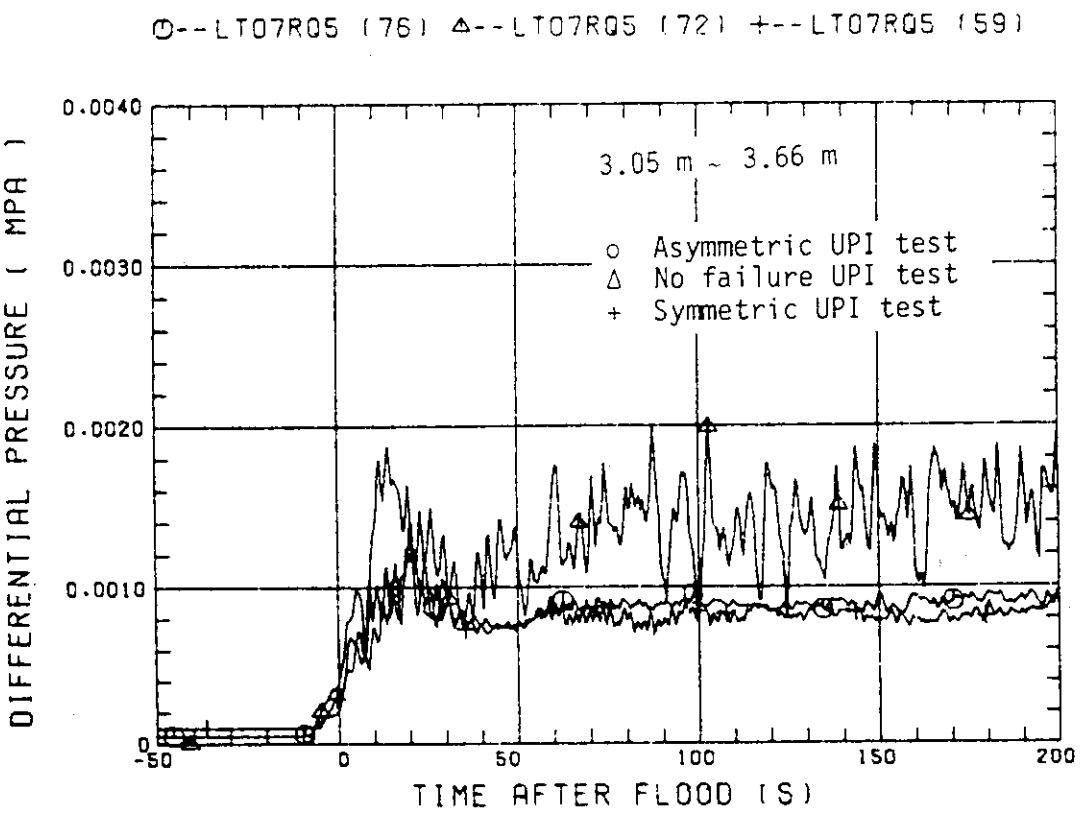

Fig. 4.8(6) Comparison of core sectional differential pressure

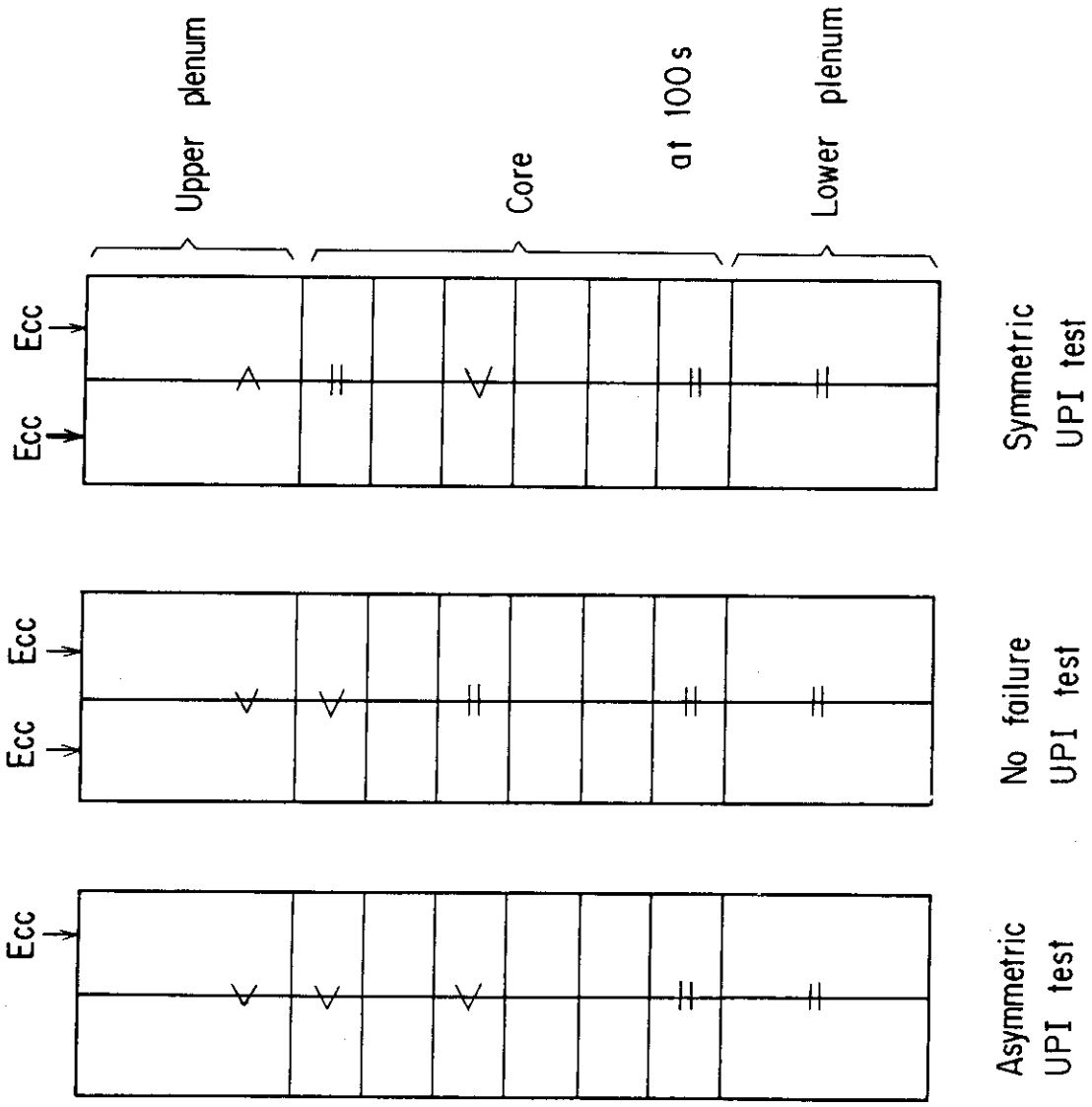

Fig. 4.9 Overall azimuthal distribution of the differential pressure

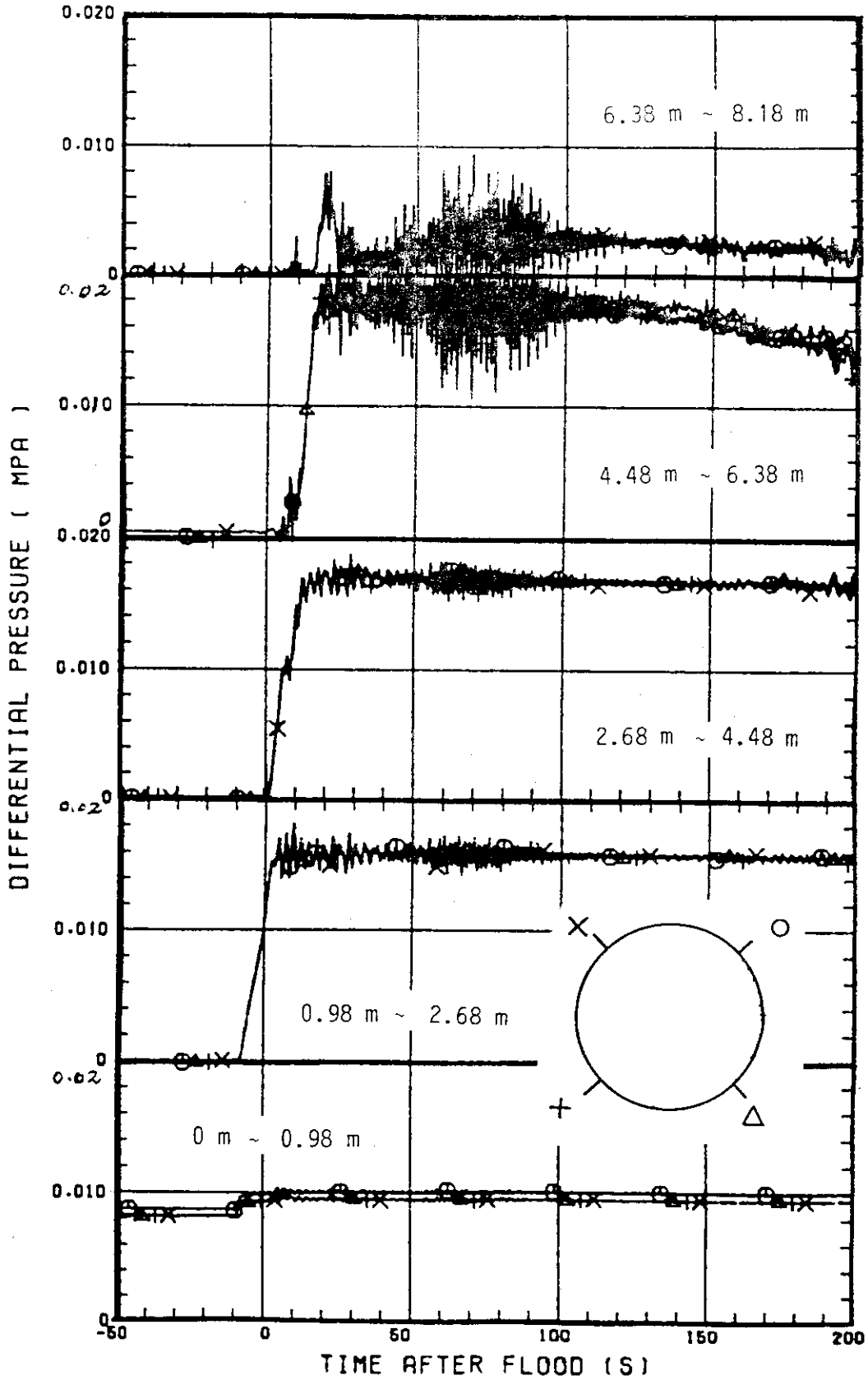

Fig. 4.10 Azimuthal distribution of the downcomer sectional differential pressure

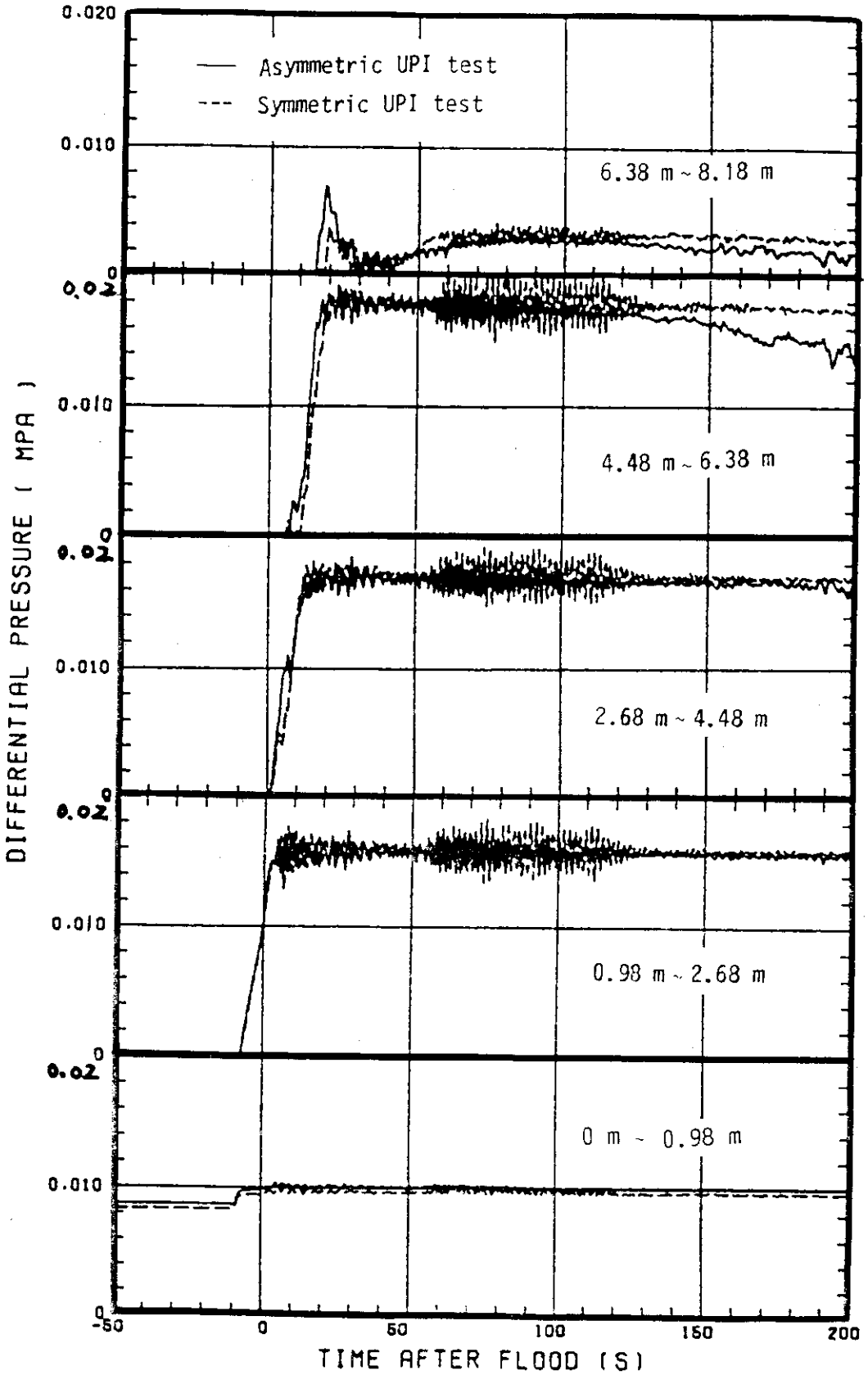

Fig. 4.11 Comparison of downcomer differential pressure

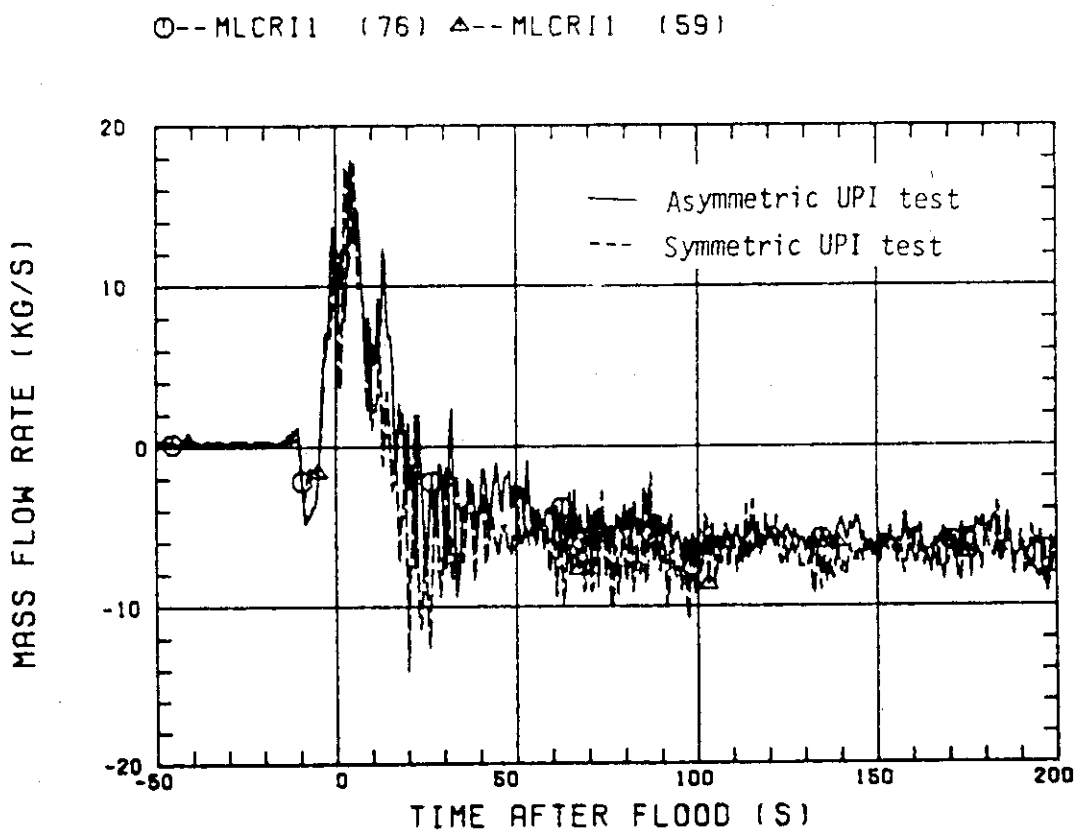

Fig. 4.12 Core inlet mass flow rate

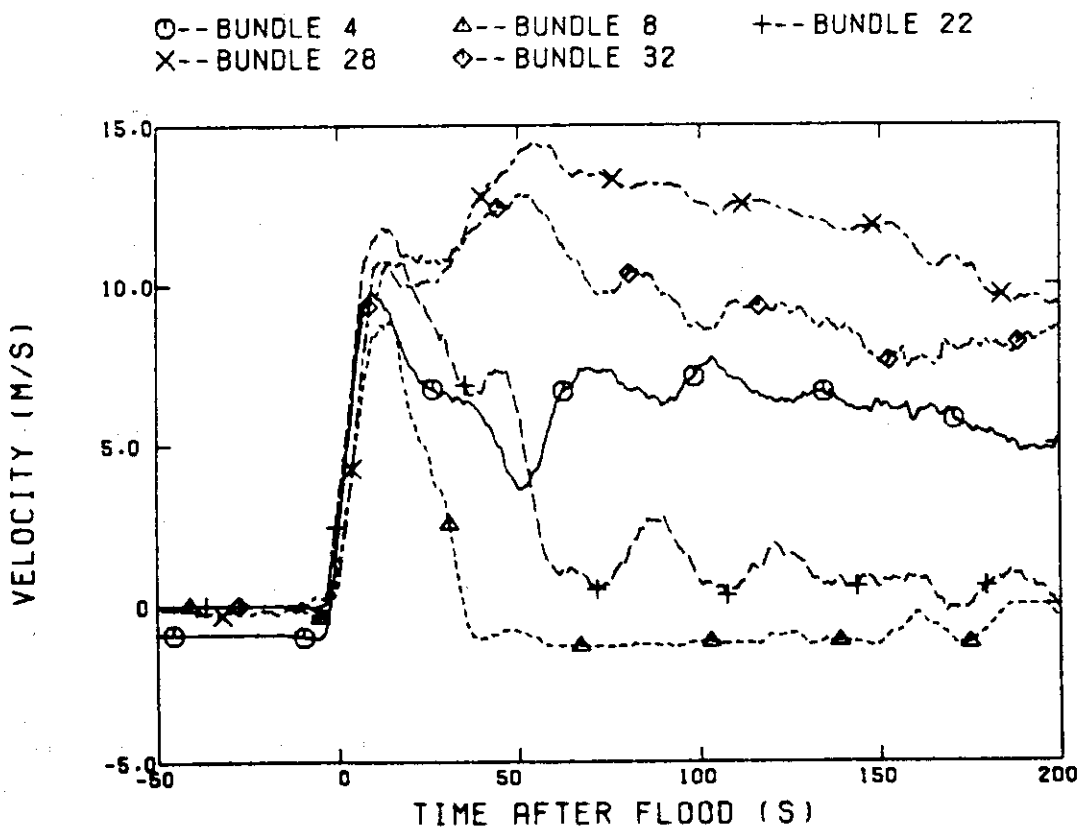

Fig. 4.13 Fluid flow measured with turbine meters located at end box

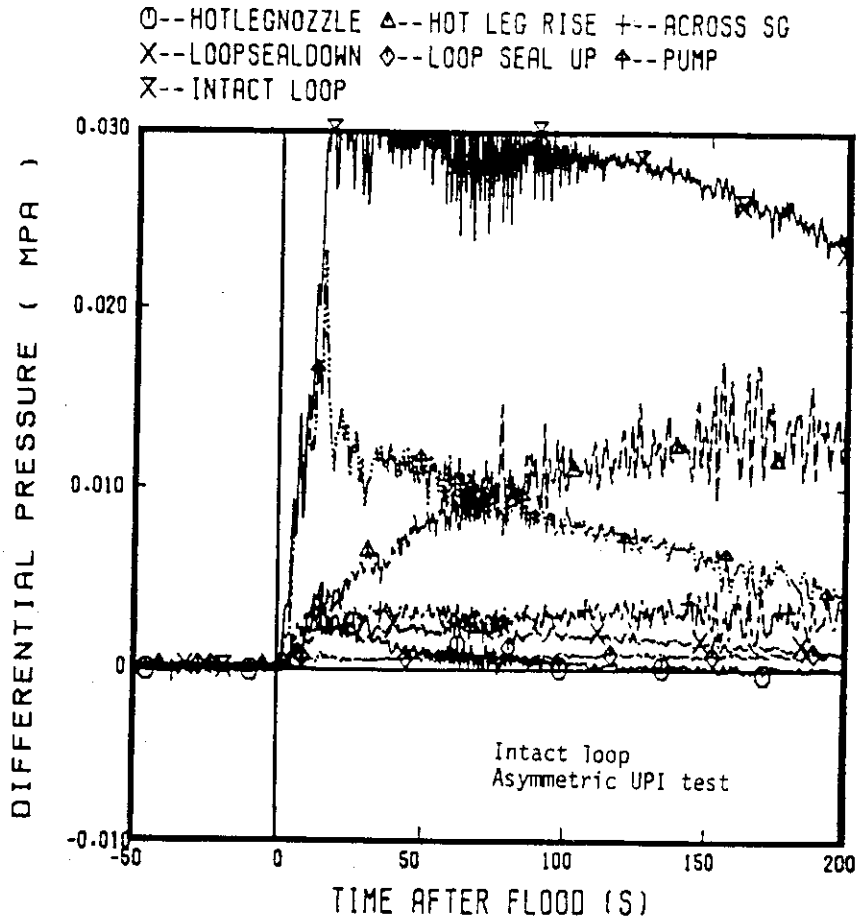

Fig. 4.14 Differential pressure through various parts of intact loops

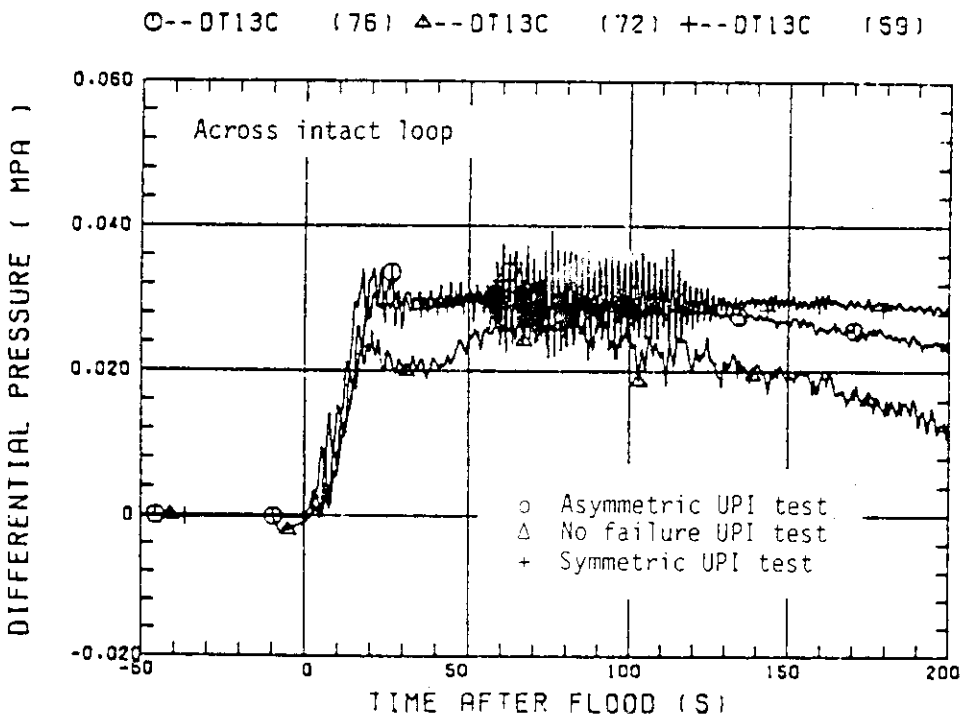

Fig. 4.15(1) Comparison of the differential pressure across intact loop

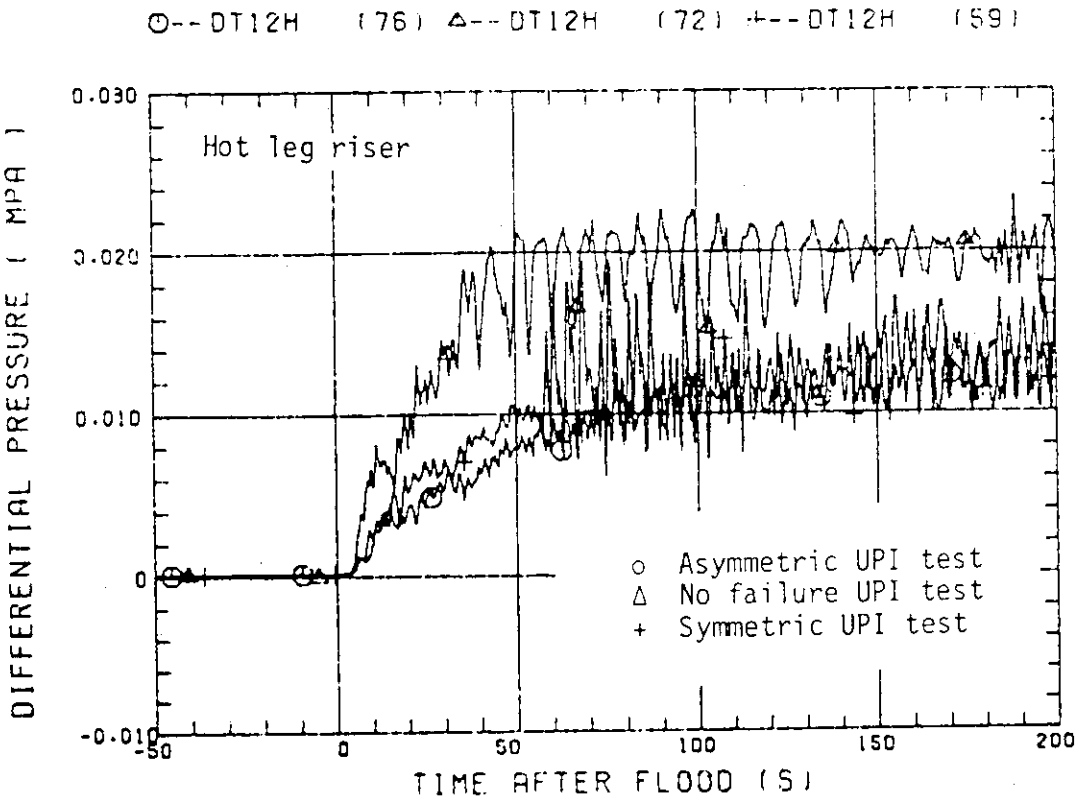

Fig. 4.15(2)

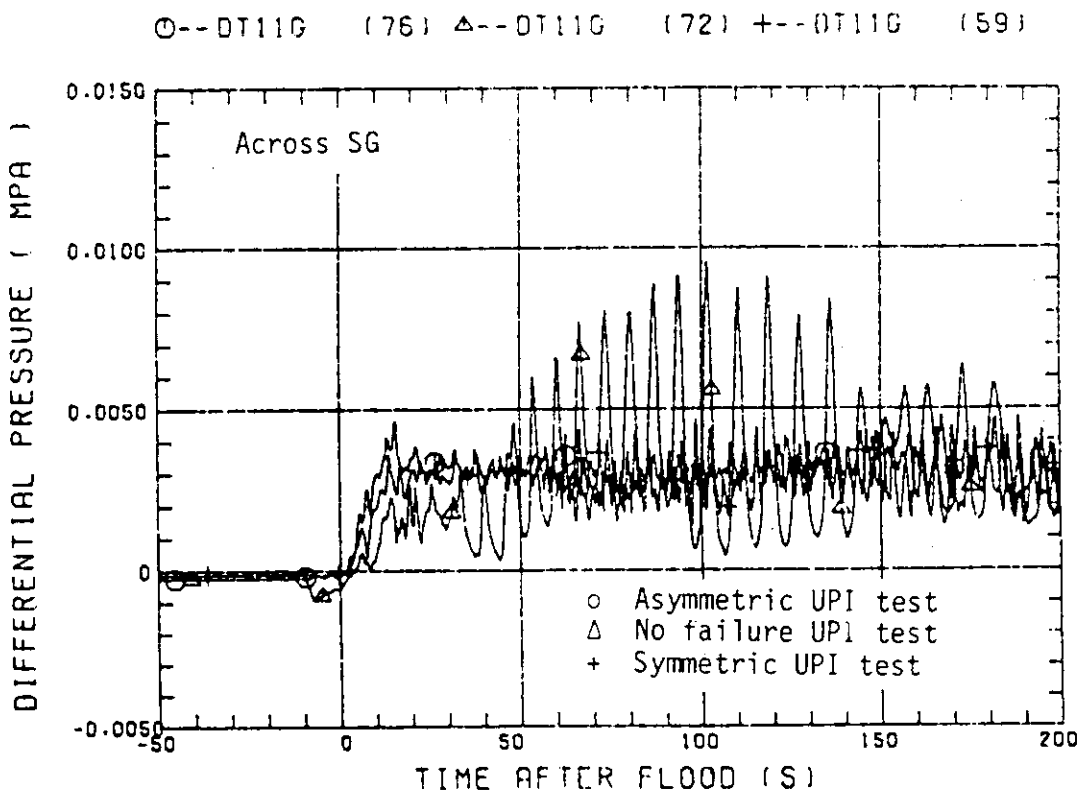

Fig. 4.15(3)

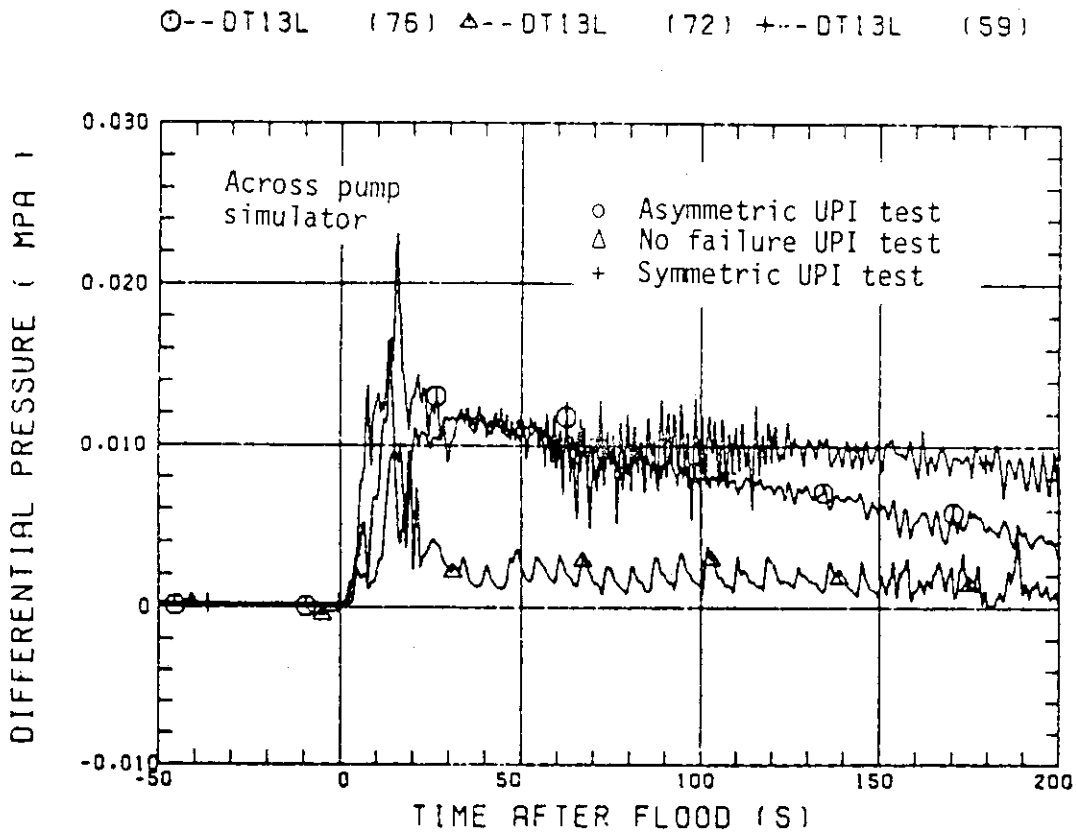
⊙--DT13L (76) △--DT13L (72) +--DT13L (59)
Across pump simulator
○ Asymmetric UPI test
△ No failure UPI test
+ Symmetric UPI test
DIFFERENTIAL PRESSURE (MPA)
0.030
0.020
0.010
0
-0.010
-50
0
50
100
150
200
TIME AFTER FLOOD (S)

Fig. 4.15(4)

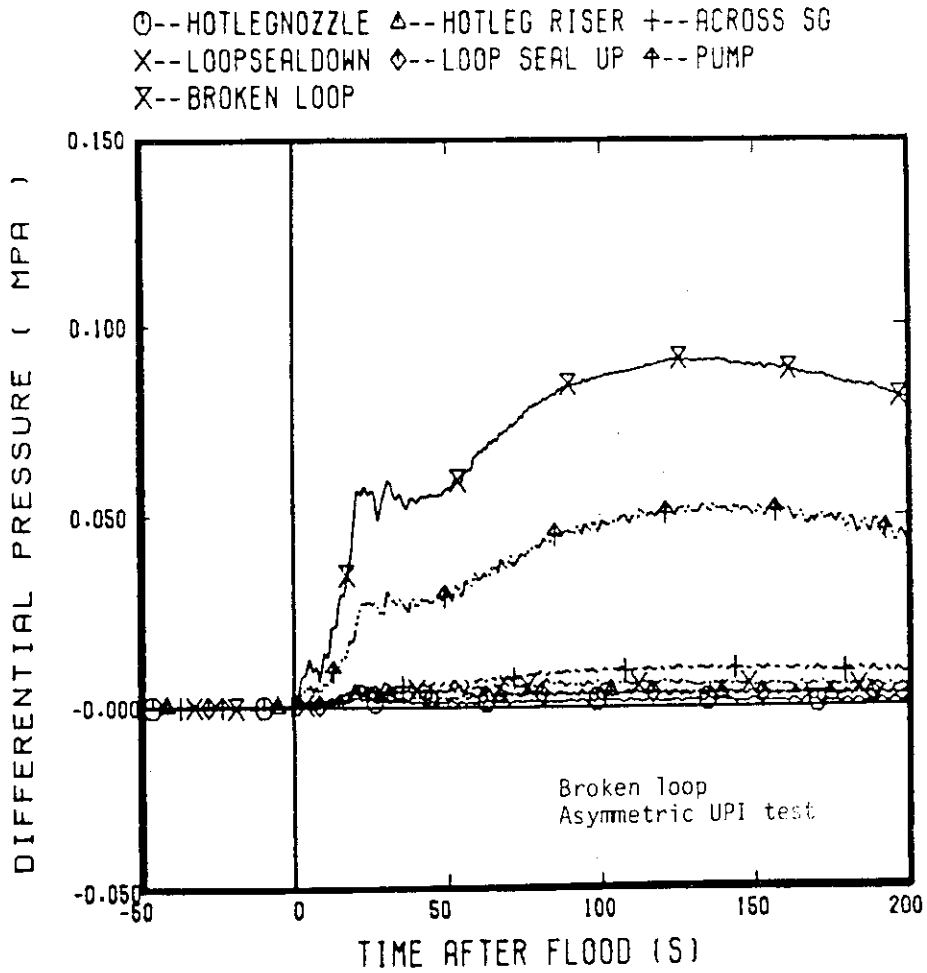

Fig. 4.16(1) Comparison of the differential pressure across the broken loop SG side

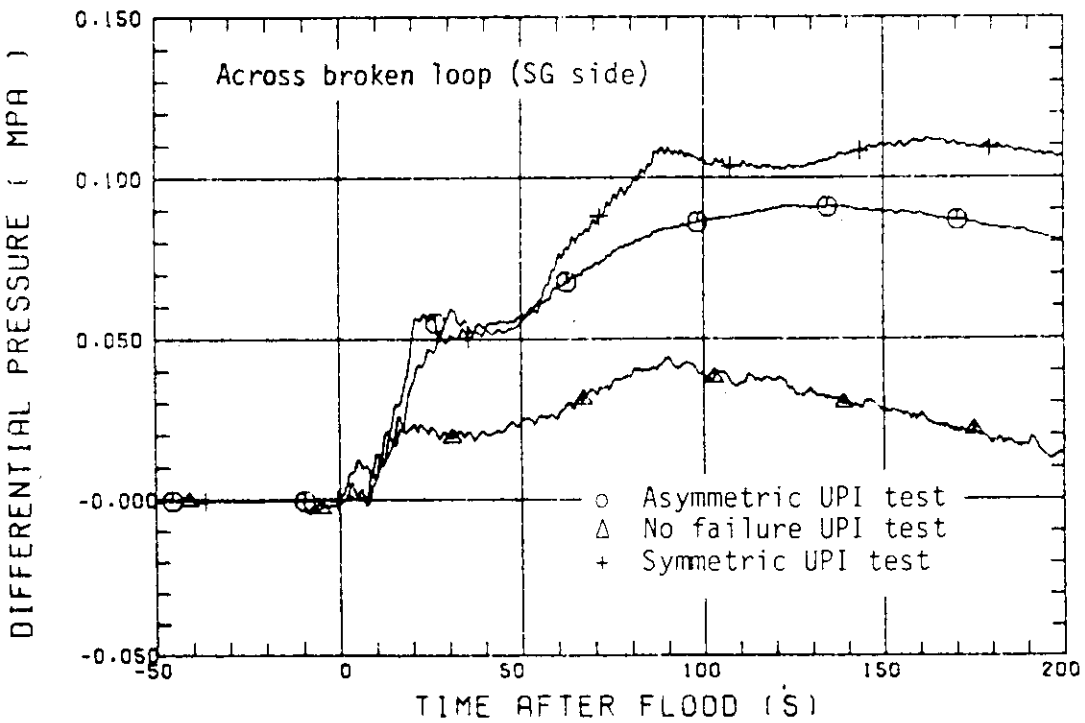

Fig. 4.16(2)

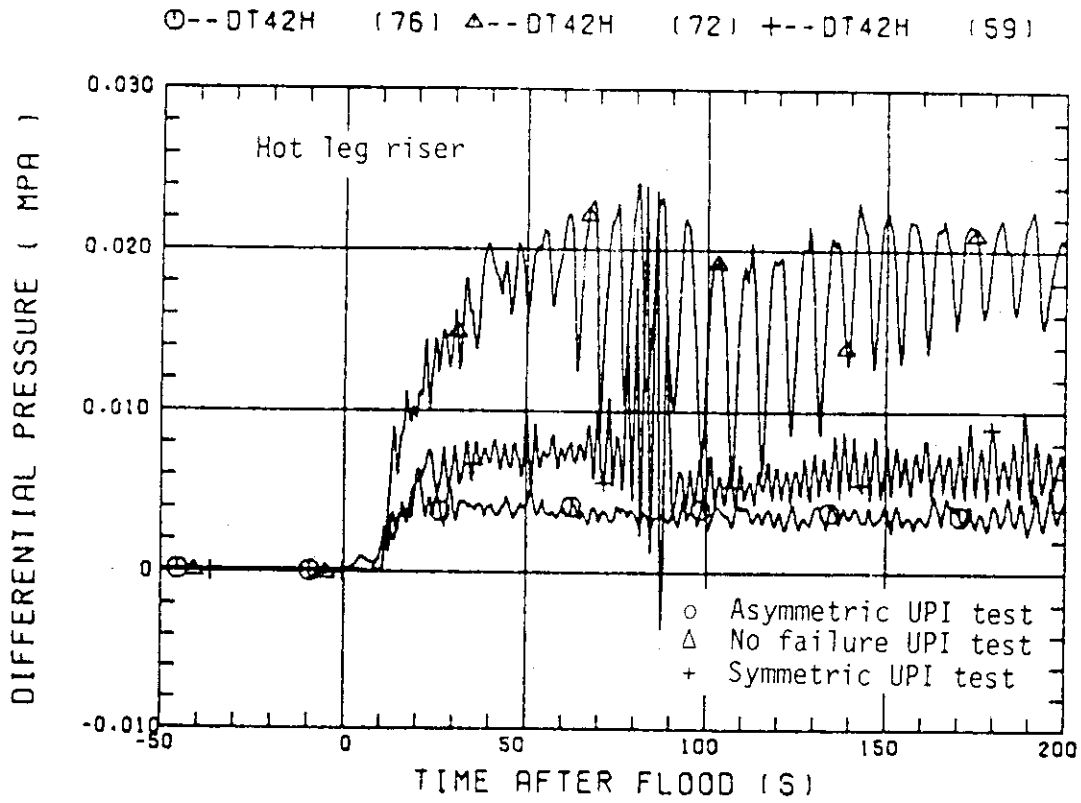

Fig. 4.16(3)

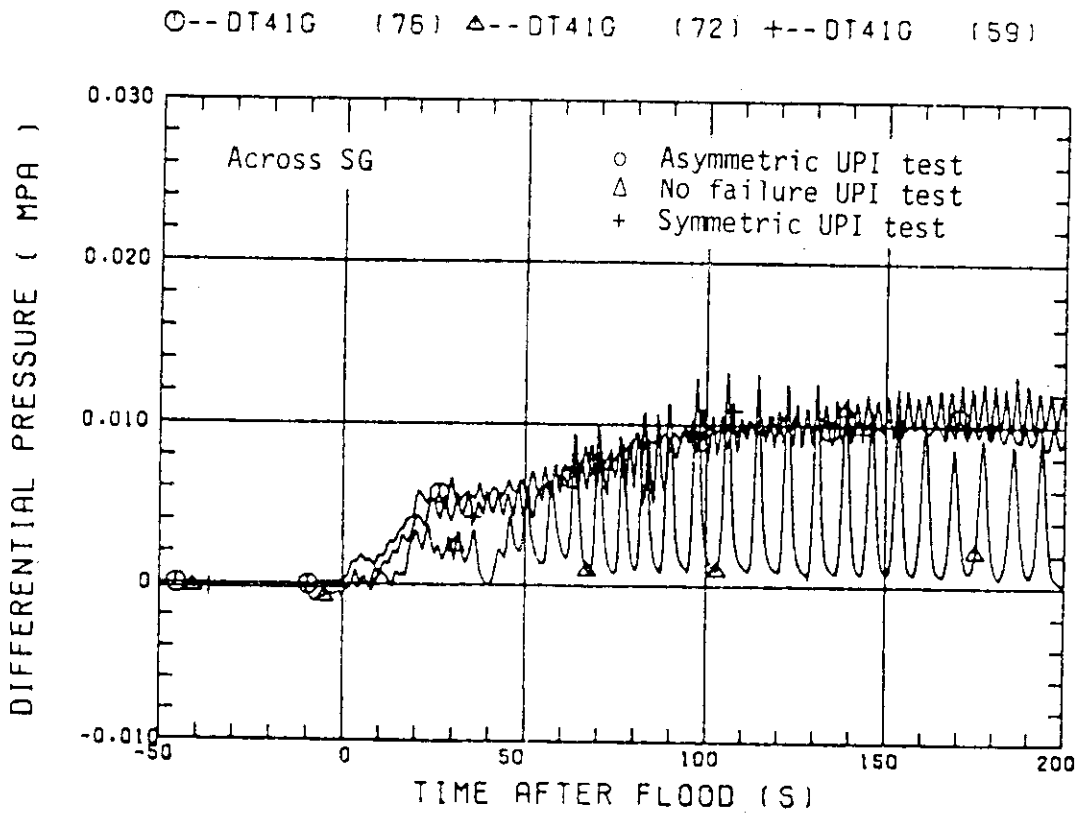

Fig. 4.16(4)

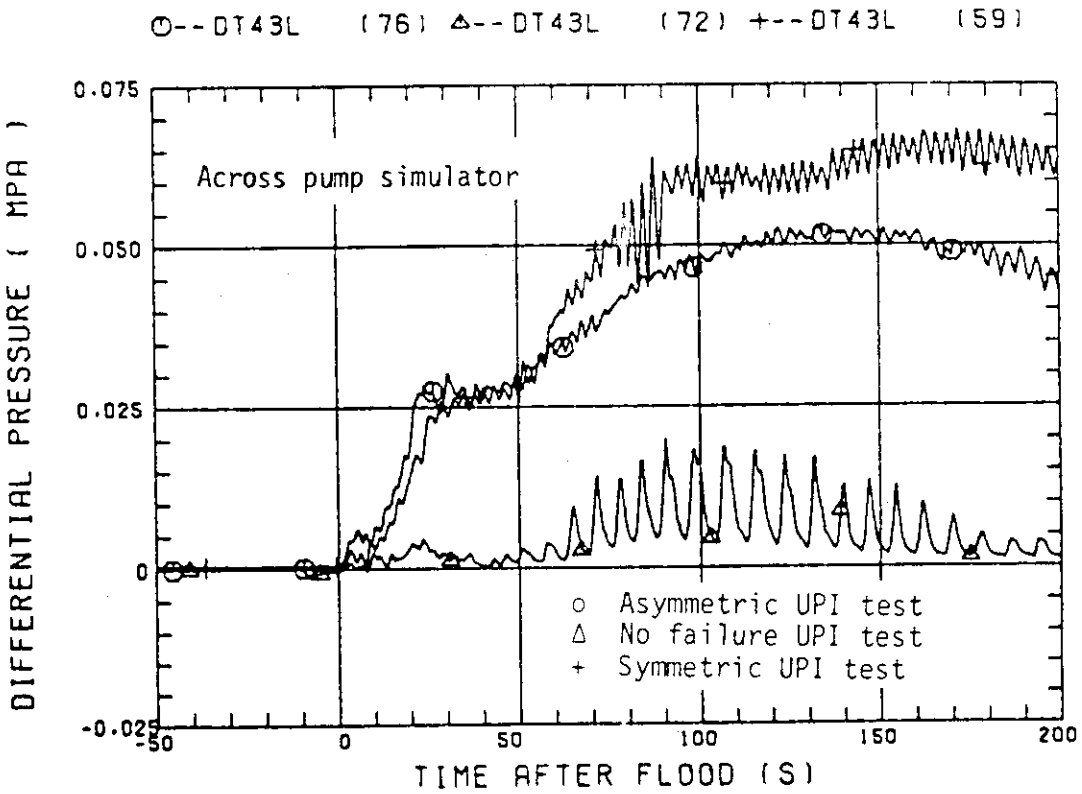

Fig. 4.16(5)

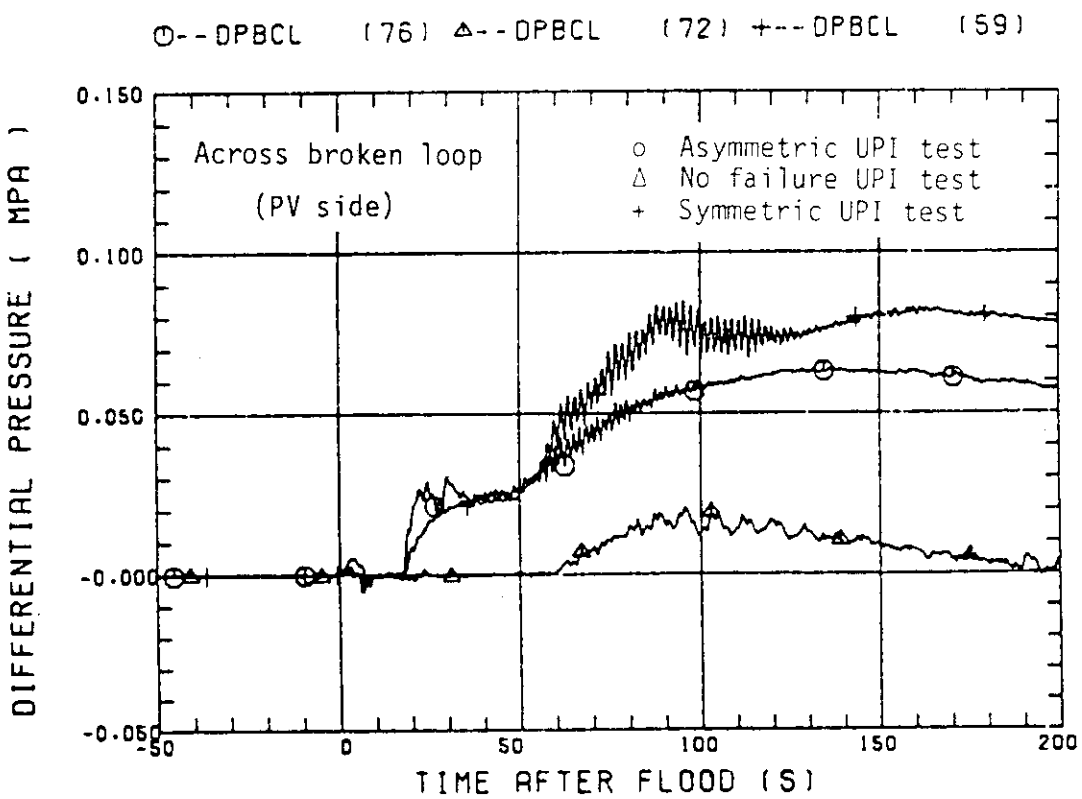

Fig. 4.17 Comparison of the differential pressure across the broken loop downcomer side

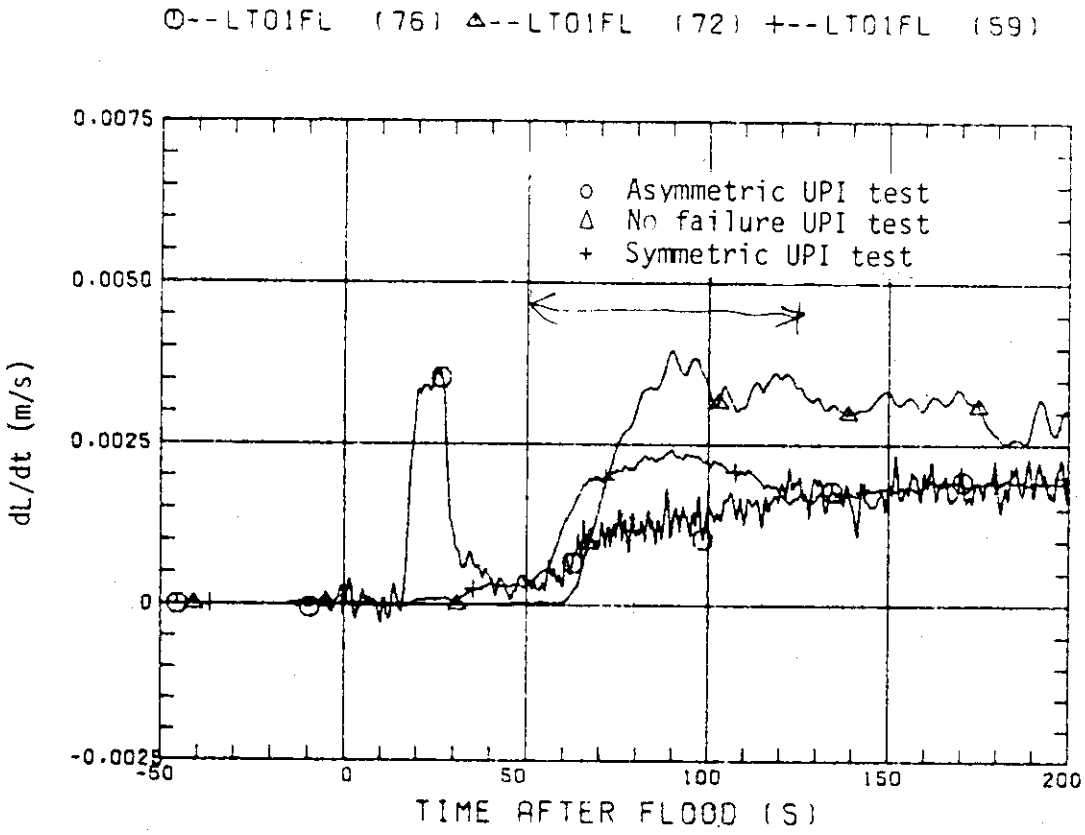

Fig. 4.18 Overflowing mass from the downcomer

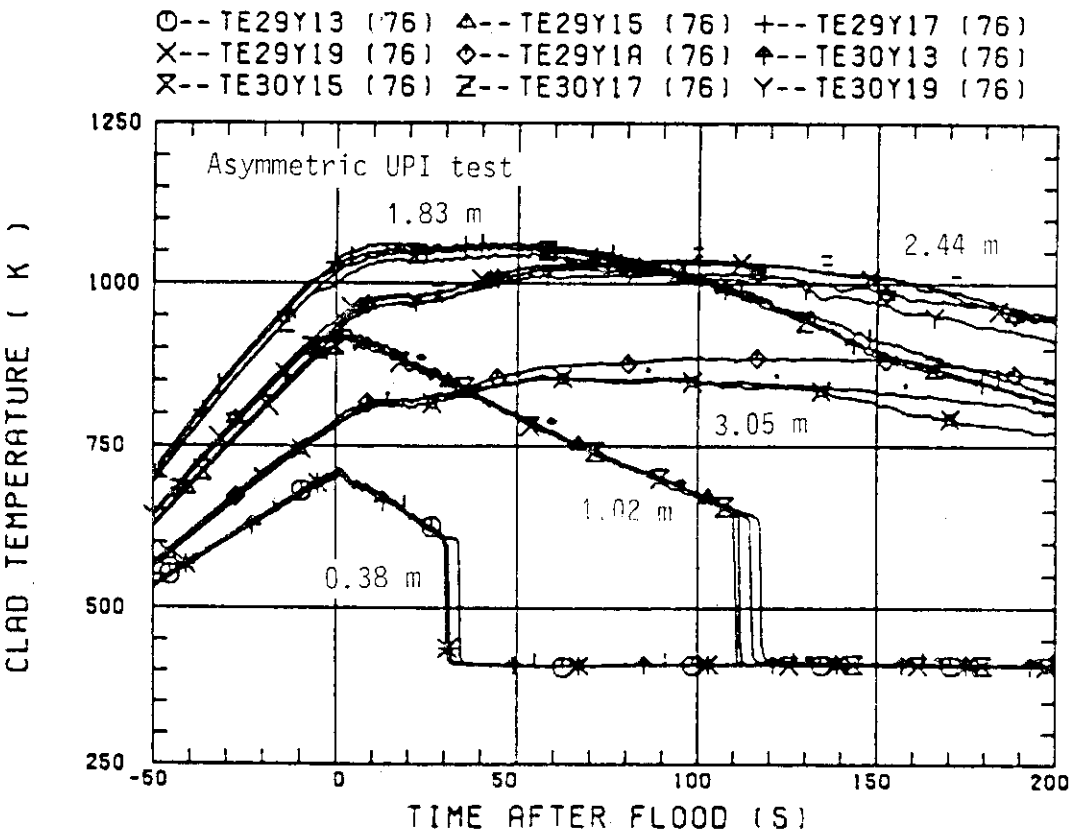

Fig. 4.19(1) Clad temperature in the high power region

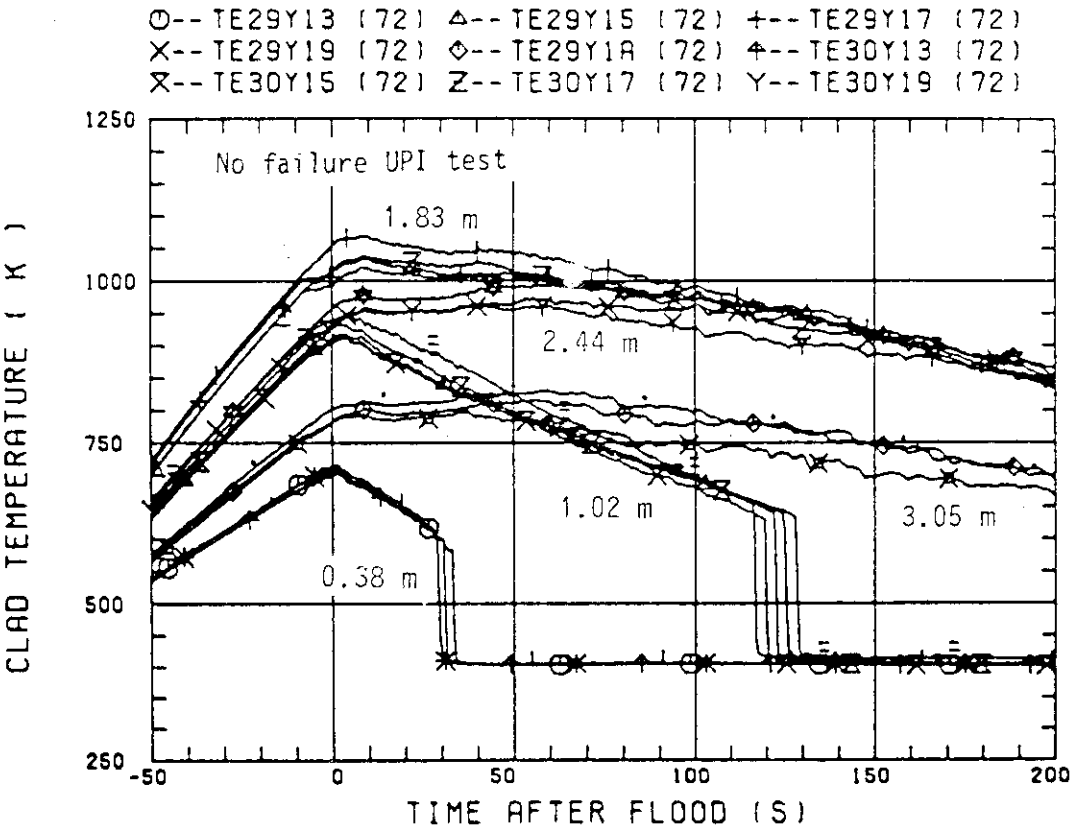

Fig. 4.19(2)

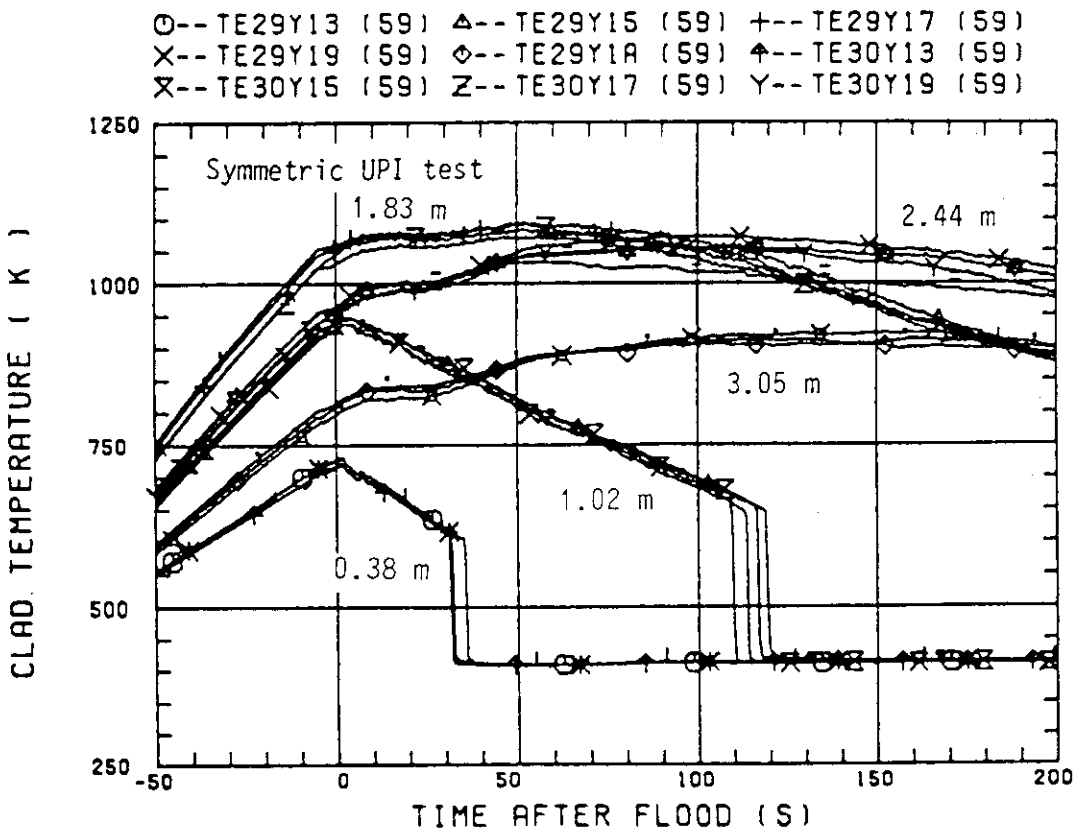

Fig. 4.19(3)

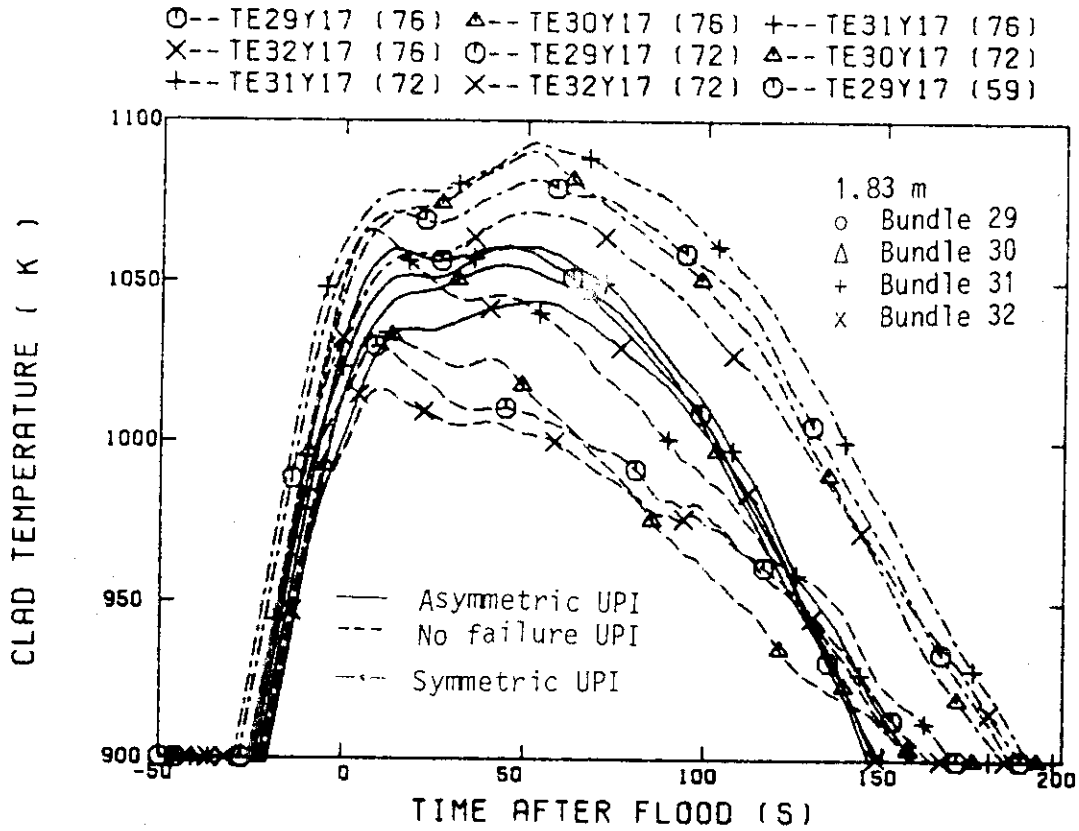

Fig. 4.19(4)

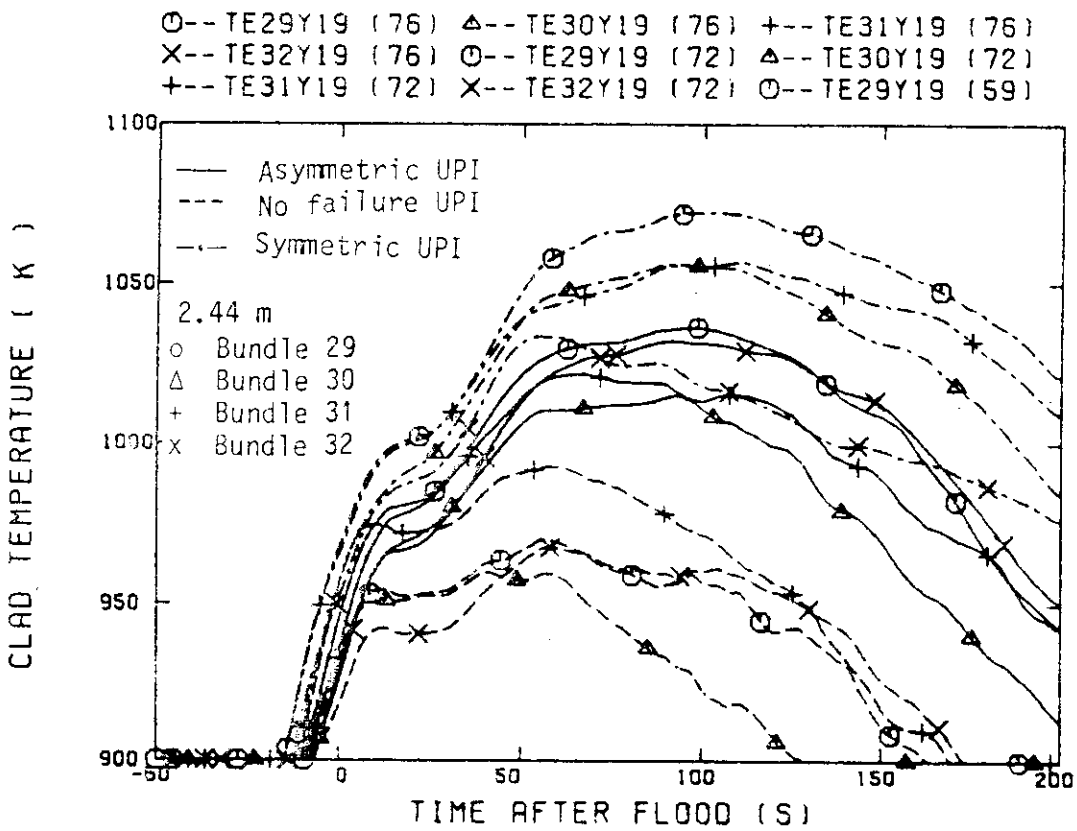

Fig. 4.19(5)

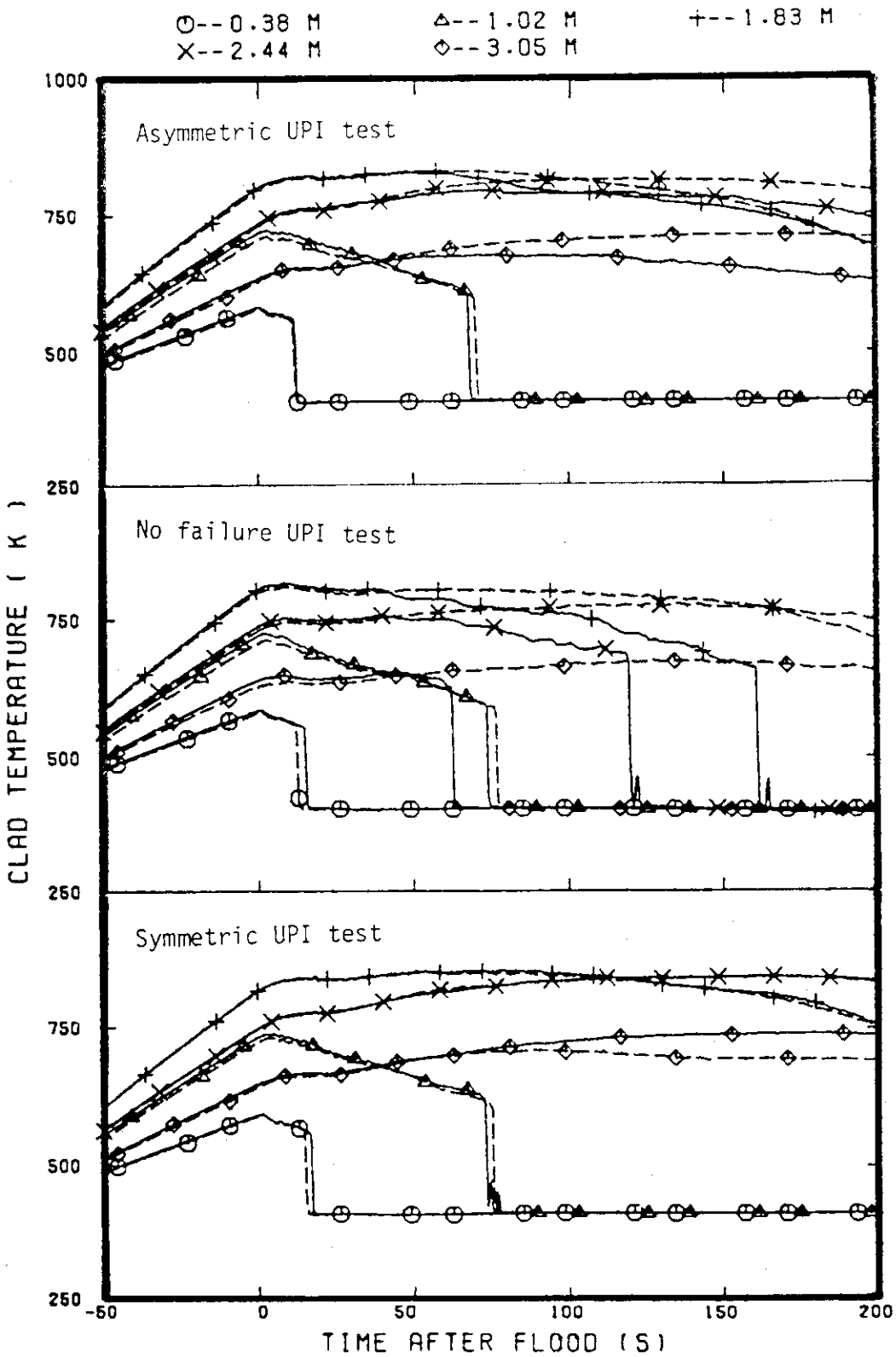

Fig. 4.20 Clad temperature in the low power region

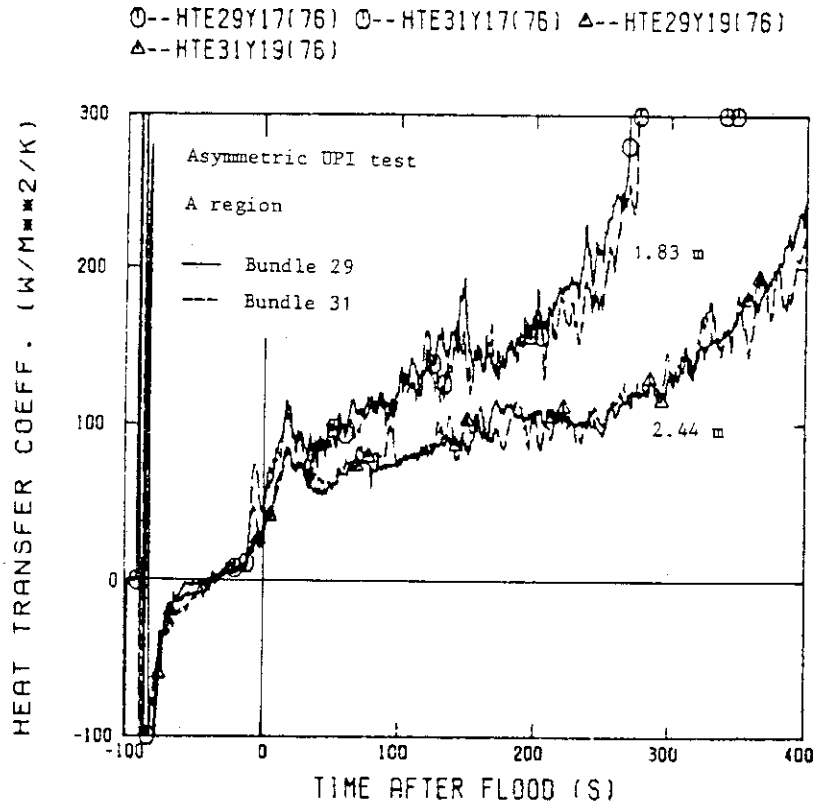

Fig. 4.21(1) Uniformity of heat transfer coefficient for high power rod

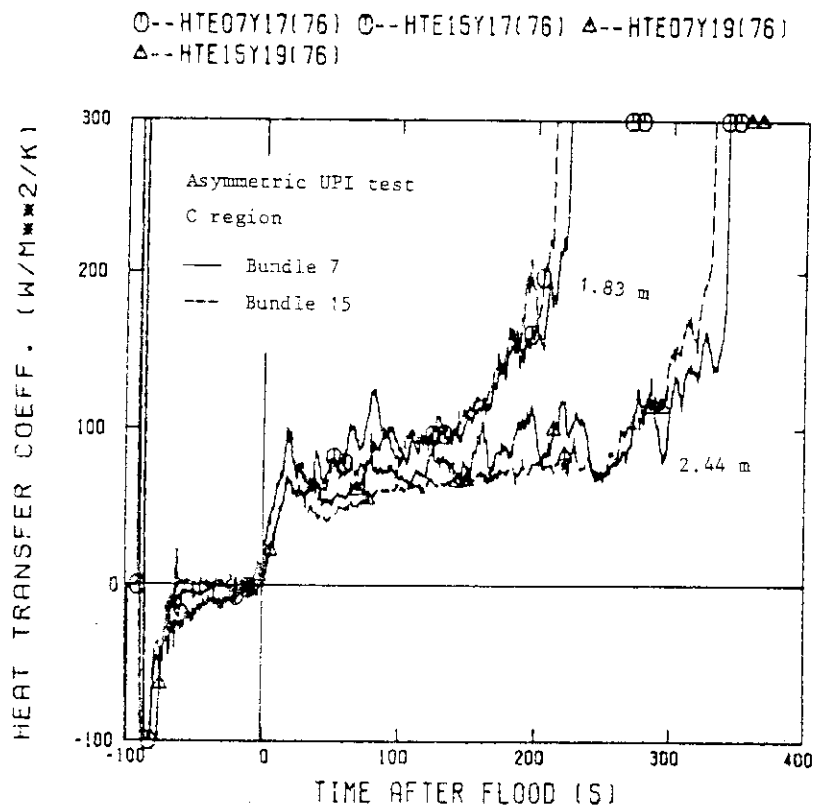

Fig. 4.21 (2) Uniformity of heat transfer coefficient for low power rod

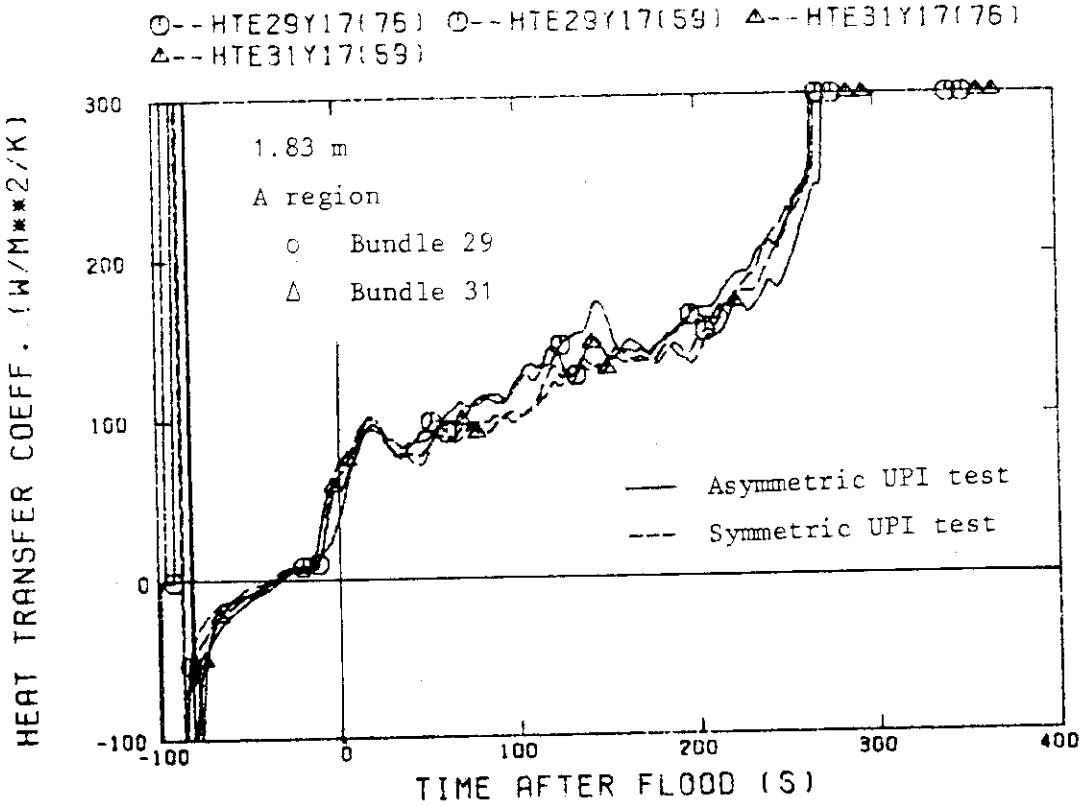

Fig. 4.22(1) Comparison of heat transfer coefficient between the present asymmetric UPI test and the relatively symmetric UPI test C2-AS1 (Run 59)

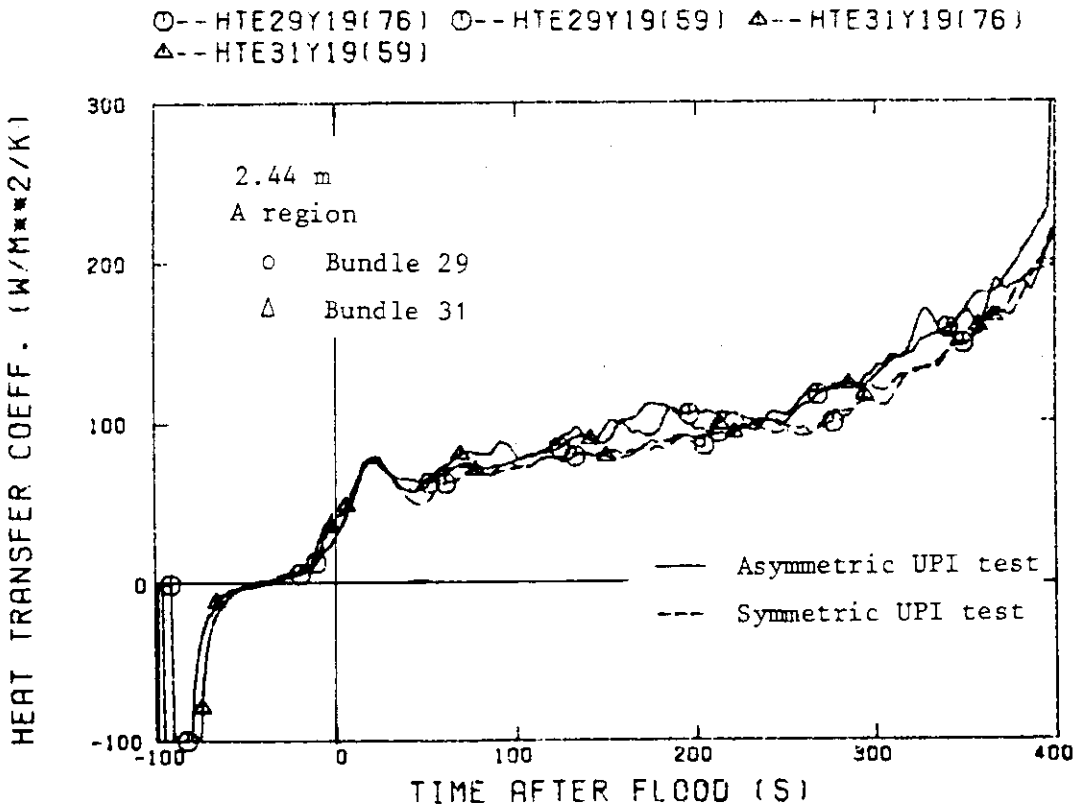

Fig. 4.22(2)

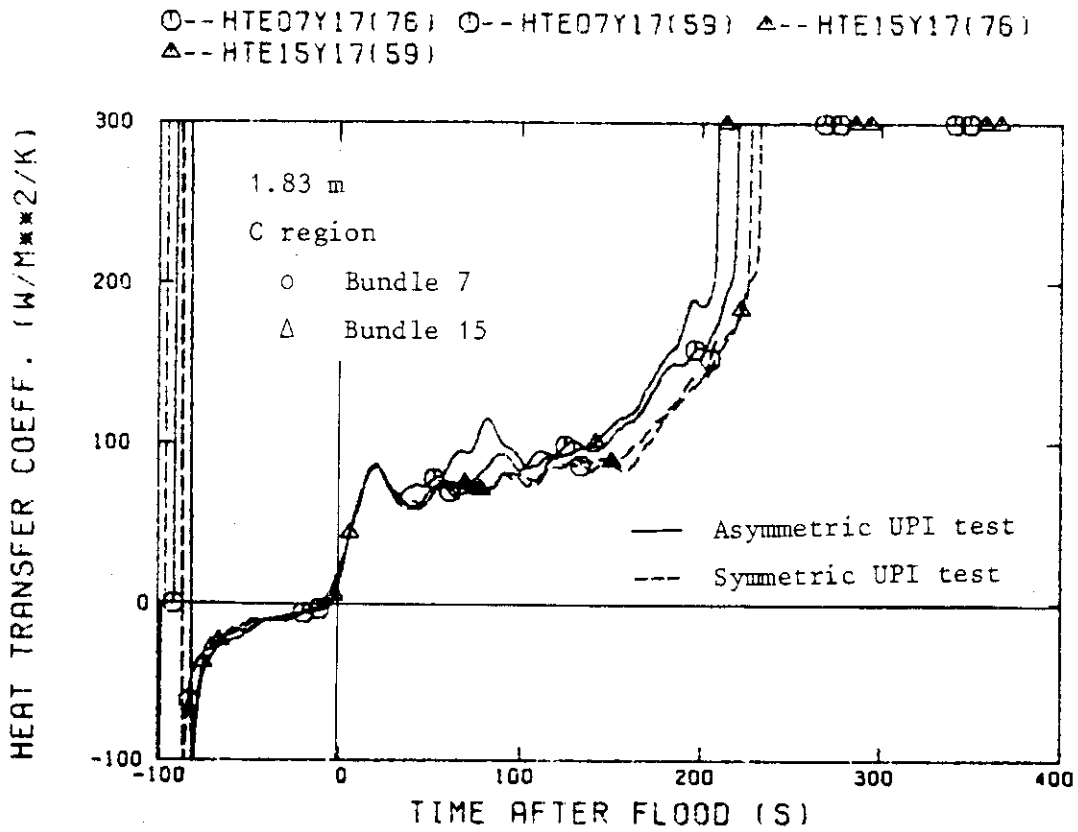

Fig. 4.22(3)

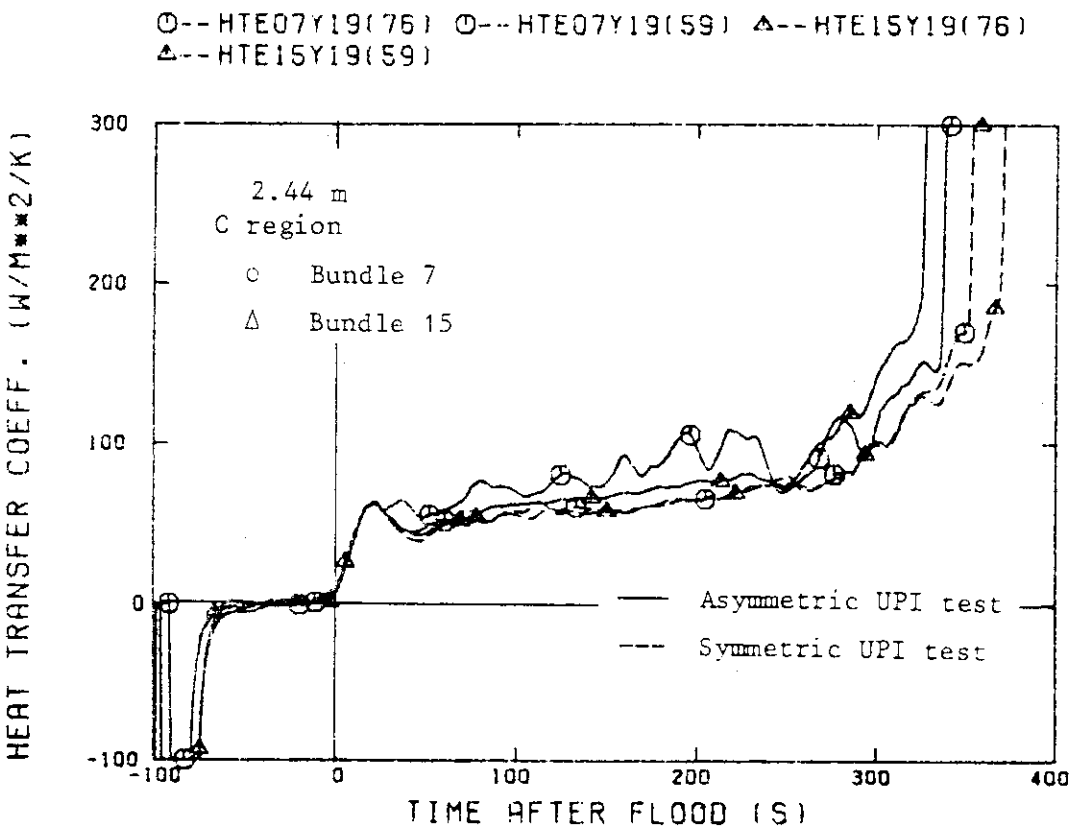

Fig. 4.22(4)

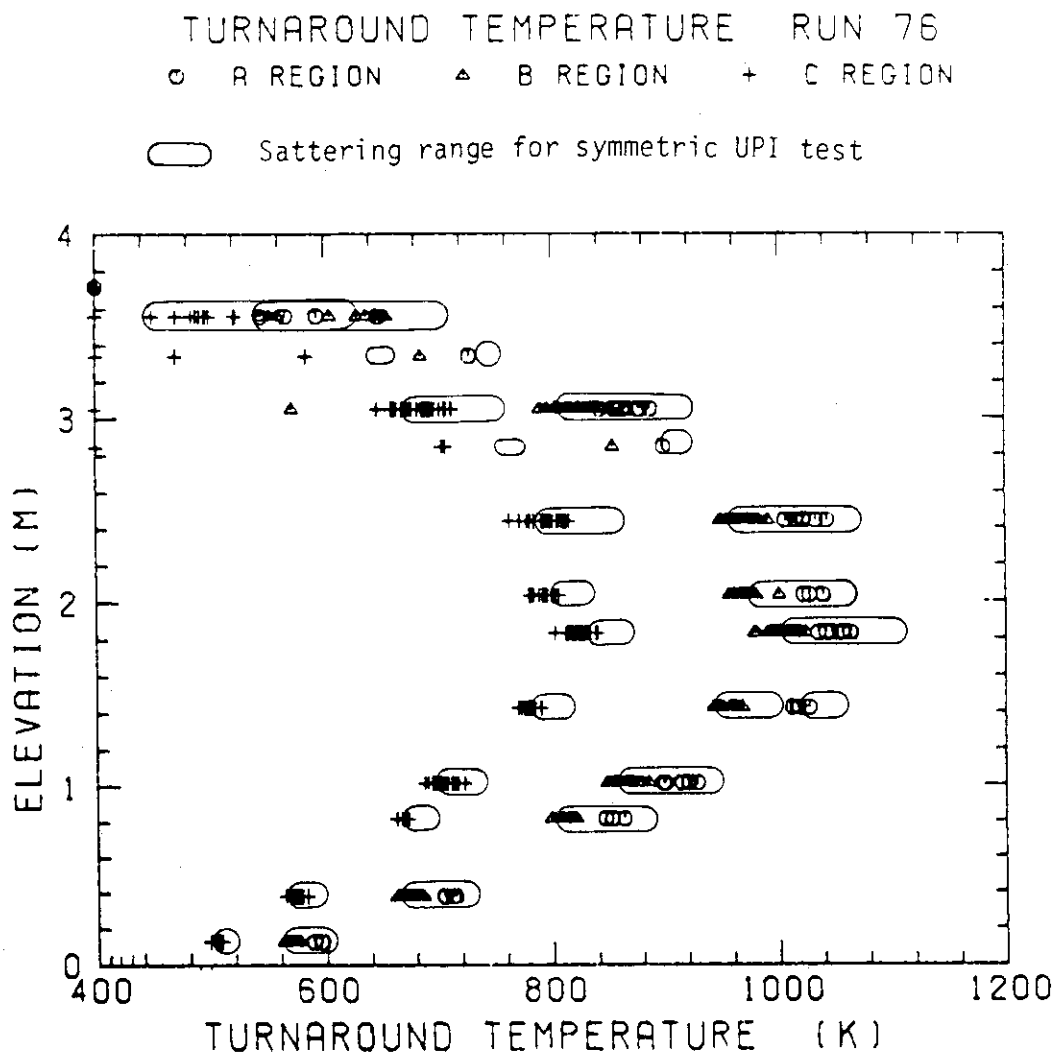

Fig. 4.23 Comparison of turnaround temperature between the present asymmetric UPI test and the relatively symmetric UPI test C2-AS1 (Run 59)

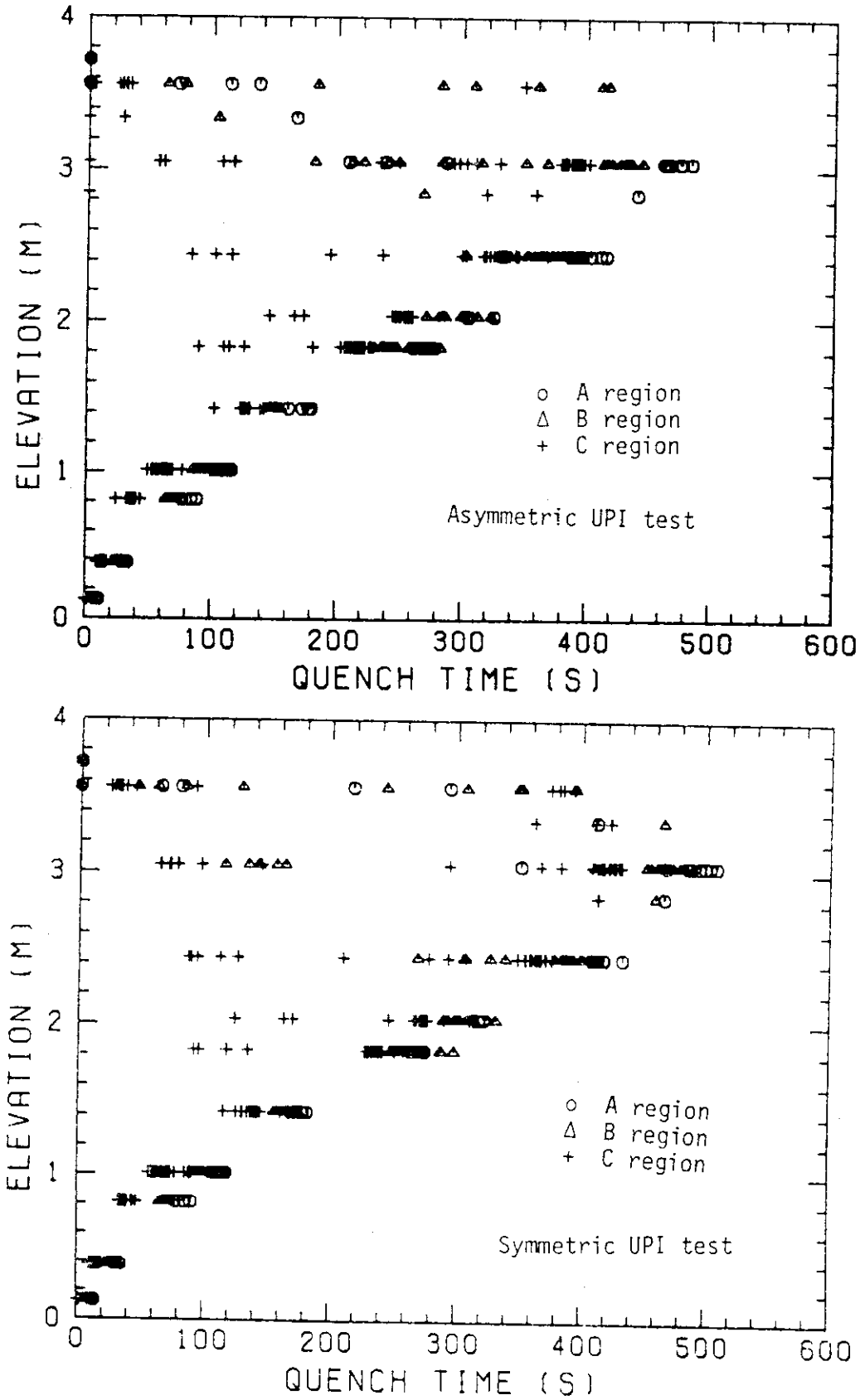

Fig. 4.24 Comparison of quench time between the present asymmetric UPI test and the relatively symmetric UPI test C2-AS1 (Run 59)

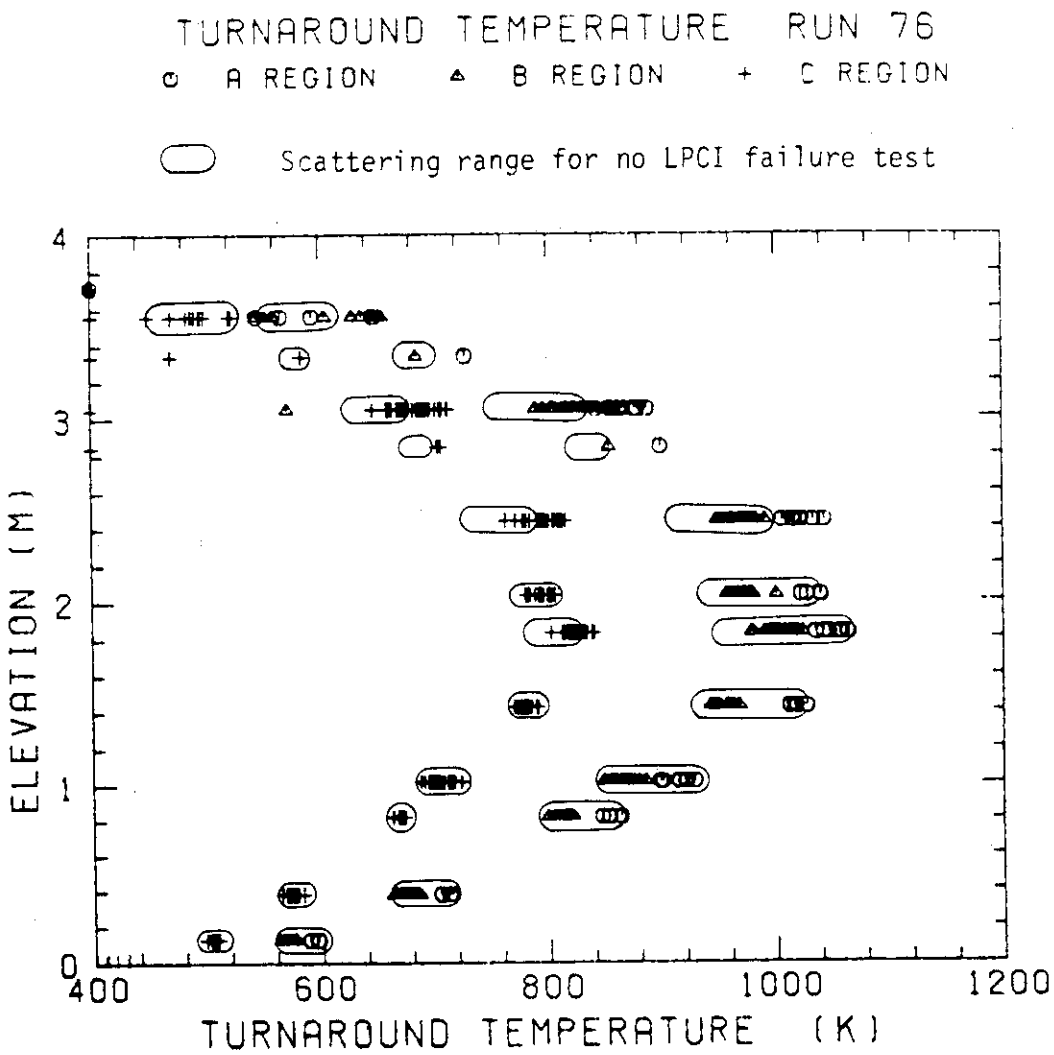

Fig. 4.25 Comparison of turnaround temperature between the present asymmetric UPI test and no failure UPI test (C2-13/ Run 72)

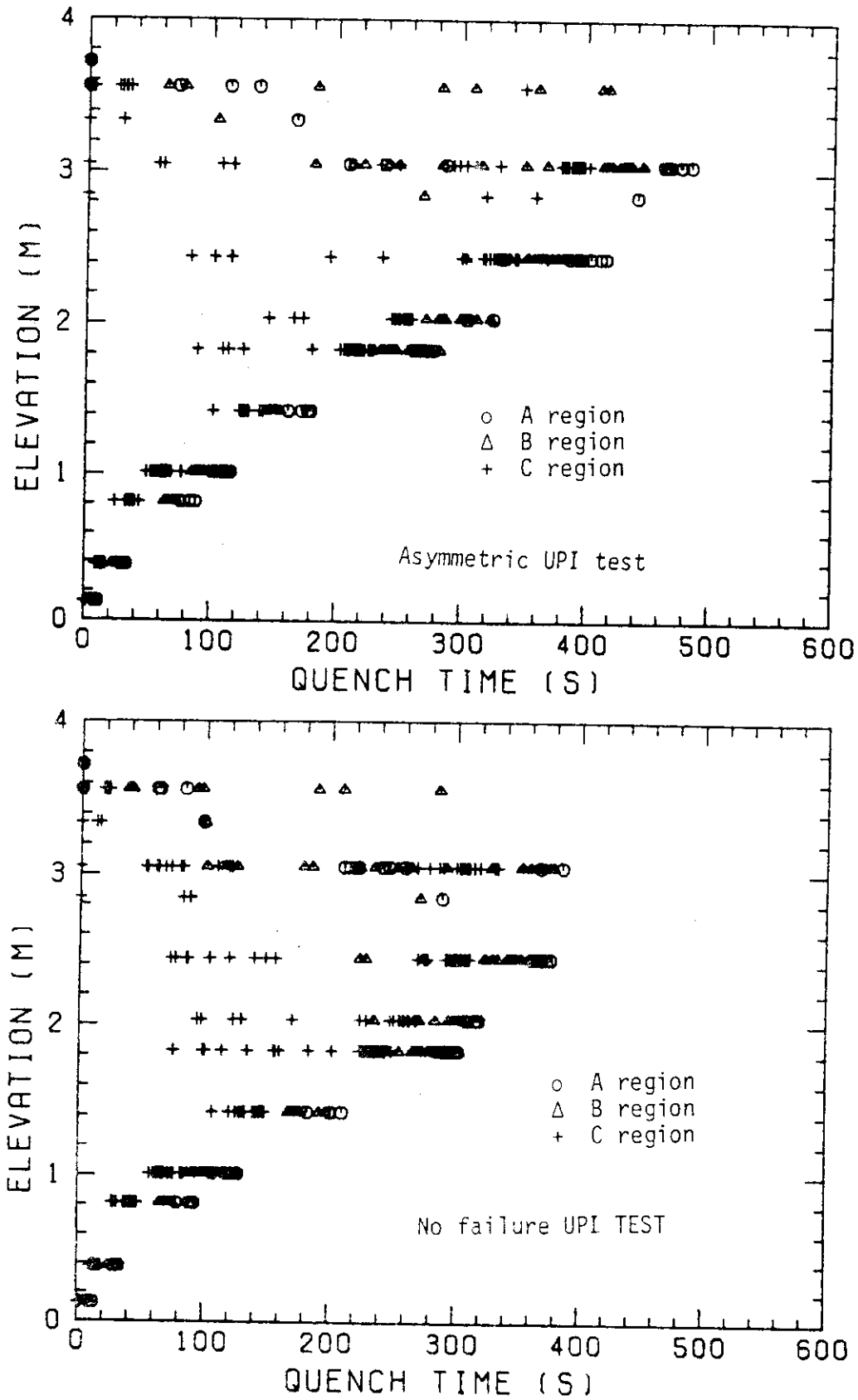

Fig. 4.26 Comparison of quench time between the present asymmetric UPI test and no failure UPI test (C2-13/ Run 72)

Early transient (< 50 S) → uniform (ΔP_c, T_c, h, u_g)

Except early transient (> 50 S) → Partially ununiform

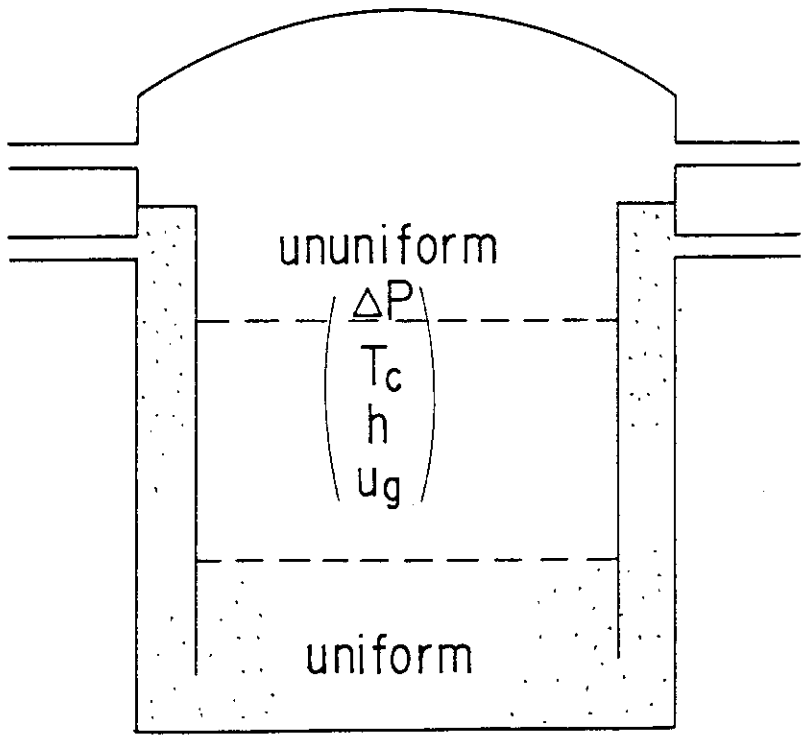

Fig. 4.27 Qualitative effect of asymmetric UPI

Early transient → Negligiblly small difference
(< 50 S)

Except for early transient → Differences in some aspects
(> 50 S)

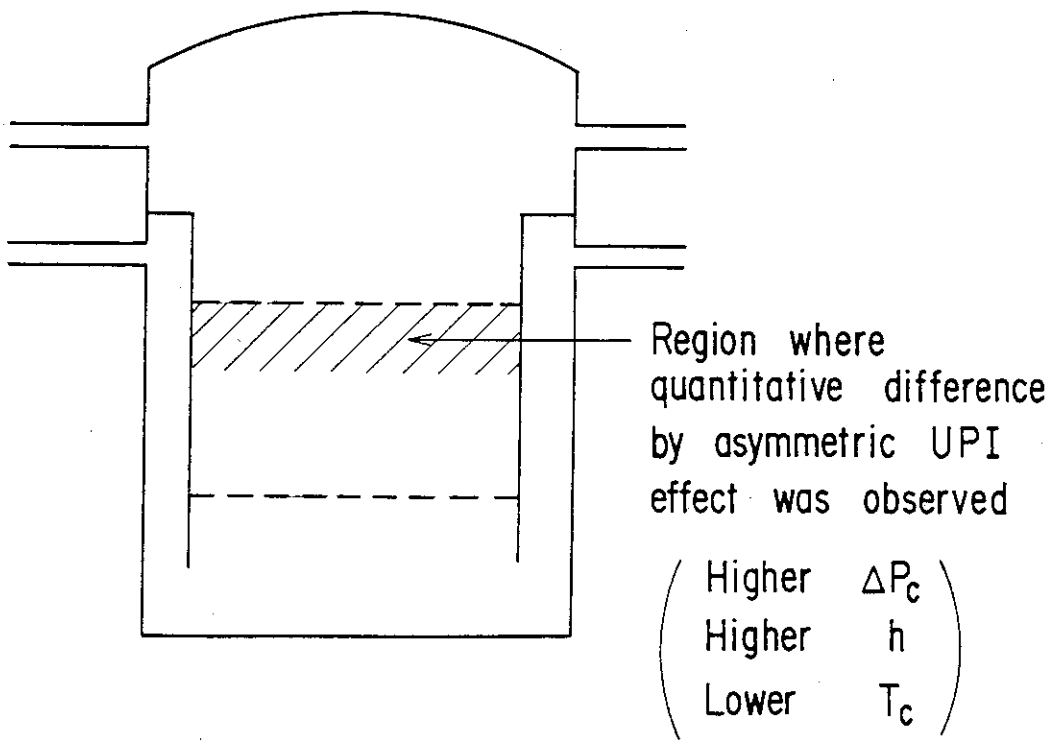

Fig. 4.28 Quantitative effect of asymmetric UPI

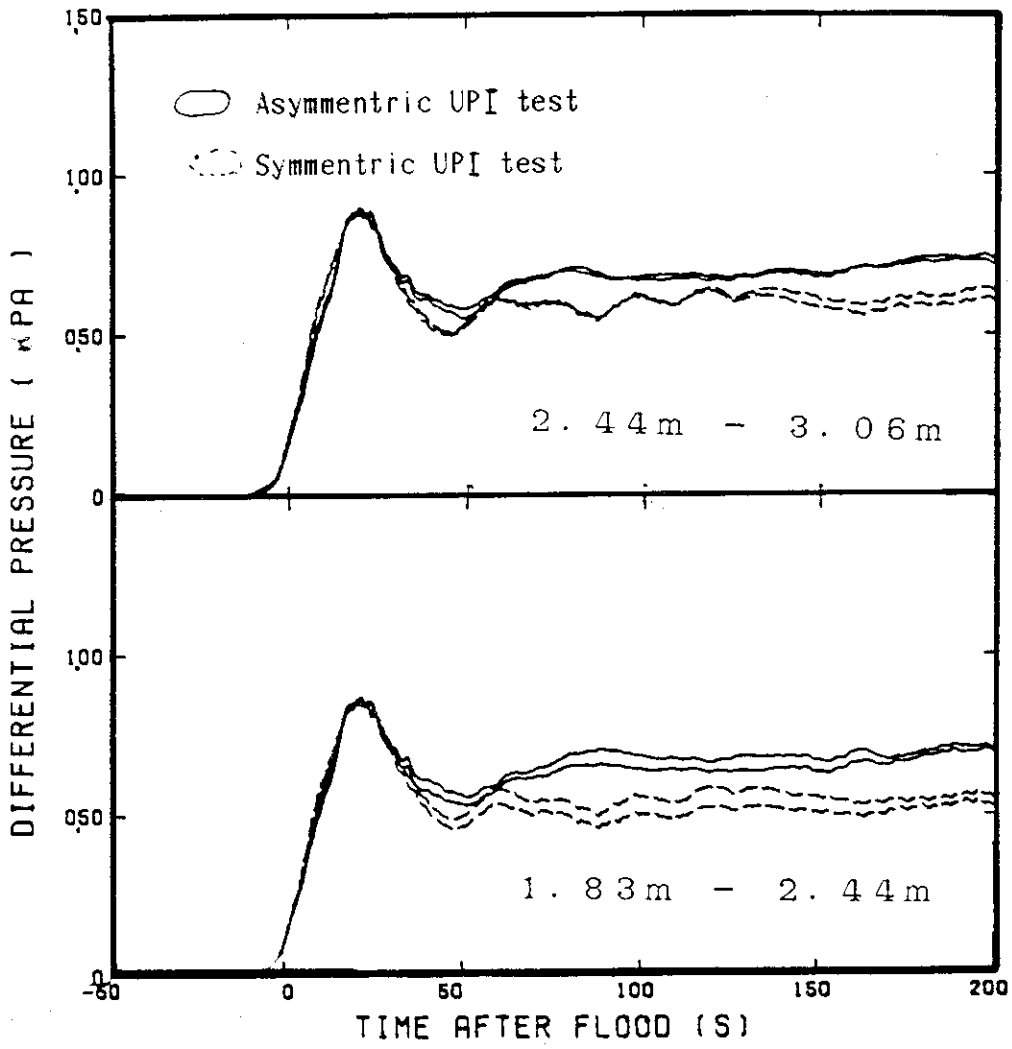

Fig. 4.29 Comparison of axial differential pressure in core

5. Conclusions

1. A UPI test simulating no LPCI pump failure (C2-13/Run 72) gave the slightly lower peak clad temperature than a UPI test simulating single LPCI pump failure (C2-16/Run 76). It indicated that no LPCI pump failure assumption gave the more conservative core cooling than single LPCI pump failure assumption for UPI condition.

2. A UPI test simulating single LPCI pump failure with asymmetric UPI rate (C2-16/Run 76) gave the lower peak clad temperature than a UPI test with the same injection rate but more symmetric UPI condition (C2-AS1/Run 59). It indicated that the asymmetric UPI condition did not give a locally poor core cooling.

3. Effect of asymmetric UPI was observed only in the upper plenum and upper part of core for later period concerning the items summarized in 4.8.

   Asymmetric UPI test lead to a higher water accumulation causing the higher heat transfer and better core cooling in upper part of core than symmetric UPI test.

Acknowledgements

The authors are much indebted to Drs. K. Sato, and T. Shimooke of JAERI for their guidance and encouragement for this program.

They would like to express their appreciation to the member of their analysis group, especially Messrs. H. Adachi, T. Iwamura, A. Ohnuki and Y. Abe.

They also would like to express their thanks to the 2D/3D project members of USA and FRG for valuable discussion.

They are deeply indebted to Messrs. A. Kamoshida, T. Ohyama, T. Wakabayashi, Y. Niitsuma, K. Nakajima, T. Chiba, J. Matsumoto, K. Komori and H. Sonobe of JAERI for their contribution to the test conduction.

References

(1) Hirano, K. and Murao, Y. ; J. At. Energy Soc. Japan, (in Japanese), 22 [10], 681 (1980)

(2) Murao, Y. et al. ; J. Nucl. Sci. Technol, 19 (9), 705 (1982)

(3) Adachi, H. et al. ; JAERI-M 83-080, (1983)

(4) For instance, Adachi, H. et al. ; NUREG/CP-0041, vol.1, pp.287 (1983)

(5) Iguchi, T. and Murao, Y. ; J. Nucl. Sci. Technol, 22 (8), 637 (1985)

(6) Murao, Y. et al. ; "Results of CCTF Upper Plenum Injection Tests", 12th water reactor safety research information meeting, Gaithersburg, Maryland (1984)

(7) An audit analysis for evaluation of ECCS of Takahama Nuclear Power Station Unit 3 & 4 (in Japanese), Prepared by JAERI (1978)

Acknowledgements

The authors are much indebted to Drs. K. Sato, and T. Shimooke of JAERI for their guidance and encouragement for this program.

They would like to express their appreciation to the member of their analysis group, especially Messrs. H. Adachi, T. Iwamura, A. Ohnuki and Y. Abe.

They also would like to express their thanks to the 2D/3D project members of USA and FRG for valuable discussion.

They are deeply indebted to Messrs. A. Kamoshida, T. Ohyama, T. Wakabayashi, Y. Niitsuma, K. Nakajima, T. Chiba, J. Matsumoto, K. Komori and H. Sonobe of JAERI for their contribution to the test conduction.

References

(1) Hirano, K. and Murao, Y. ; J. At. Energy Soc. Japan, (in Japanese), 22 [10], 681 (1980)

(2) Murao, Y. et al. ; J. Nucl. Sci. Technol, 19 (9), 705 (1982)

(3) Adachi, H. et al. ; JAERI-M 83-080, (1983)

(4) For instance, Adachi, H. et al. ; NUREG/CP-0041, vol.1, pp.287 (1983)

(5) Iguchi, T. and Murao, Y. ; J. Nucl. Sci. Technol, 22 (8), 637 (1985)

(6) Murao, Y. et al. ; "Results of CCTF Upper Plenum Injection Tests", 12th water reactor safety research information meeting, Gaithersburg, Maryland (1984)

(7) An audit analysis for evaluation of ECCS of Takahama Nuclear Power Station Unit 3 & 4 (in Japanese), Prepared by JAERI (1978)

Appendix A

Definitions of Tag IDs

Figure List

1. Definition of Tag. ID for clad surface temperatures and heat fransfer coefficients

Notation : TEnnYlm (temperature)

HTEmmYlm (heat transfer coefficient)

nn : Bundle number (see Fig. A-1)

m : Elevation number

	Elevation (m)	Axial power factor
3	0.38	0.651
5	1.015	1.147
7	1.83	1.40
9	2.44	1.256
A	3.05	0.854

2. Definition of power zone and boundle number

See Fig. A-1

3. Definition of Tag. ID for void fraction

See Fig. A-2

4. Definition of Tag. ID for average linear power of heater rod in each power unit zone

See Fig. A-3

5. Definition of Tag. ID for differential pressure through downcomer, upper plenum, core and lower plenum

See Fig. A-4

6. Definition of Tag. ID for differential pressure through intact and broken loop and broken cold leg nozzle

See Fig. A-5

7. Definition of Tag. ID for fluid temperature in inlet and outlet plenum and secondary side of steam generator

See Fig. A-6

8. Definition of Tag. ID for ECC water injection rate, ECC water temperature and vented steam flow rate

   See Fig. A-7

9. Definition of initial temperature, turnaround temperature quench temperature, temperature rise, turnaround time and quench time. (See Fig. A-8)

   T_i : Initial temperature (Clad surface temperature at reflood initiation)

   T_t : Turnaround temperature (Maximum clad surface temperature in each temperature history)

   ΔT_r : Temperature rise ($= T_t - T_i$)

   T_q : Quench temperature (Clad surface temperature at quenching)

10. Definition of quenching

   See Fig. A-8

Quench time t_t is determined as

$$t_t = i \times \Delta t - \text{(reflood initiation time)}$$

In above equation, i is determined by the following criteria.

(1) Clad surface temperature is high, compared with the saturation temperature.

$$T_i > T_{sat} + \Delta T_1$$

(2) Decreasing rate of clad surface temperature is large.

$$\frac{T_{i+1} - T_i}{\Delta t} < - C_{st}$$

(3) Clad surface temperature falls around the saturation temperature.

$$T_{i+k_1} \leq T_{sat} + \Delta T_1$$

(4) If the determined i is inadequate, the value i is manually re-determined.

Δt : Data sampling period (s)

T_i : Clad surface temperature (K)

T_{sat}: Saturation temperature at the pressure in upper plenum (K)

ΔT_1 : Temperature discrepancy (K)
Default value = 50.0

C_{st} : Decreasing rate of clad surface temperature (K/S)
Default value = 25.0

k_1 : Number of referred data (-)
Default value = 6

11. Definition of Tag. ID for core inlet mass flow rate, time-integral core inlet mass flow rate and carry-over rate fraction

(1) Core inlet mass flow rate : $\dot{m}_F$
Notation : MLCRI□ (□ = N, 1 or 11)

(2) Time-intefral core inlet mass flow rate : $\int \dot{m}_F dt$
Notation : IMLCRI□ (□ = N, 1 or 11)

(3) Carry-over rate fraction : $(\dot{m}_F - \dot{m}_{CR})/\dot{m}_F$
Natation : CRF□ (□ = N, 1 or 11)

where $\dot{m}_F$: Core inlet mass flow rate (See item 12)

$\dot{m}_{CR}$: Water accumulation rate in core

Suffix	$\dot{m}_F$ base on
N	Eq.(A.2)
1	Eq.(A.1) with K=15
11	Eq.(A.1) with K=20

12. Evaluation of core inlet mass flow rate

The reflood phenomena is a relatively slow transient and a steady state condition can be applied. In a steady state condition, based on the mass balance relations of the system, the core flooding mass flow rates $\dot{m}_F$s can be written as follows:

By using the data measured at the downstream of the core inlet, $\dot{m}_F$ is derived as,

$$\dot{m}_F = \dot{m}_C + \dot{m}_U + \dot{m}_B + \Sigma \dot{m}_I \quad , \qquad (A.1)$$

where $\dot{m}_C$ and $\dot{m}_U$ are the mass accumulation rates in the core and the upper plenum respectively. The $\dot{m}_B$ and $\dot{m}_I$ are the mass flow rates in the broken loop and the intact loop, respectively.

By using the data measured at the upstream of the core inlet, $\dot{m}_F$ is derived as,

$$\dot{m}_F = \Sigma\, \dot{m}_{DL} - \dot{m}_D - \dot{m}_O + \dot{m}_{ECC/LP} \quad , \tag{A.2}$$

where $\dot{m}_{DL}$ and $\dot{m}_O$ are the mass flow rates of the water flowing into and overflowing from the downcomer, $\dot{m}_{ECC/LP}$ and $\dot{m}_D$ are the mass flow rate of the ECC water injected into the lower plenum and the water accumulation rate in the dowmcomer respectively.

The $\dot{m}_I$s and $\dot{m}_B$ can be obtained from the pressure drops at the pump simulators with orifices by assuming the K-factor of the orifice is constant. The values of $\dot{m}_C$, $\dot{m}_D$ and $\dot{m}_U$ can be evaluated with the differential pressure ΔP_C, ΔP_D and ΔP_U, respectively, as follows:

$$\dot{m}_n = d(\Delta P_n S_n/g)/dt \quad (n : C, D, U) \quad , \tag{A.3}$$

where g is the gravitational acceleration and S_n is the cross sectional area. The value of $\dot{m}_O$ can be obtained from the liquid level X in the Containment tank 1 as,

$$\dot{m}_O = d(X\rho_\ell S_o)/dt \ , \tag{A.4}$$

where ρ_ℓ is the liquid density and S_o is the cross sectional area of the containment tank 1.

The value of $\dot{m}_{DL}$, $\dot{m}_{DV}$ and h, which are liquid flow rate, steam flow rate and enthalpy of two phase mixture downstream each ECC port respectively, are obtained from the following mass and energy balance relations at each ECC port under the assumption of thermal equilibrium:

$$\dot{m}_{DV} + \dot{m}_{DL} = \dot{m}_{ECC} + \dot{m}_I \quad , \tag{A.5}$$

$$(\dot{m}_{DV} + \dot{m}_{DL})i = \dot{m}_{ECC}h_{ECC} + \dot{m}_I h_I \quad , \tag{A.6}$$

$$\text{if} \quad h_g \geq h \geq h_\ell \ , \ (\dot{m}_{DV} + \dot{m}_{DL})h = \dot{m}_{DV}h_g + \dot{m}_{DL}h_\ell$$

$$\text{if} \quad h \geq h_g \quad , \ \dot{m}_{DL} = 0 \quad , \tag{A.7}$$

$$\text{if} \quad h \geq h_\ell \quad , \ \dot{m}_{DV} = 0$$

where h is enthalpy of fluid and h_ℓ and h_g are enthalpies of liquid and steam at the saturation temperature, respectively.

The fluid temperatures can be measured with thermocouples immersed in the fluid and the enthalpies h_I and h_{ECC} can be estimated.

Mass balance calculations were performed with Eqs. (A.1) and (A.2). The K-factor of the orifice in the pump simulator was evaluated in the following two ways.

The K-factor of 20 was obtained with the steam and water single phase calibration tests using the flow meter and spool piece data. The K-factor of 15 was obtained with the Pitot tube measurement in a typical reflood condition assuming the flat velocity profile in the pipings. In the differentiation, higher frequency components of the data tends to be amplified more. Therefore, in the differentiation of the differential pressure data, the smoothing procedure was used to suppress the high frequency components of the data.

In the Acc injection period, the calculated $\dot{m}_F$s with Eqs. (A.1) and (A.2) are significantly different from each other. This discrepancy may be caused by inaccuracy of the mass flow rate injected into the system and by the unaccounting of the storage of water in the cold leg pipe. The former might be introduced from the slow time response of the flow meter (time constant 1 second) and the change of the gas volume in the injection line. In this period, especially before the steam generation from the core becomes noticeable, the mass flow rate, $\dot{m}_F$, calculated with Eq. (A.1) is probably reasonable, since the calculation uses the increasing rates of the masses in the core and the upper plenum and their accuracy is good enough for our estimation.

In the LPCI injection period, the calculated $\dot{m}_F$s are slightly different from each other. Judging from the time-integral values of both $\dot{m}_F$s, their average values are nearly proportional. The discrepancy was inferred to be caused by the disregard of the bypass of steam and liquid from the upper plenum without going through the hot legs in the calculation with Eq. (A.1). And additionally the discrepancy was caused by the disregard of the steam generation in the downcomer due to the hot wall of the pressure vessel in the calculation with Eq. (A.2). It was estimated that the disregard of the downcomer steam generation causes the error of 0.25 kg/s on predicted $\dot{m}_F$. The estimation was made by comparing the results of the tests with hot and cold downcomer conditions.

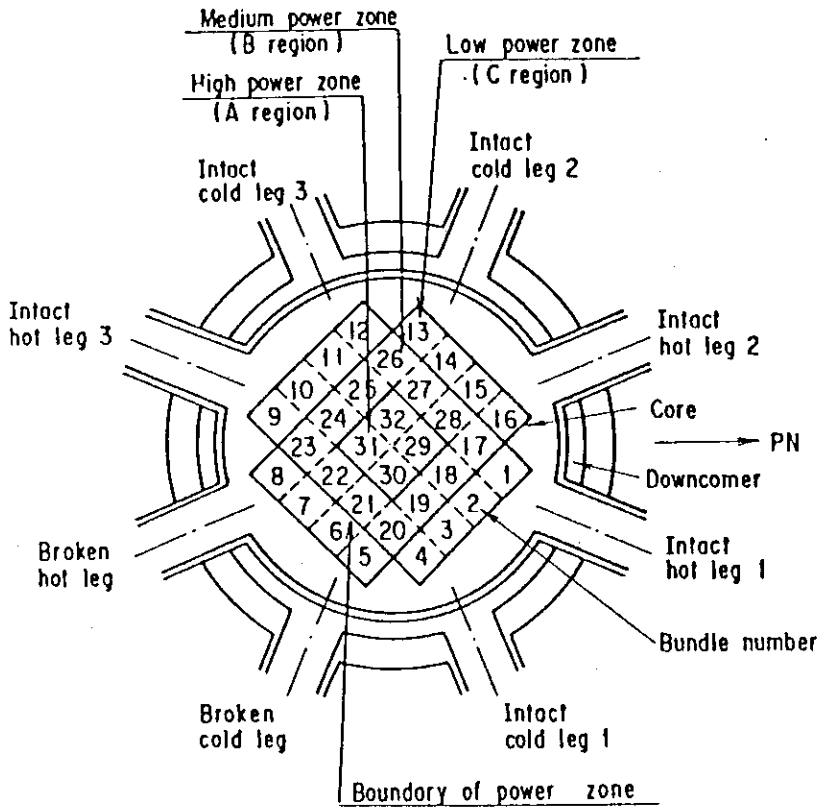

Fig. A-1 Definition of power zones and bundle numbers

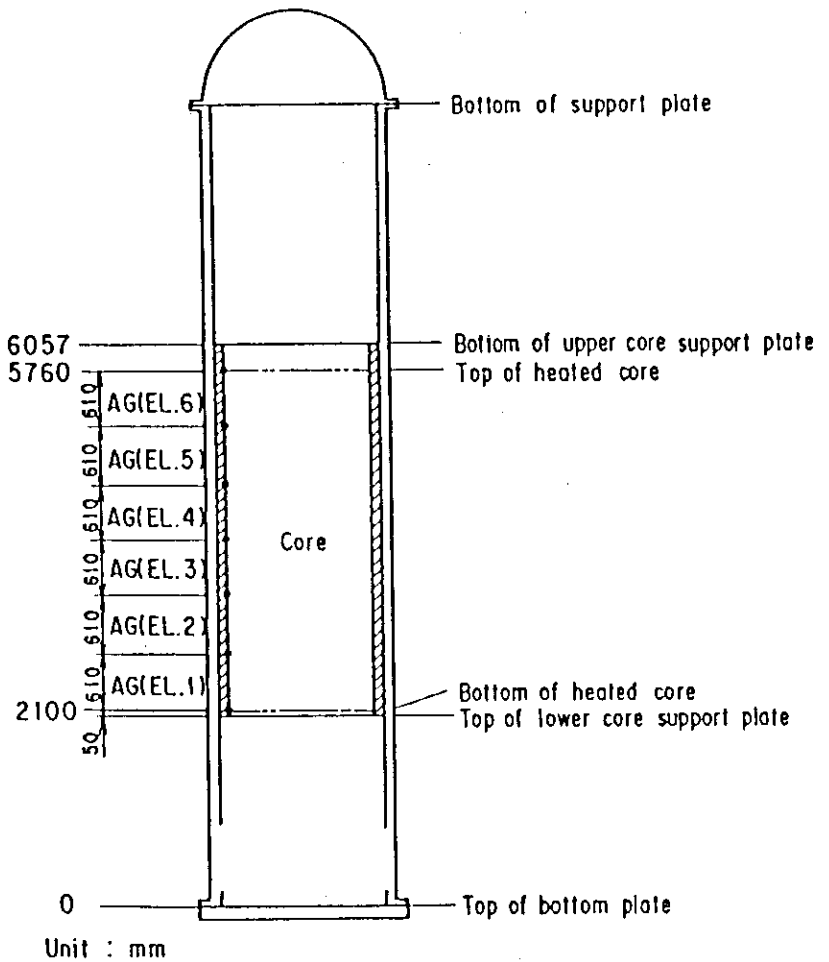

Fig. A-2 Definition of Tag ID for void fraction (AG(EL. 1) ~ AG(EL. 6))

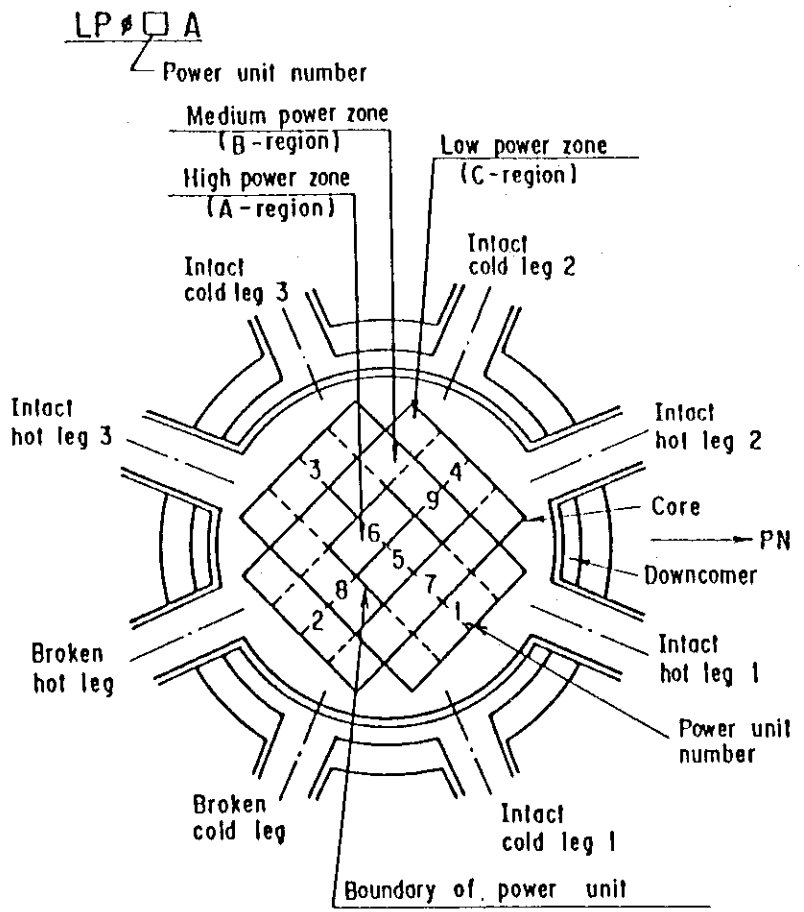

Fig. A-3 Definition of Tag. ID for average linear power of heater rod in each power unit zone
(LP01A ~ LP09A)

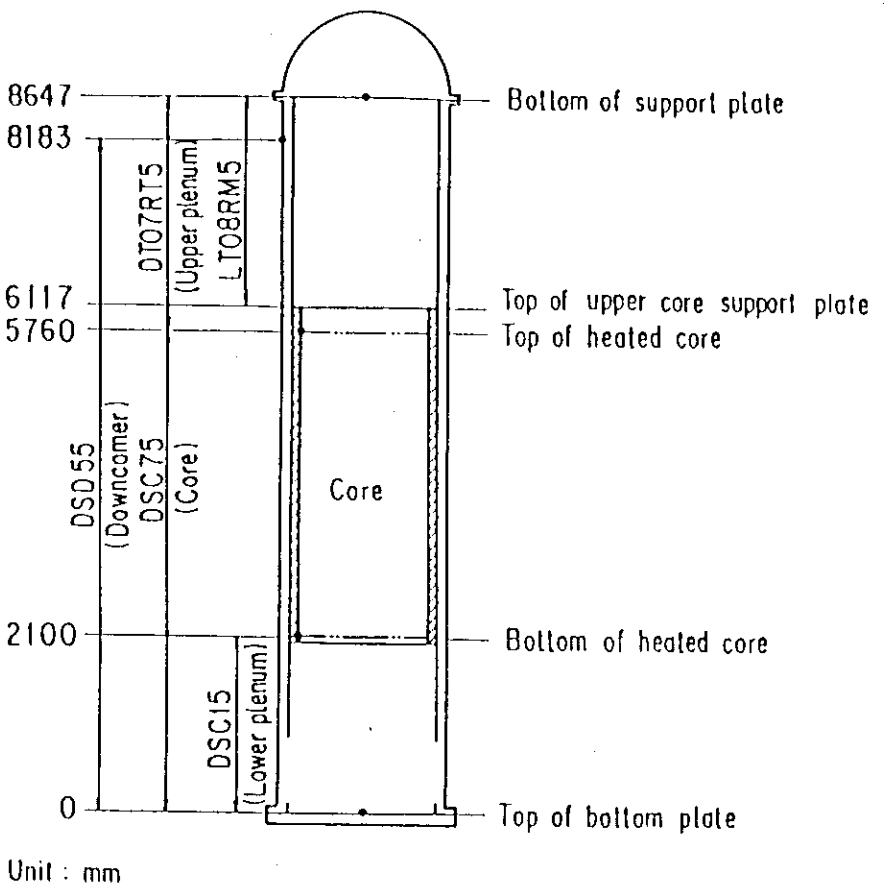

Fig. A-4 Definition of Tag. ID for differential pressure through downcomer, upper plenum, core, and lower plenum
(DSD55, DT07RT5, LT08RM5, DSC75, DSC15)

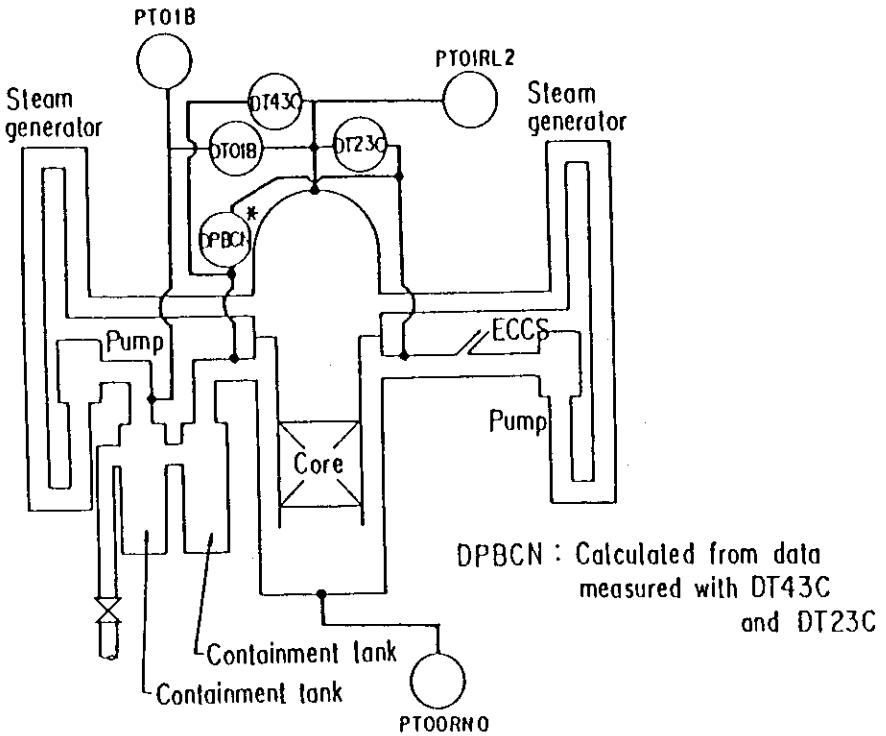

Fig. A-5 Definition of Tag. ID for pressures in upper and lower plena and containment tank 2 (PT01RL2, PT00RNO, PT01B) and for differential pressure through intact and broken loop and broken cold leg nozzle (DT23C, DT01B, DPBCN)

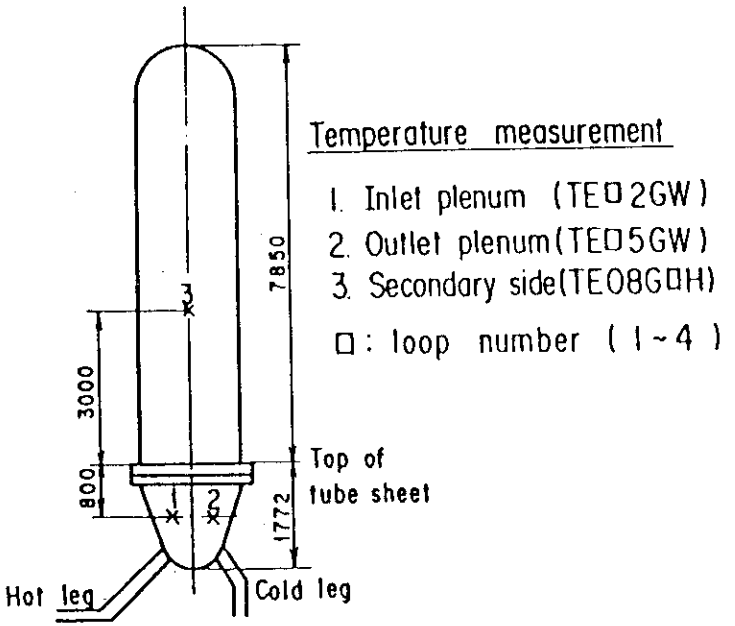

Fig. A-6 Definition of Tag. ID for fluid temperature in inlet and outlet plenum and secondary of steam generator (TE□2GW, TE□5GW, TE08G□H)

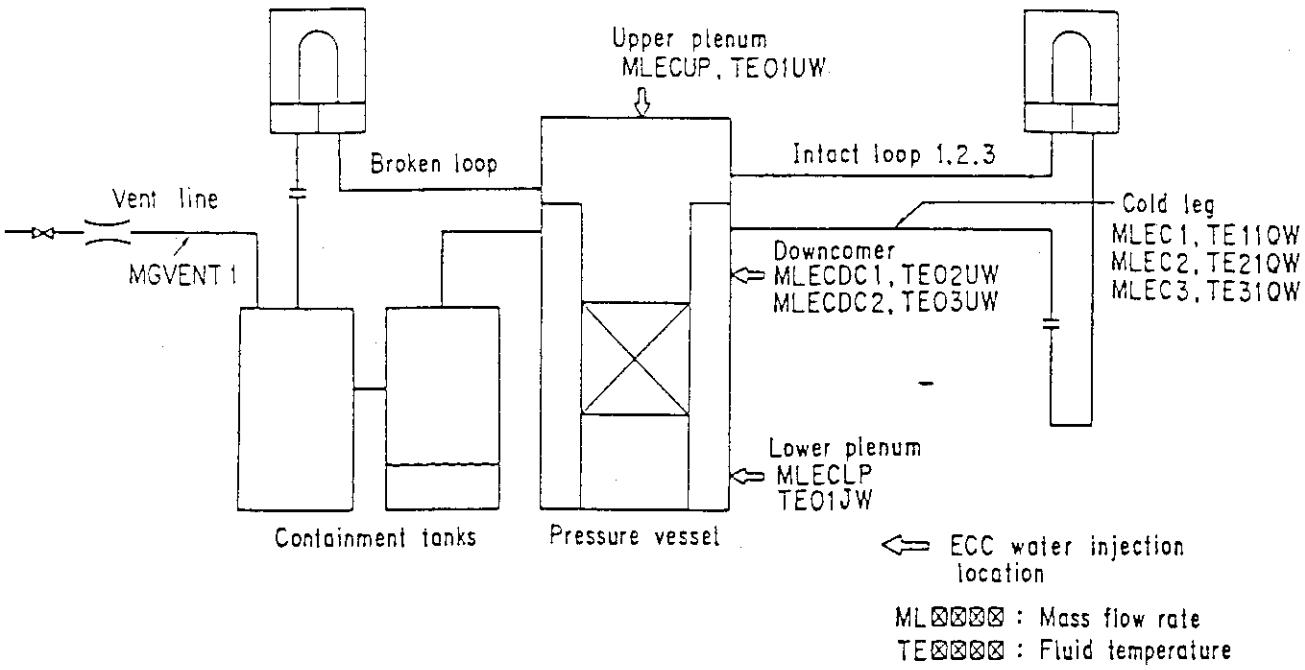

Fig. A-7 Definition of Tag. ID for ECC water injection rate, ECC water temperature and vented steam flow rate

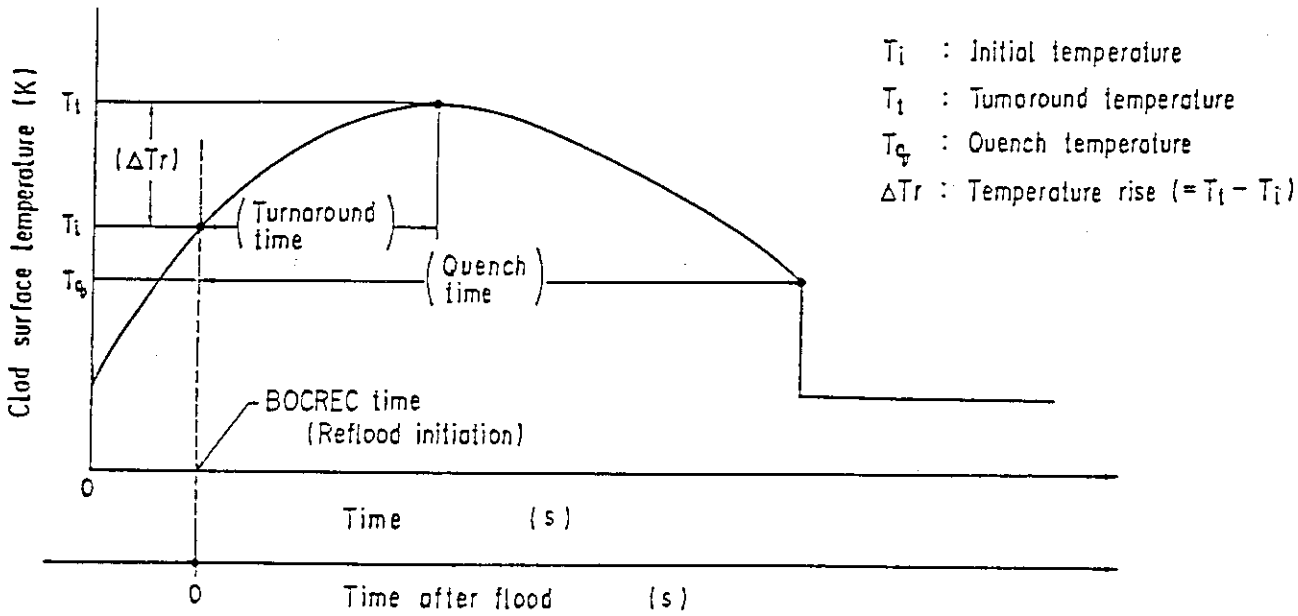

Fig. A-8 Definition of initial temperature, turnaround temperature, quench temperature, temperature rise, turnaround time and quench time

Appendix B

Selected data of CCTF Test C2-16 (Run 76)

Figure List

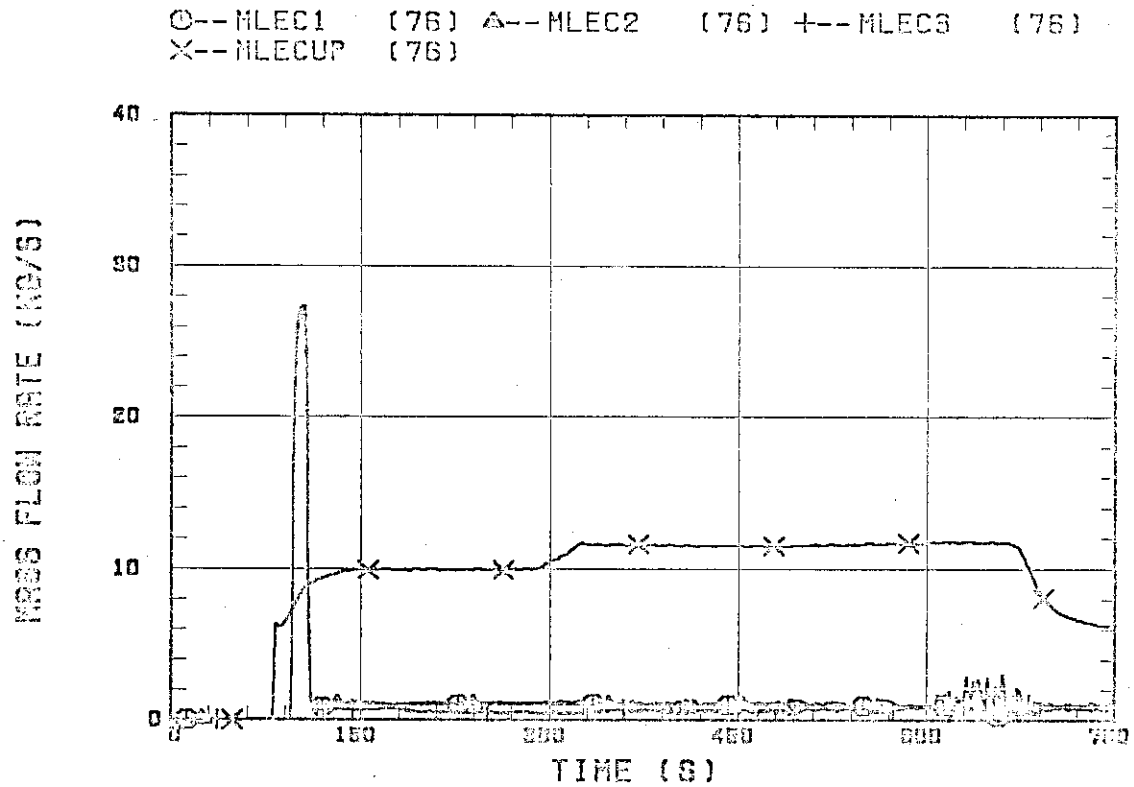

Fig. B.1 ECC water injection rates into the primary system.

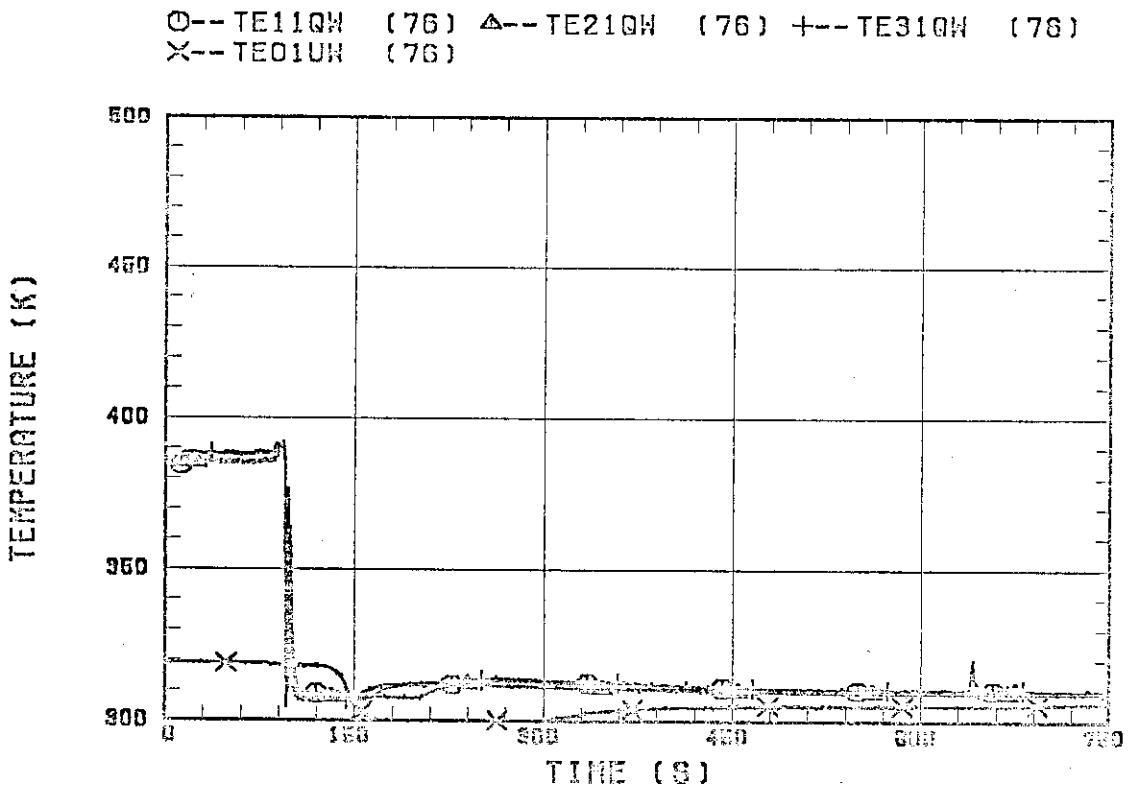

Fig. B.2 ECC water temperature.

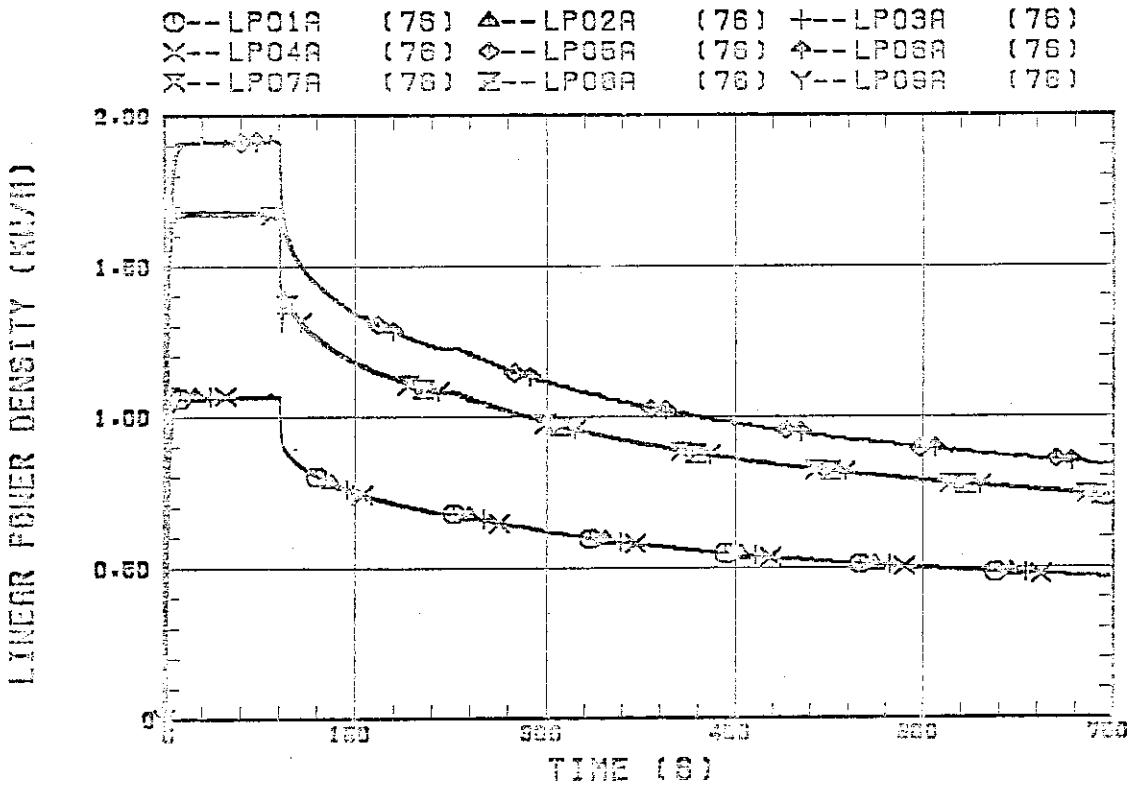

Fig. B.3 Average linear power of heater rod in each power unit zone.

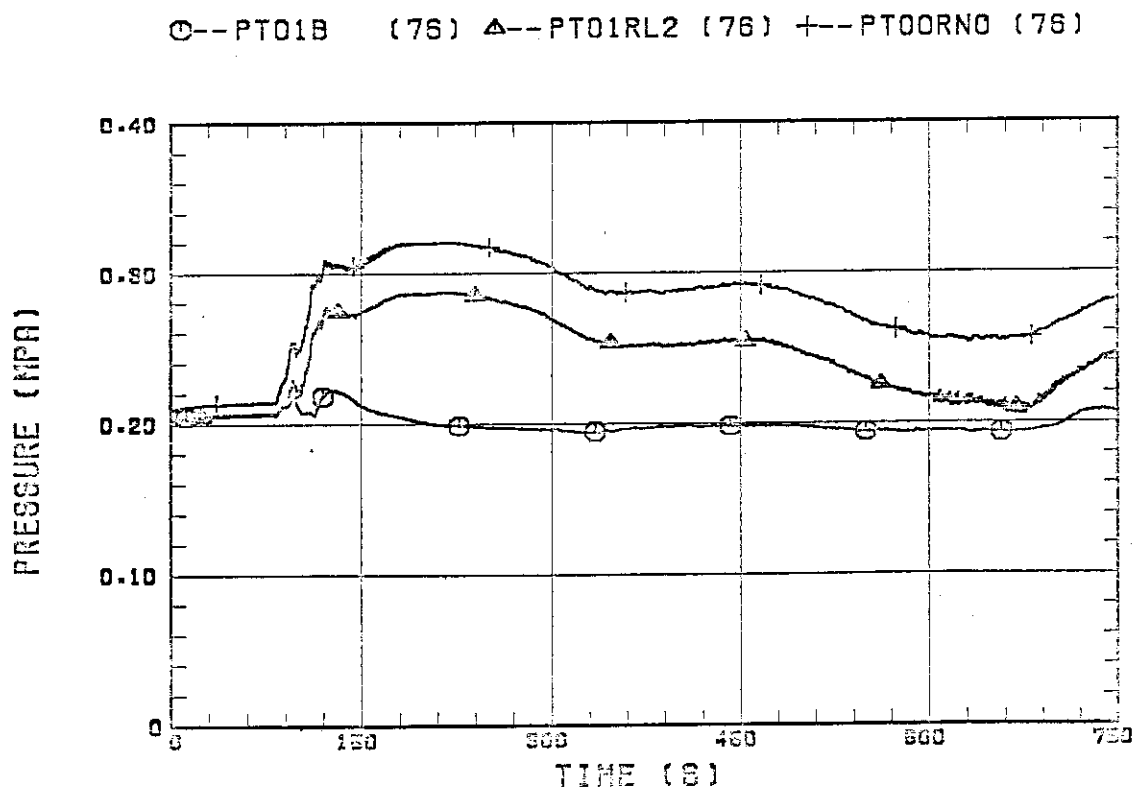

Fig. B.4 Pressure history in containment tank 2, upper plenum and lower plenum.

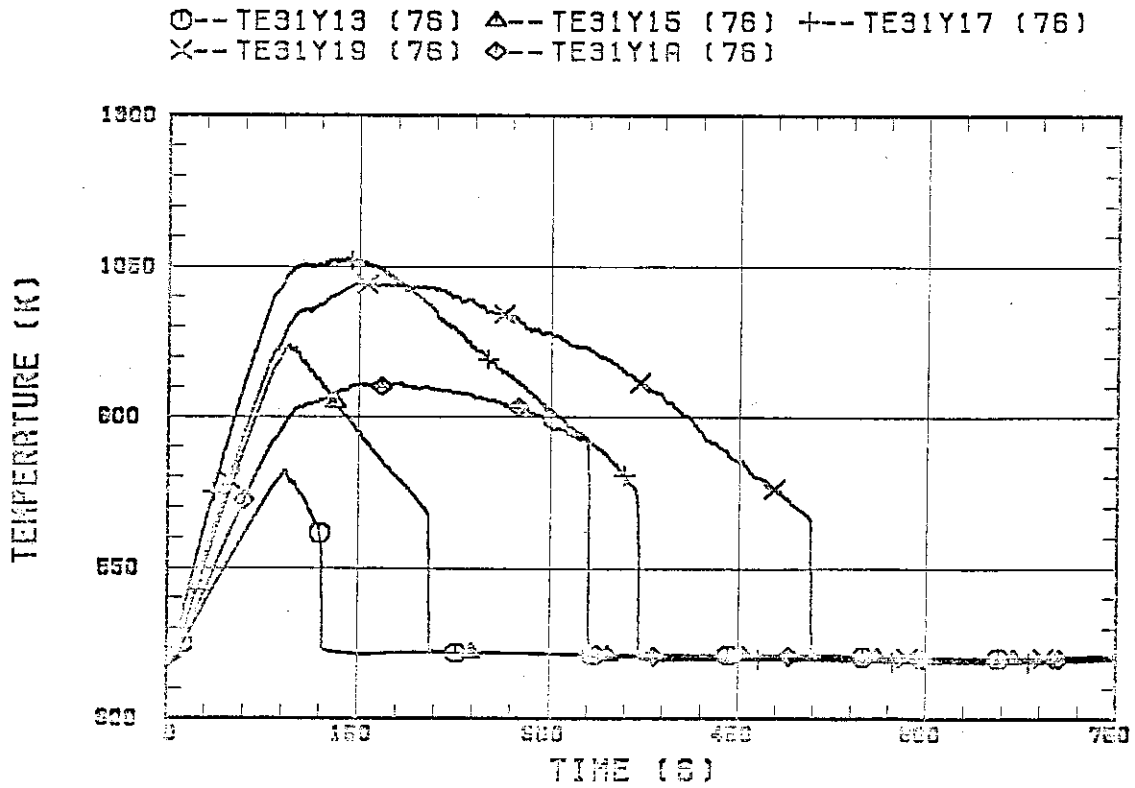

Fig. B.5 Clad surface temperature at various elevations along a heater rod in high power region (A region).

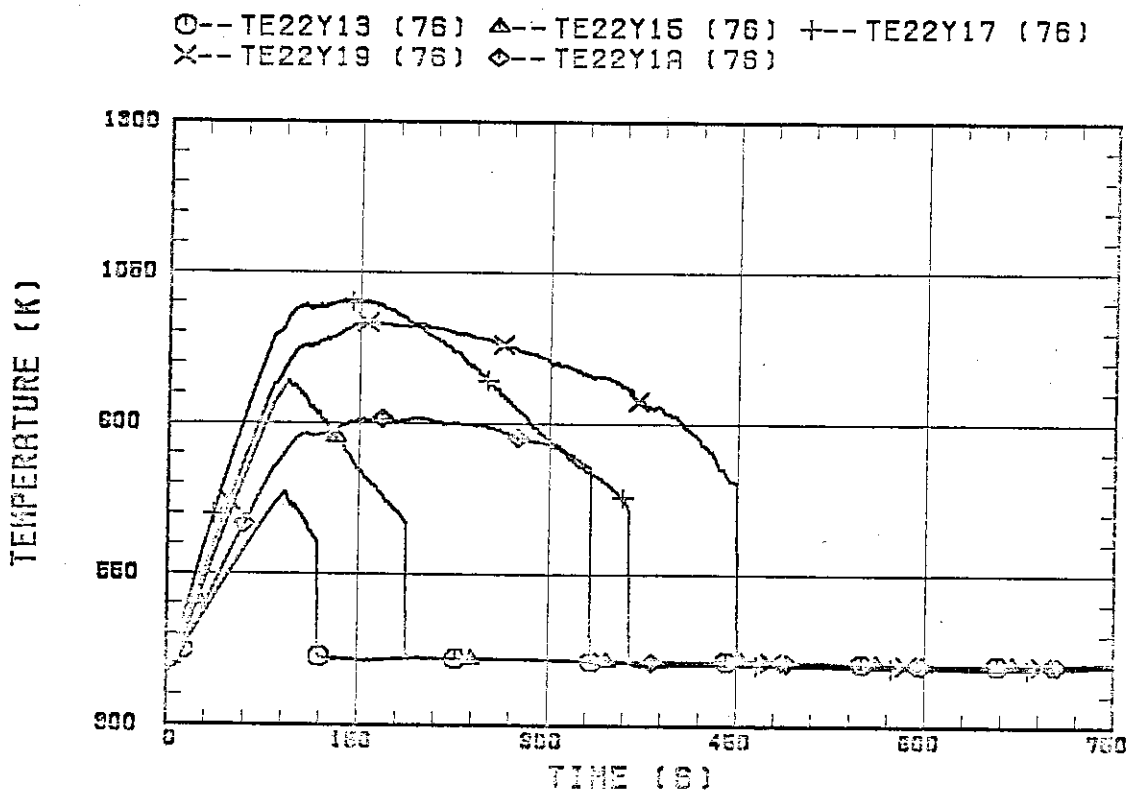

Fig. B.6 Clad surface temperature at various elevations along a heater rod in medium power region (B region).

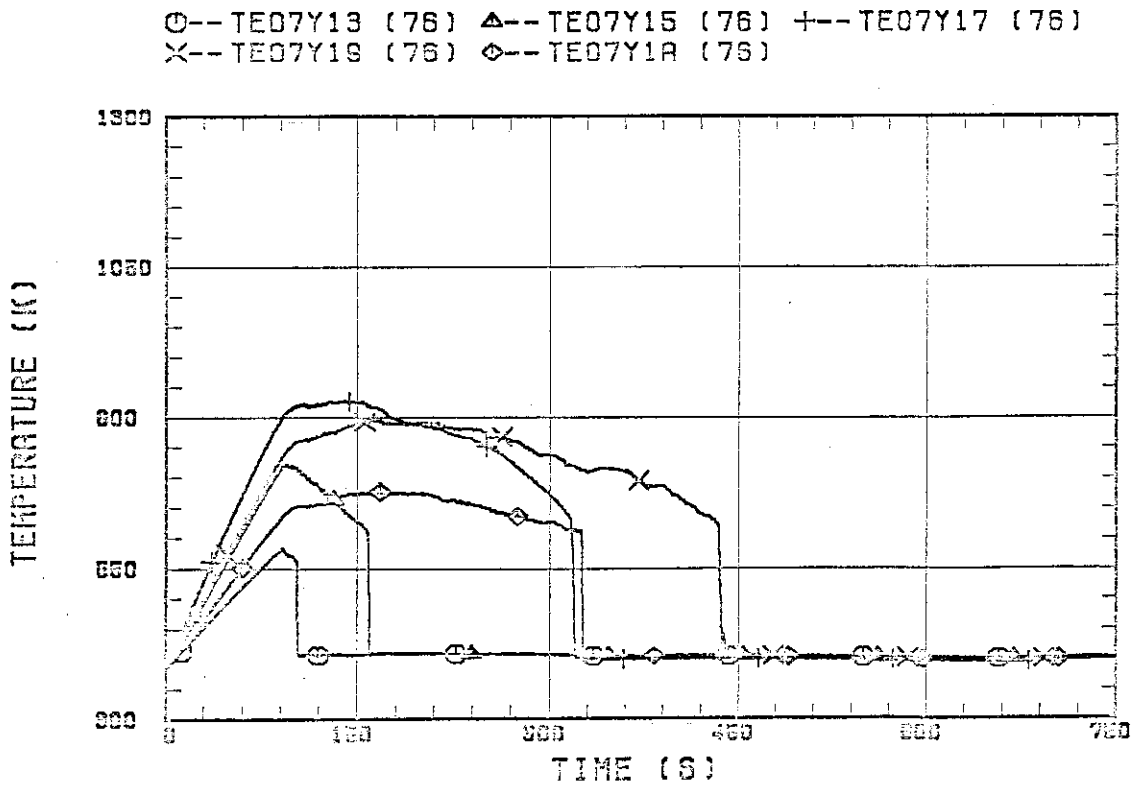

Fig. B.7 Clad surface temperature at various elevations along a heater rod in low power region (C region).

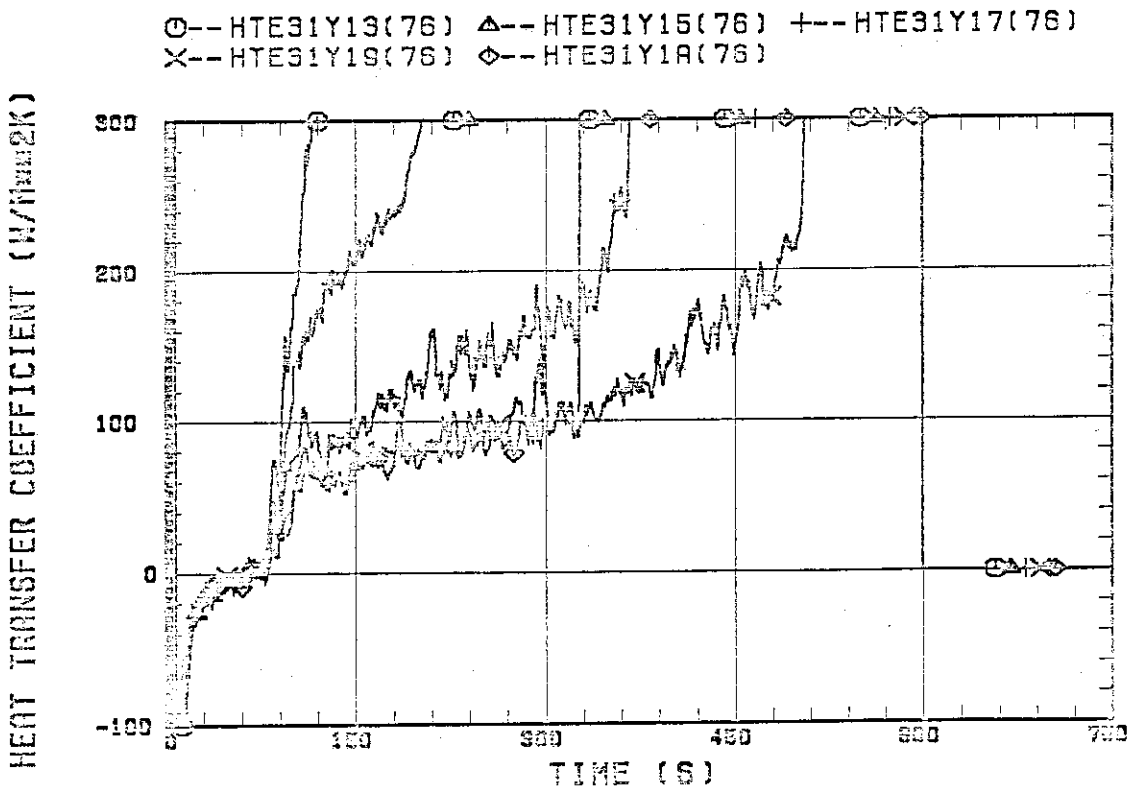

Fig. B.8 Heat transfer coefficient at various elevations along a heater rod in high power region (A region).

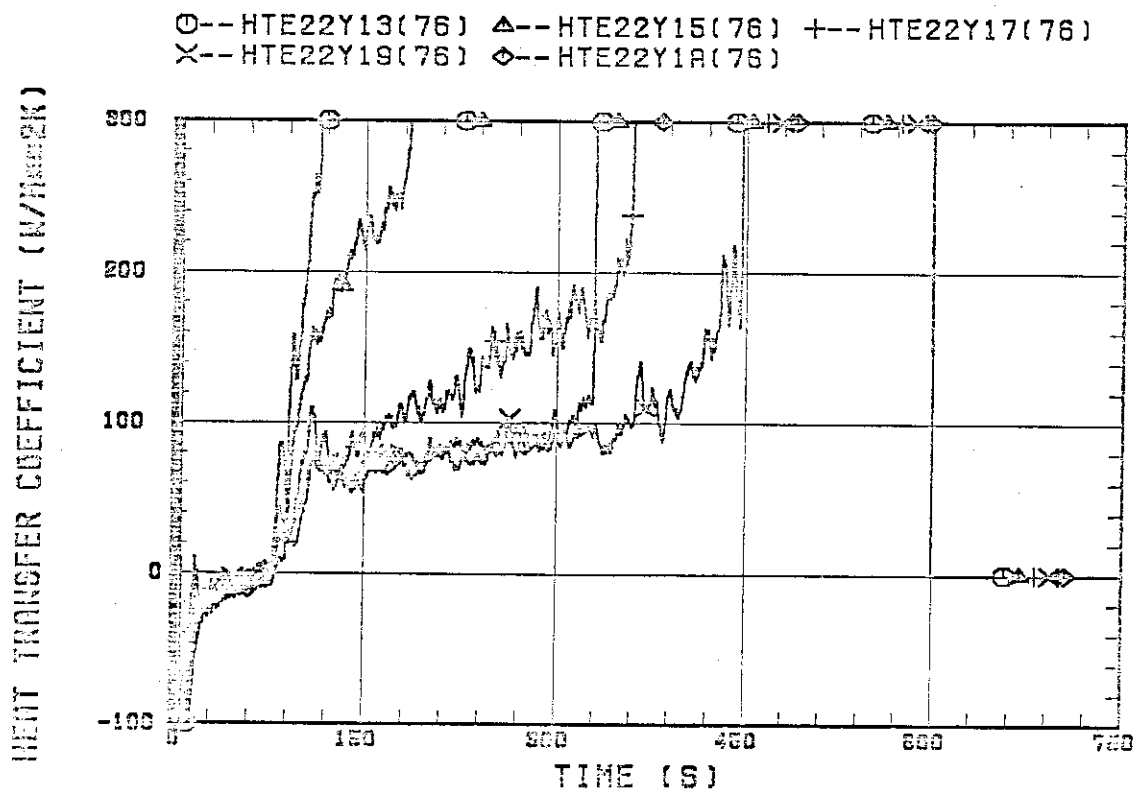

Fig. B.9 Heat transfer coefficient at various elevations along a heater rod in medium power region (B region).

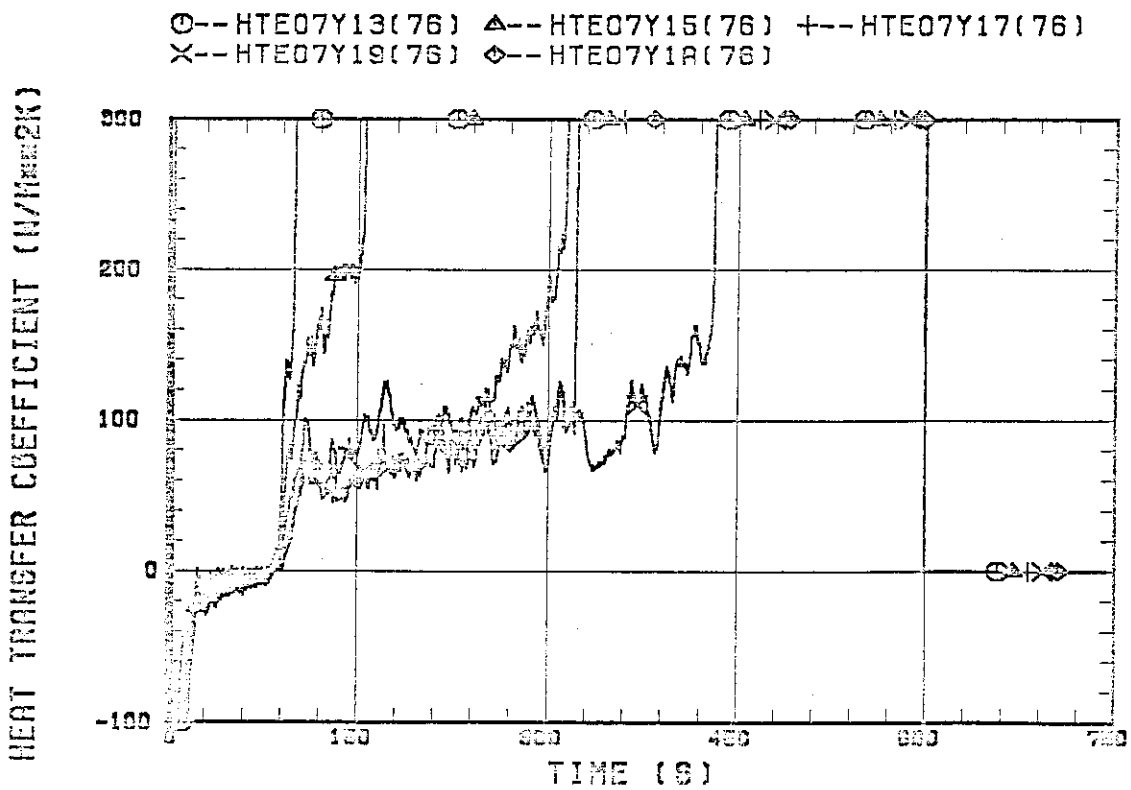

Fig. B.10 Heat transfer coefficient at various elevations along a heater rod in low power region (C region).

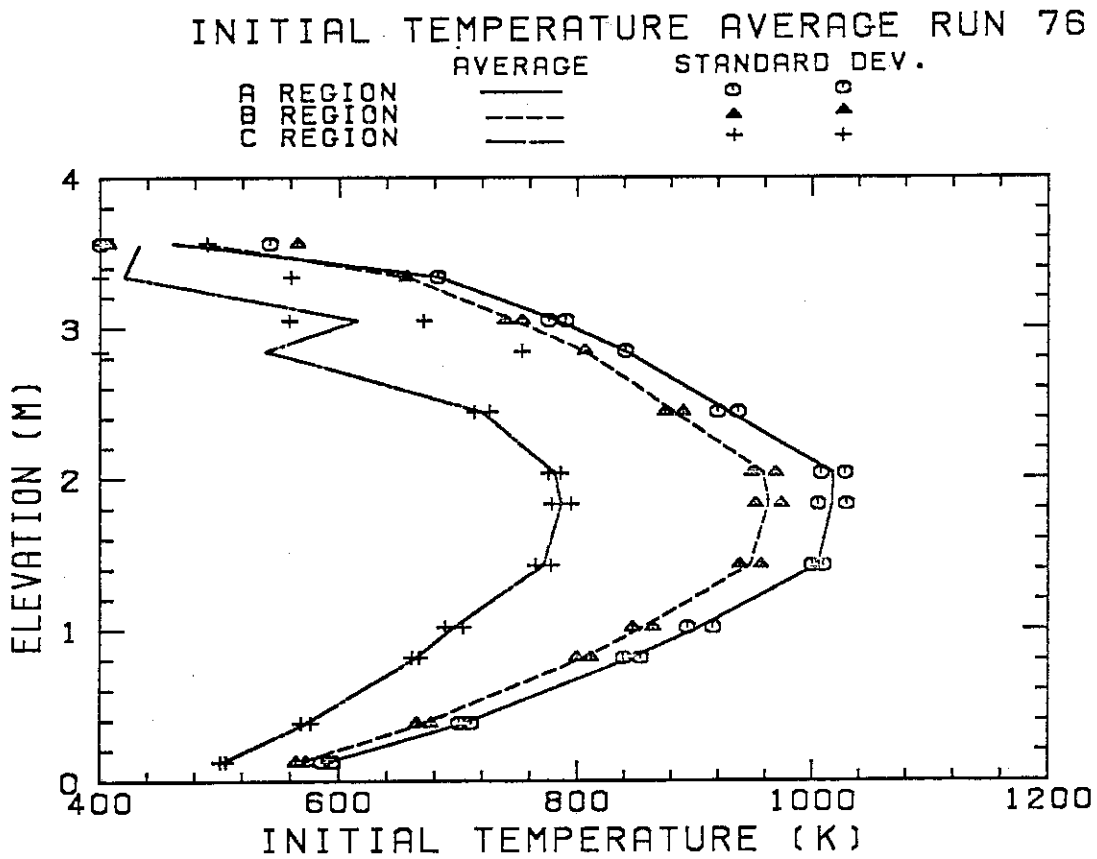

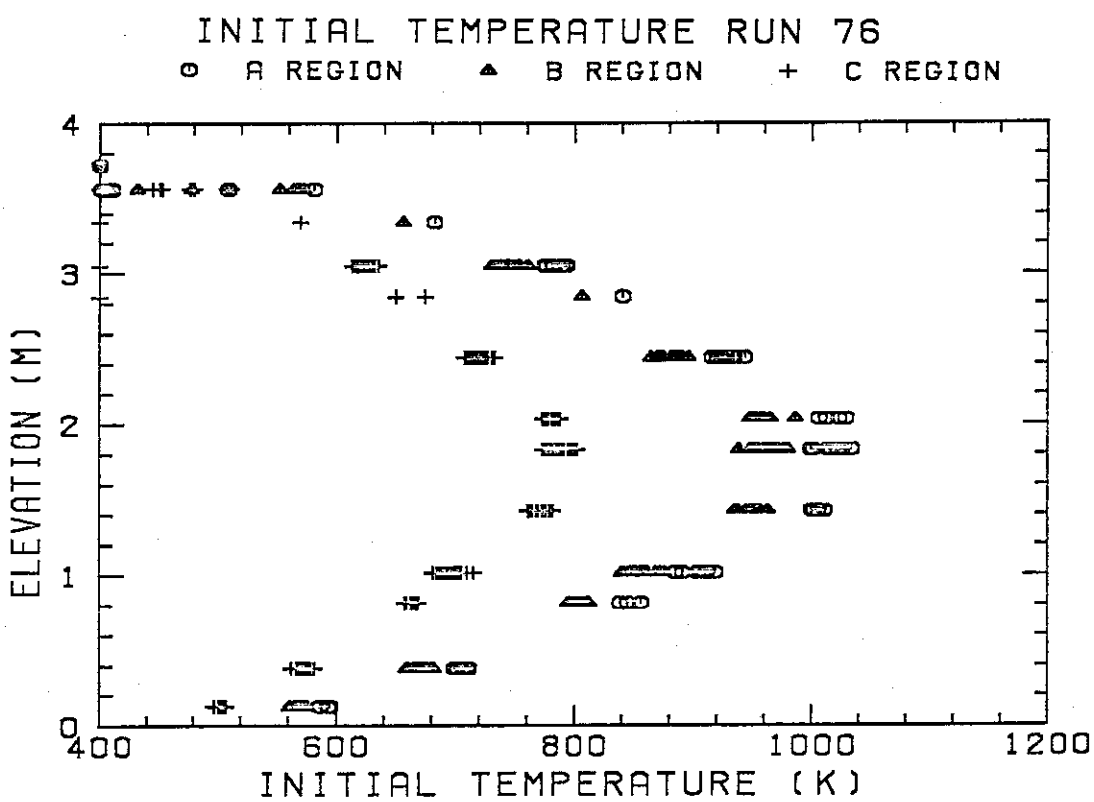

Fig. B.11 Initial clad surface temperature.

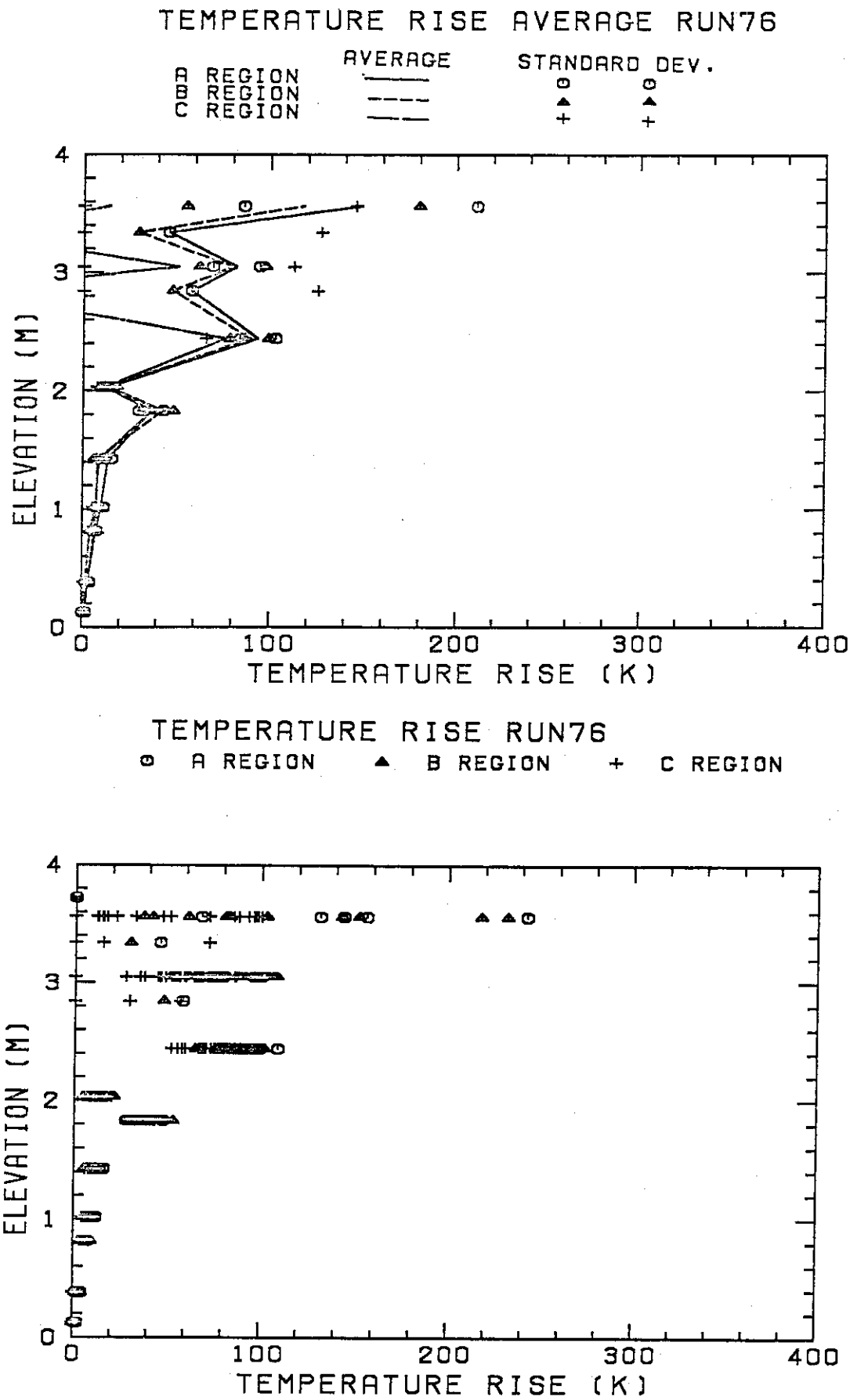

Fig. B.12 Temperature rise.

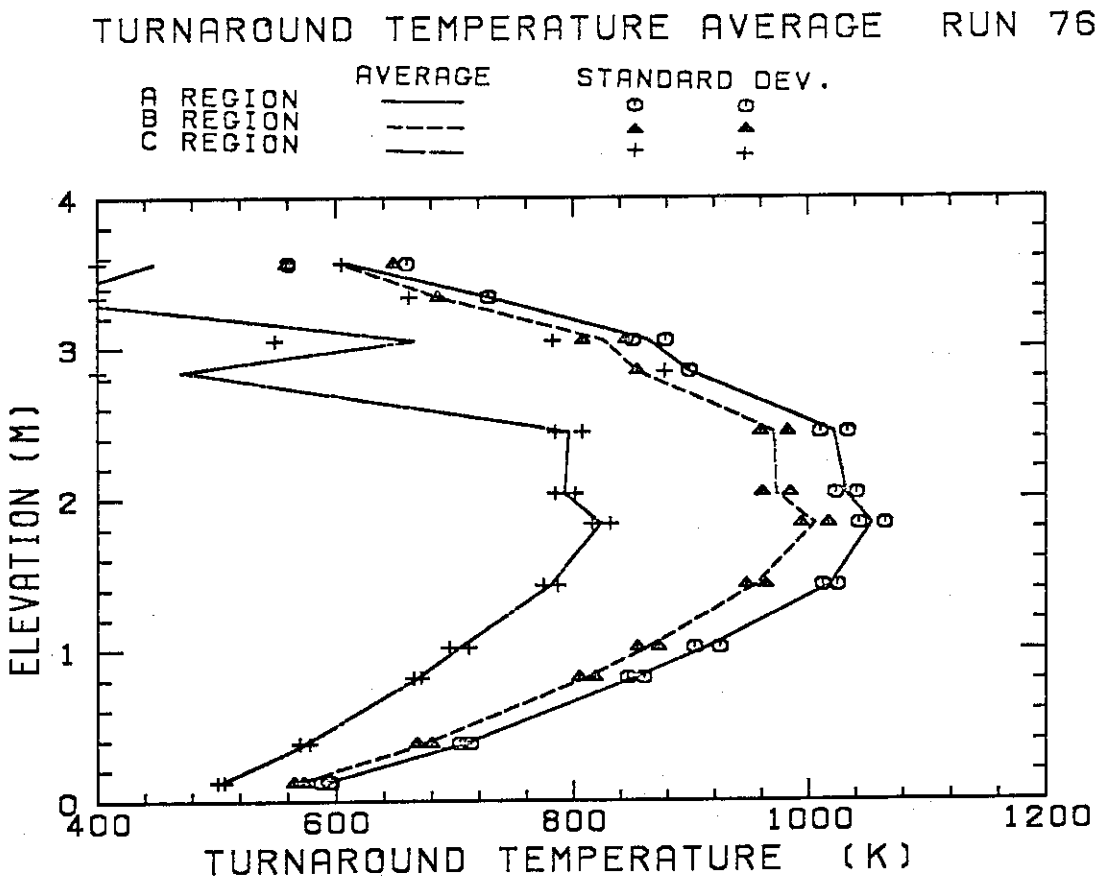

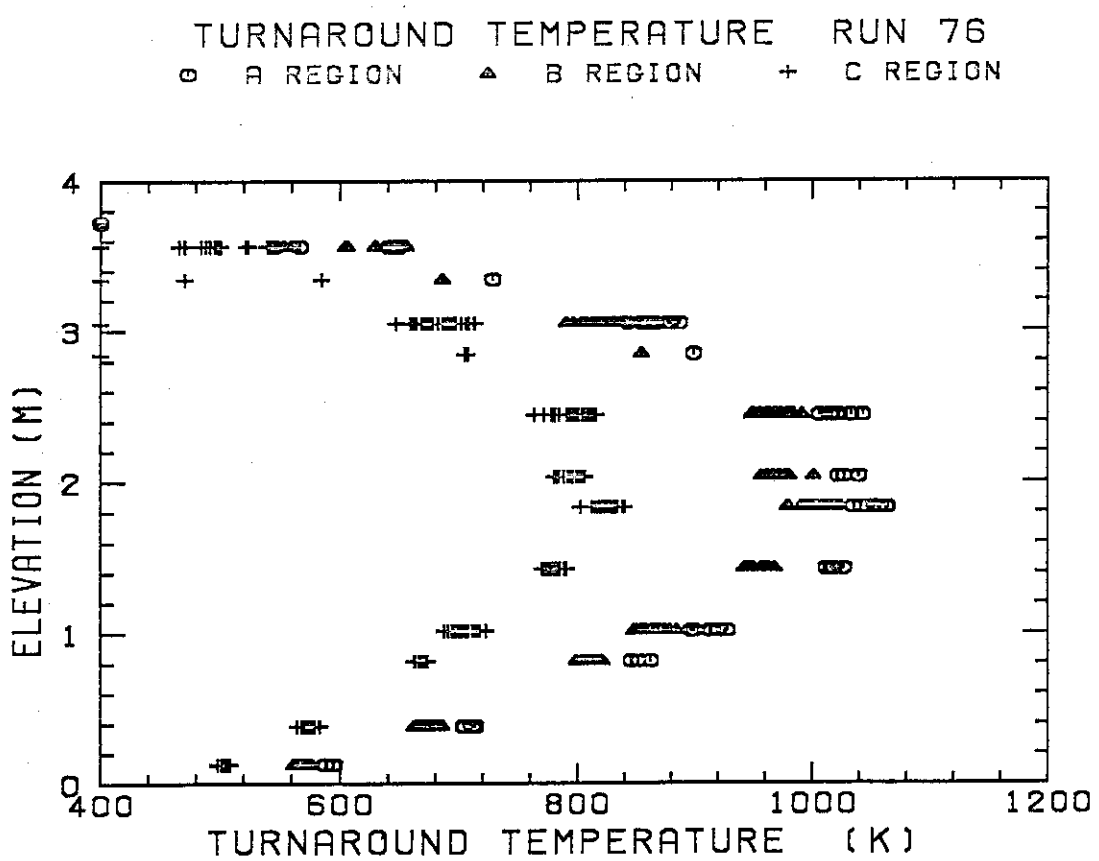

Fig. B.13 Turnaround temperature.

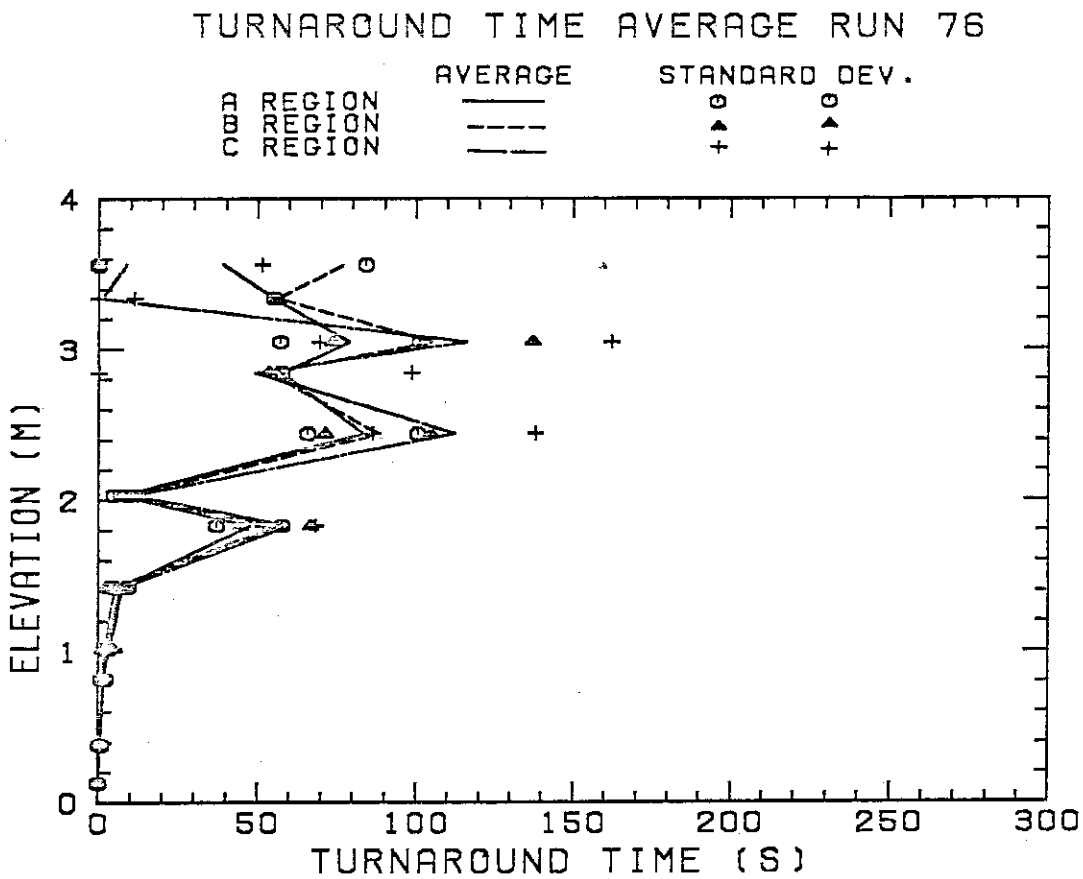

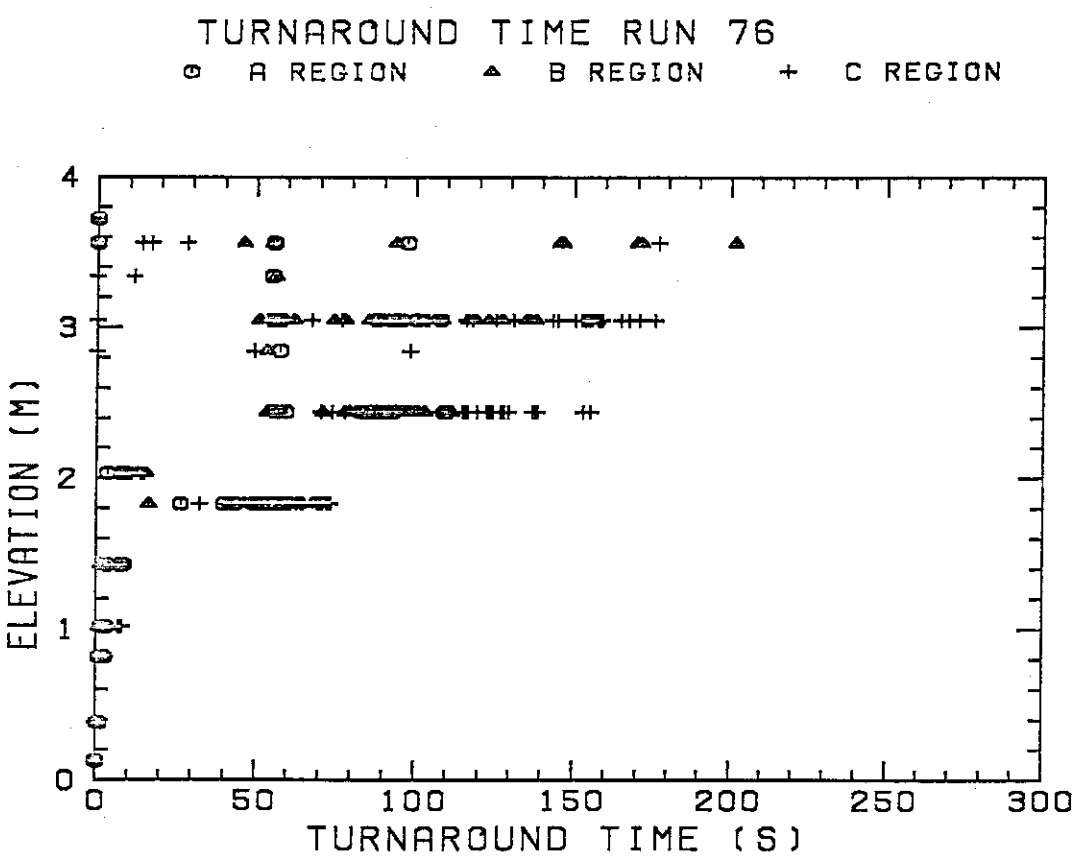

Fig. B.14 Turnaround time.

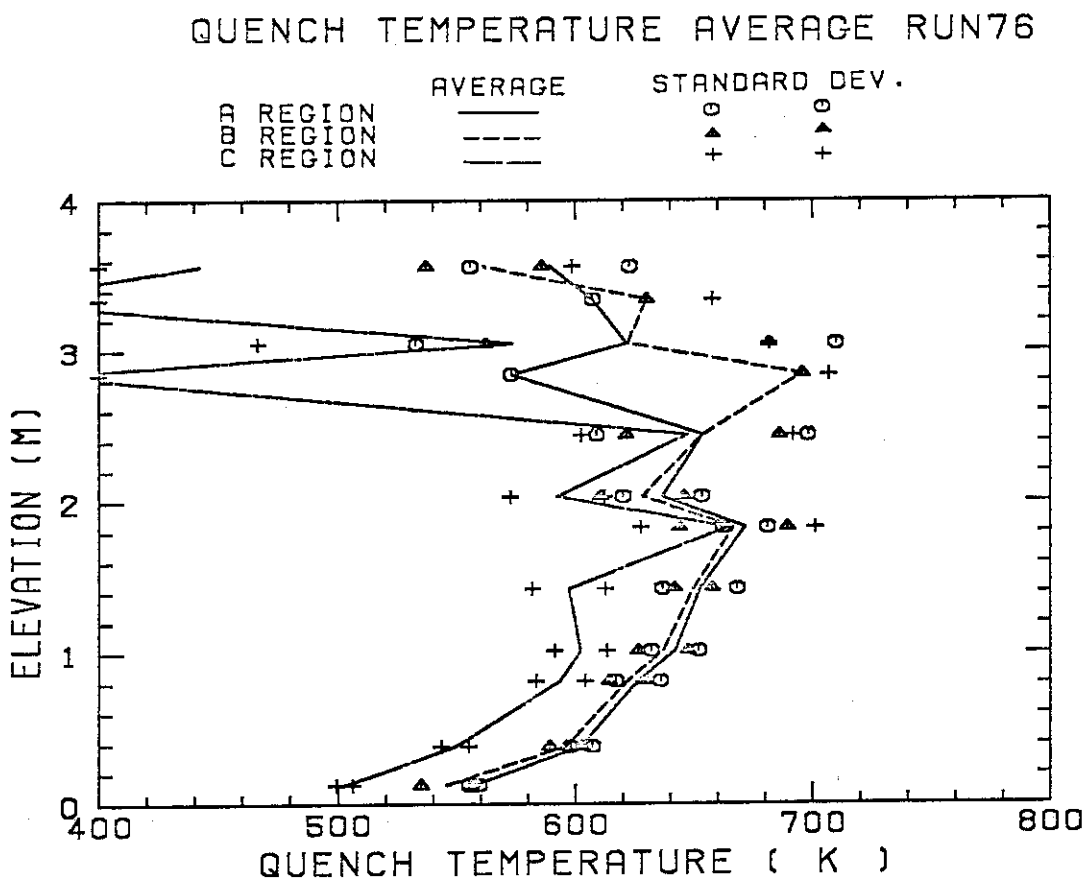

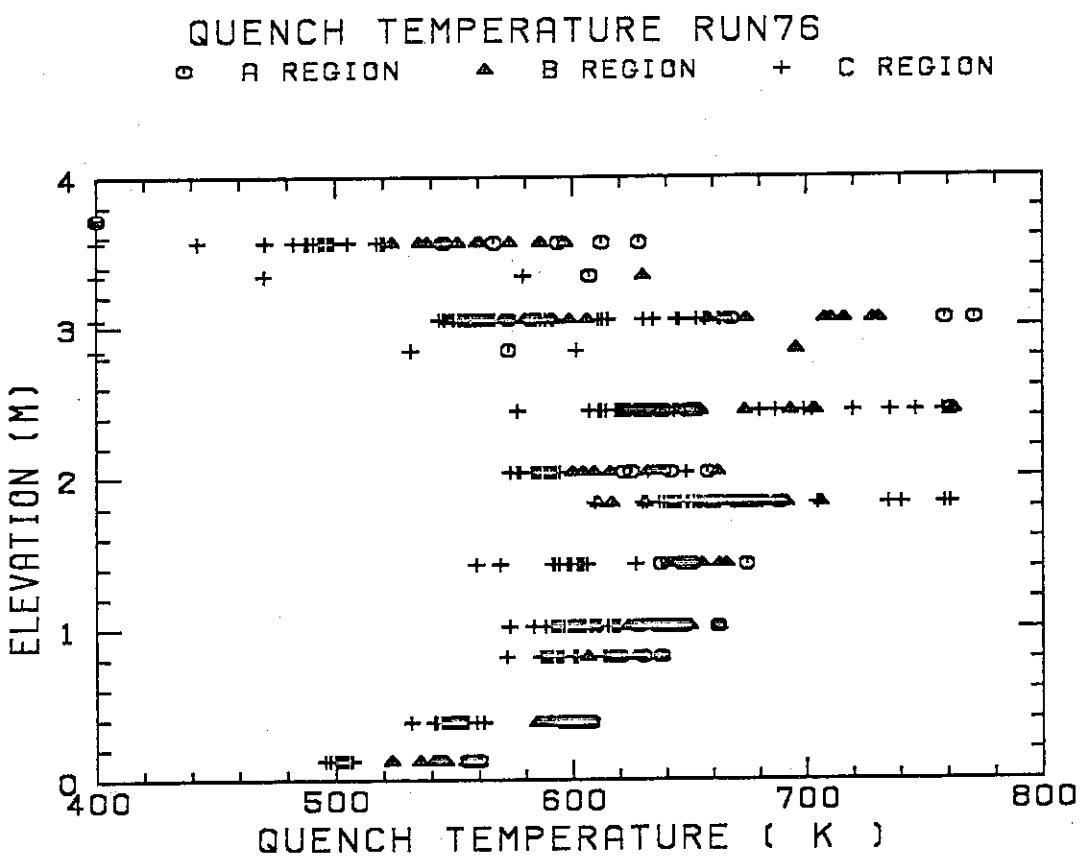

Fig. B.15 Quench temperature.

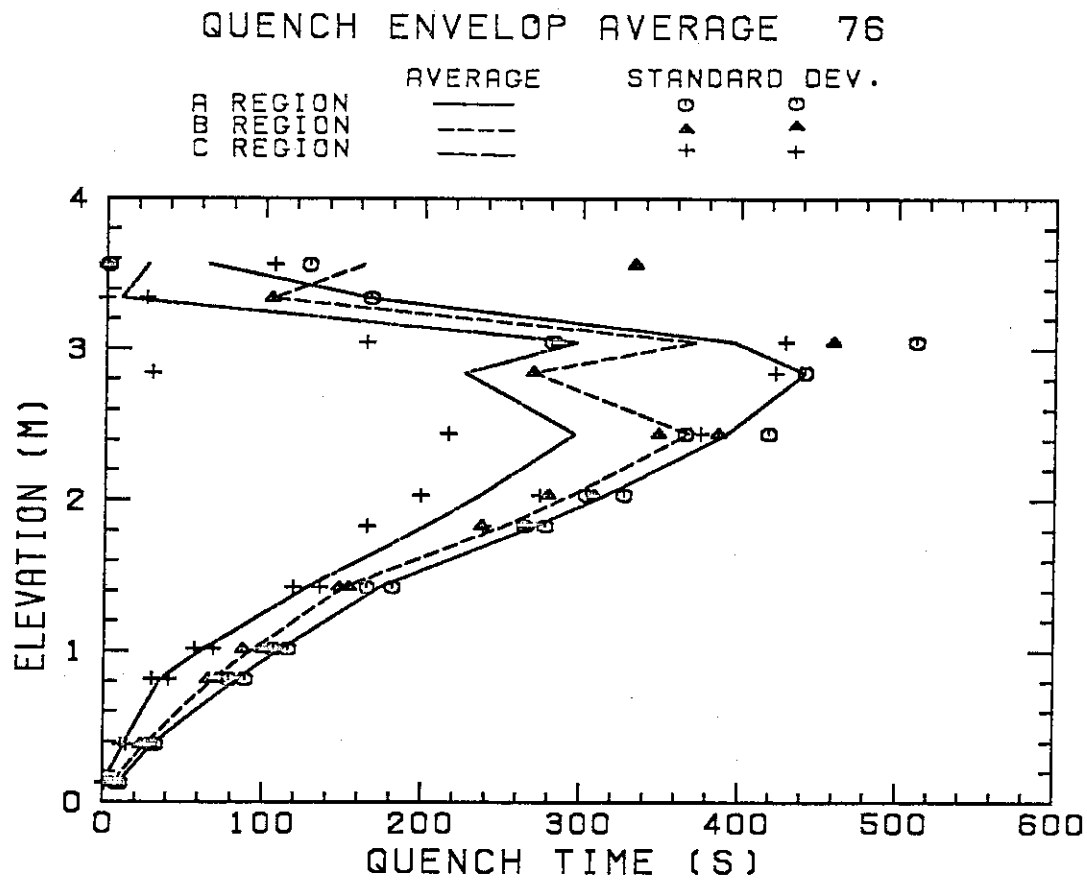

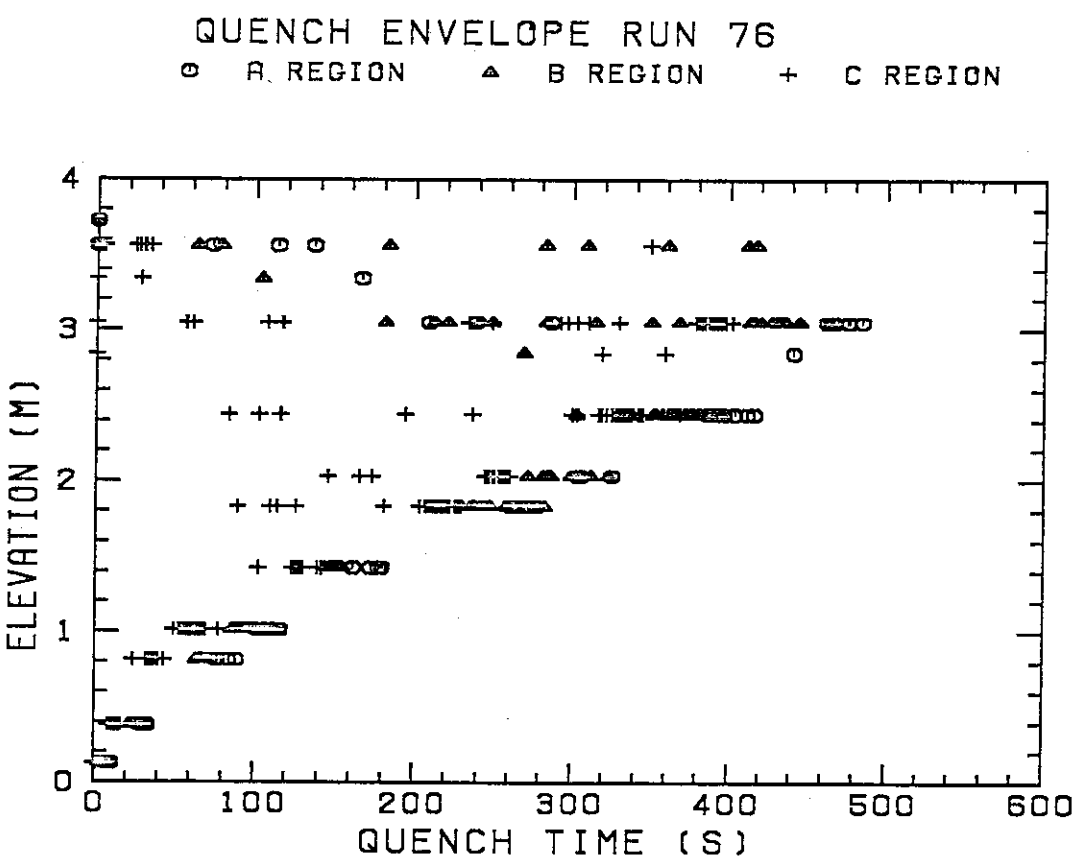

Fig. B.16 Quench time.

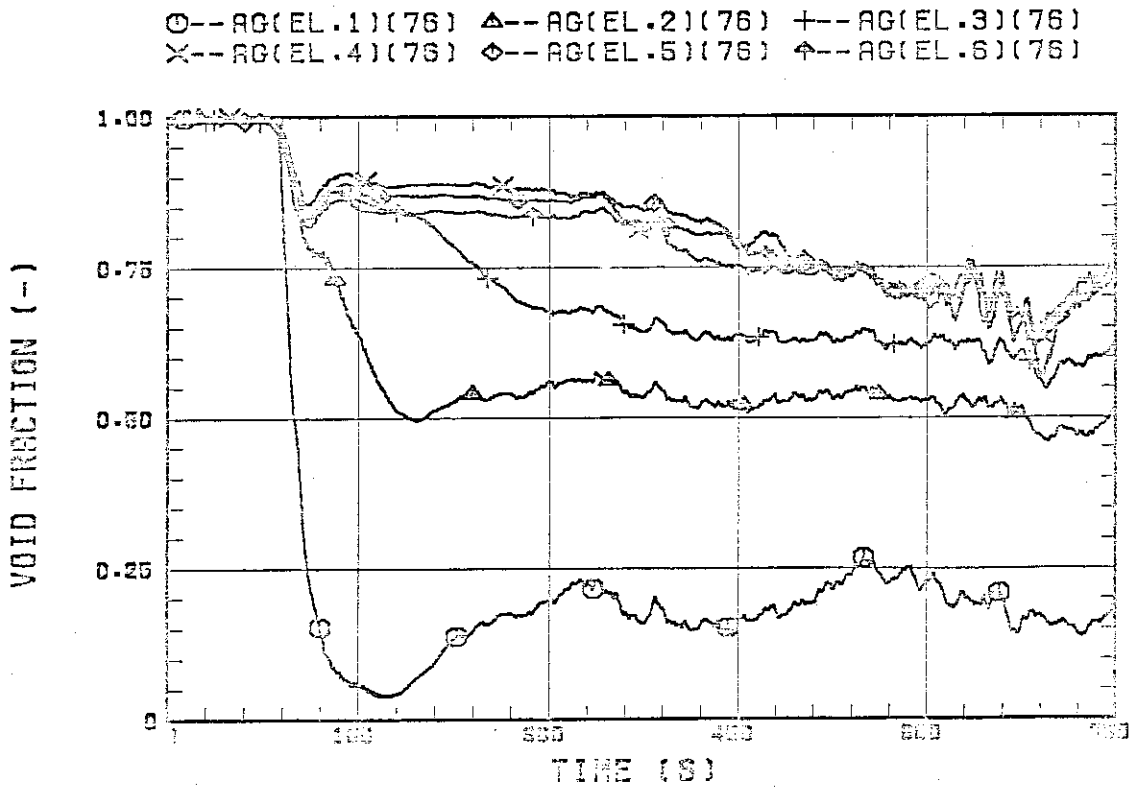

Fig. B.17 Void fraction in core.

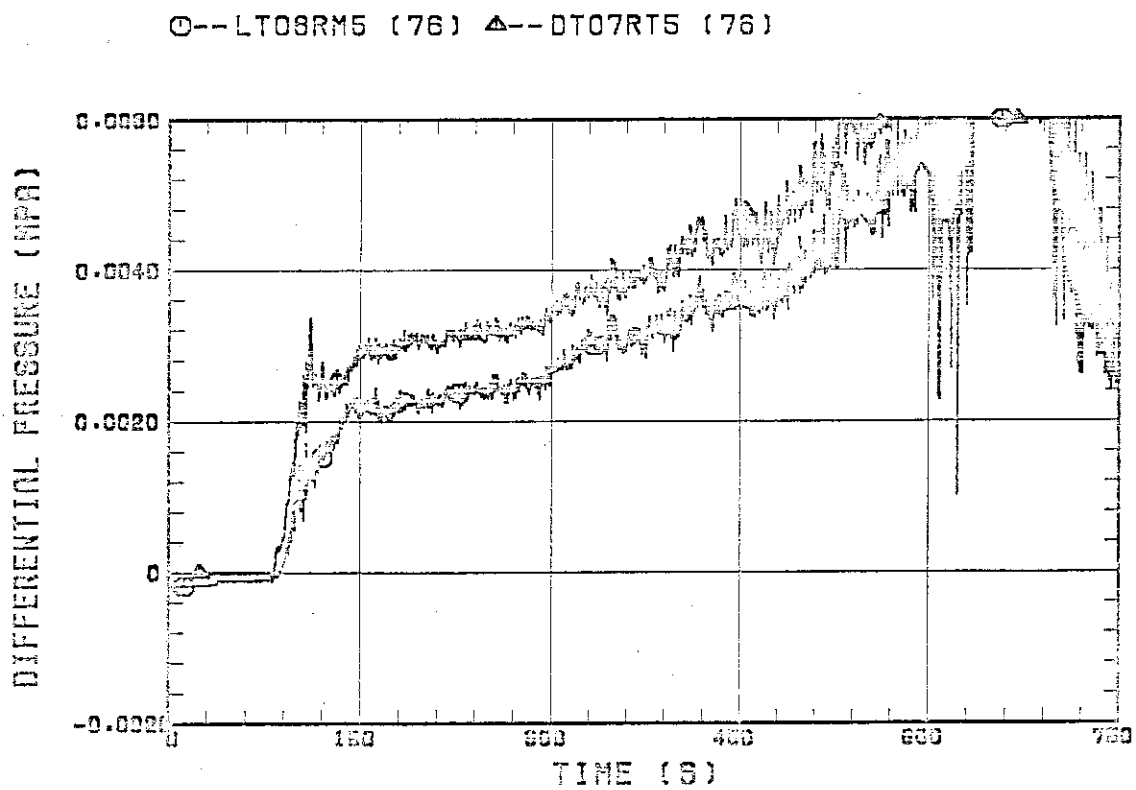

Fig. B.18 Differential pressure through upper plenum.

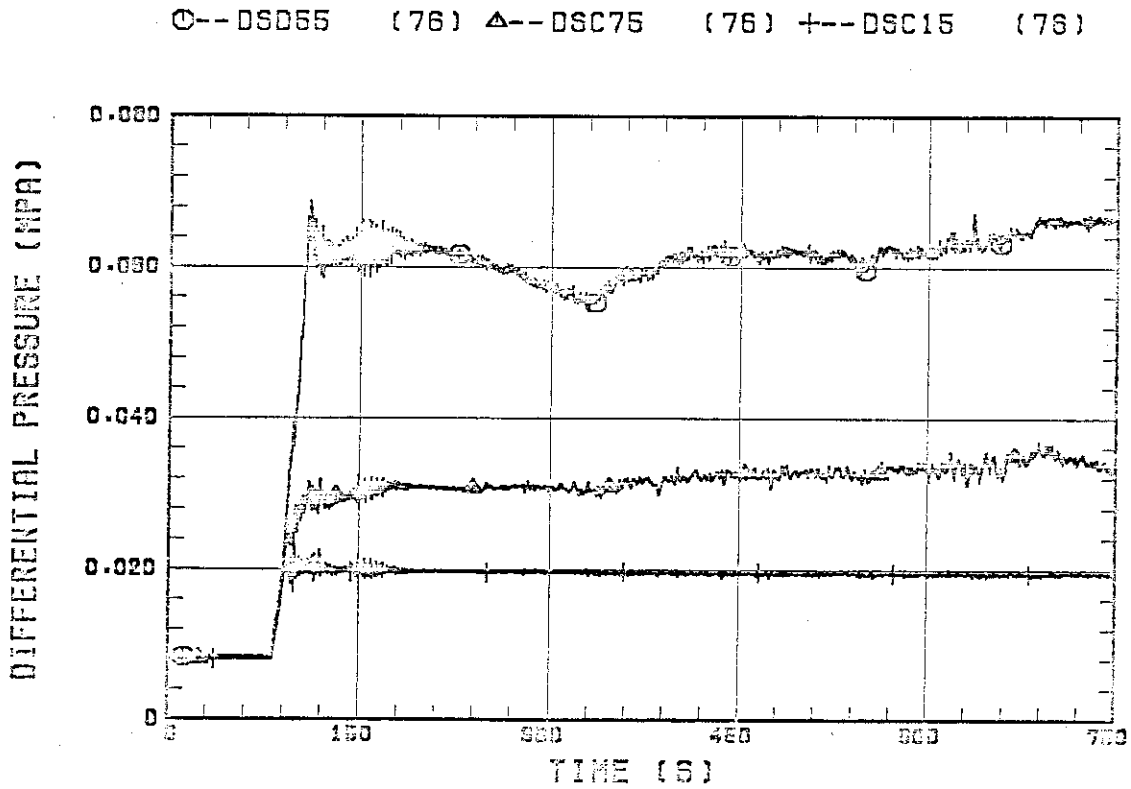

Fig. B.19 Differential pressure through downcomer, core, and lower plenum.

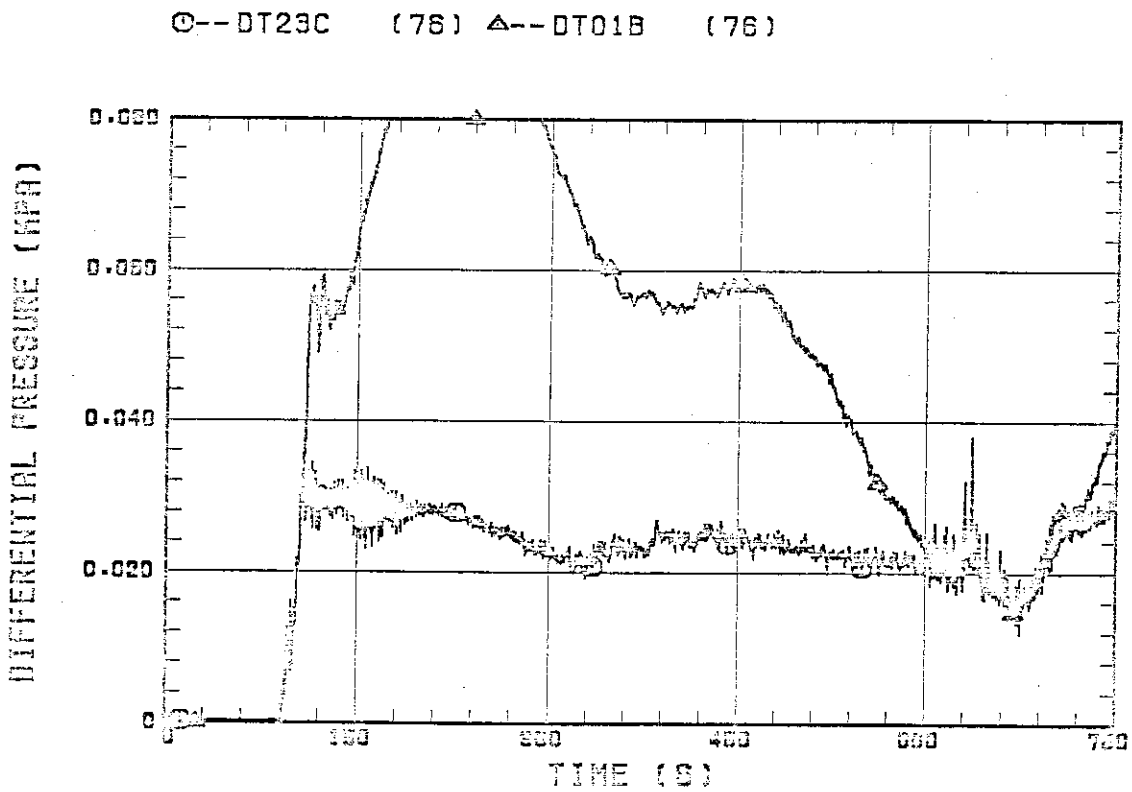

Fig. B.20 Differential pressure through intact and broken loops.

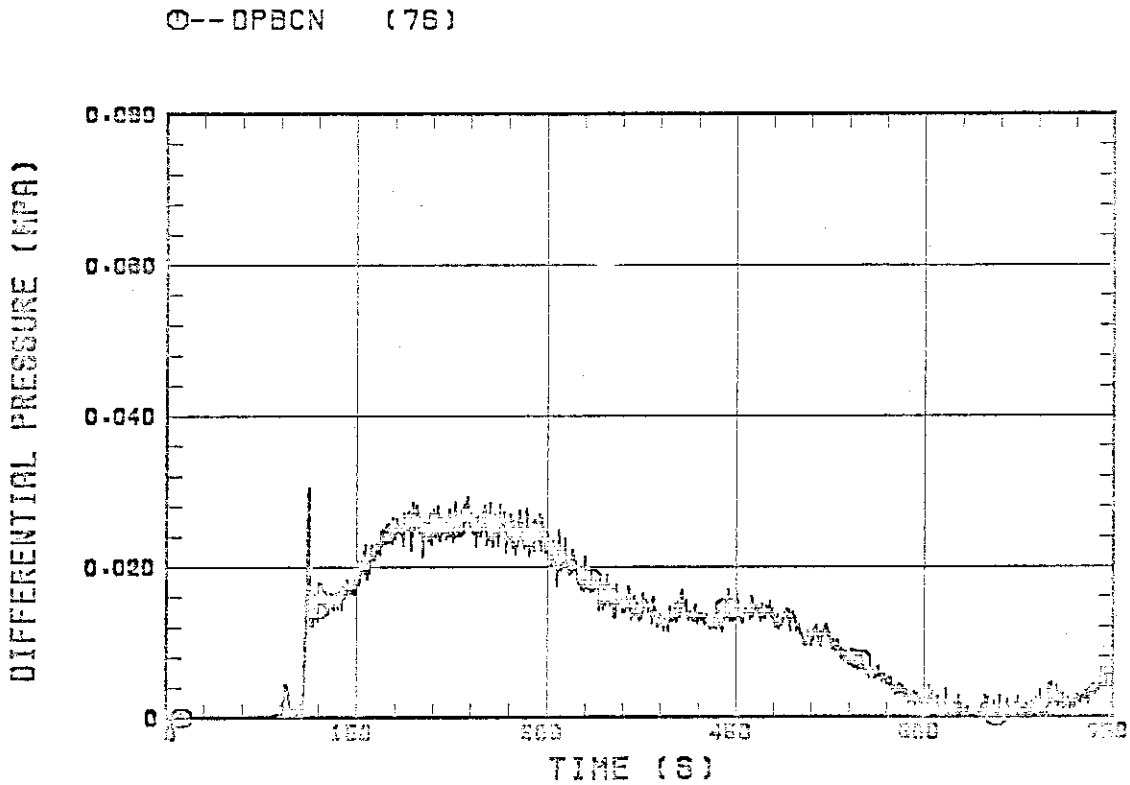

Fig. B.21 Differential pressure through broken cold leg nozzle.

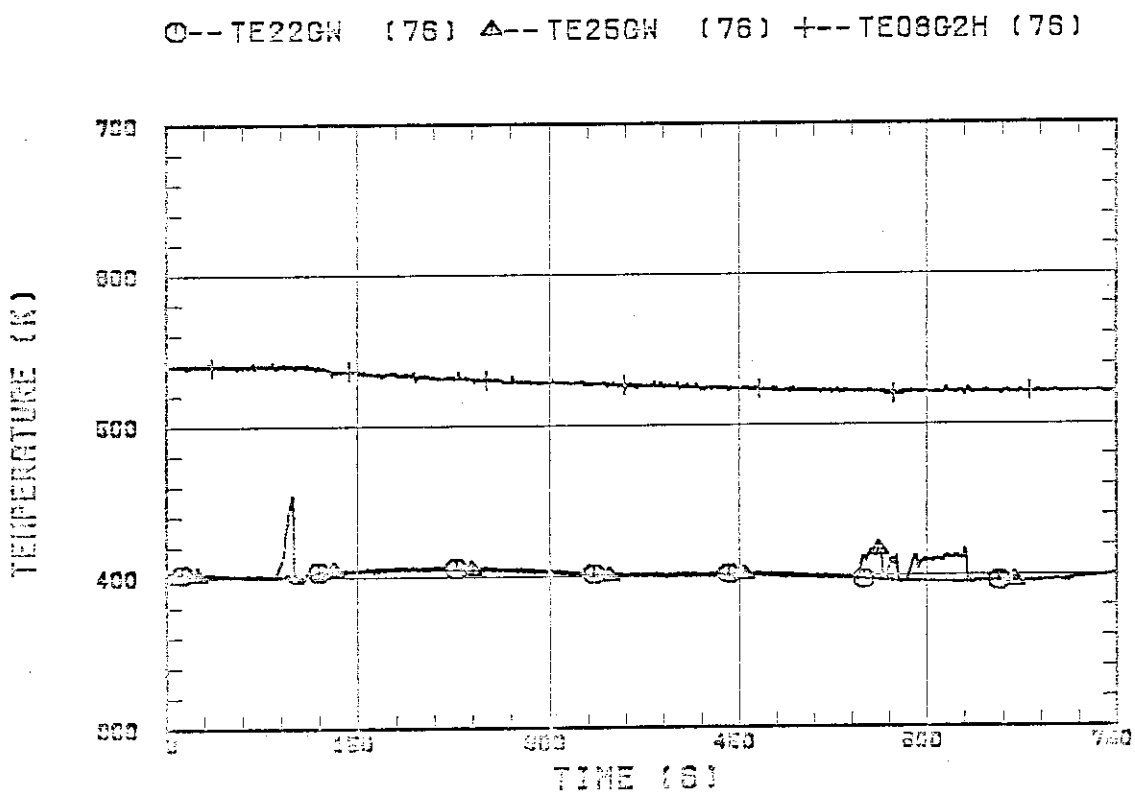

Fig. B.22 Fluid temperature in inlet plenum, outlet plenum, and secondary of steam generator 1.

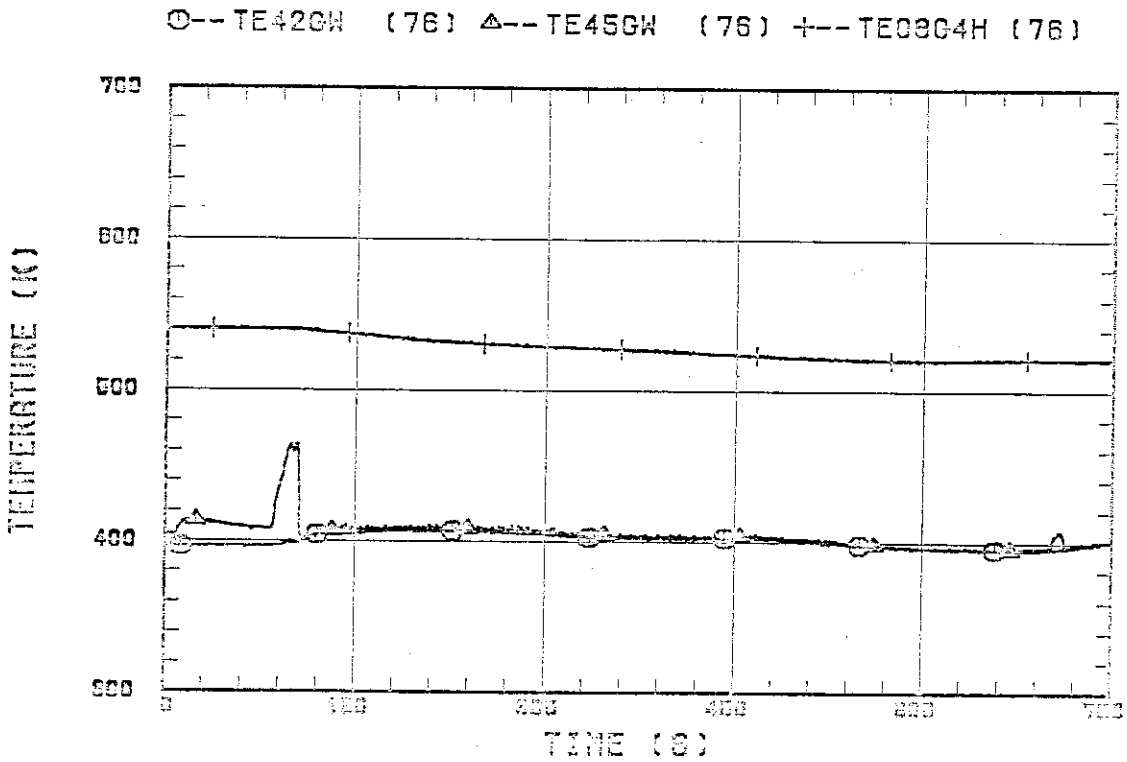

Fig. B.23 Fluid temperature in inlet plenum, outlet plenum, and secondary of steam generator 2.

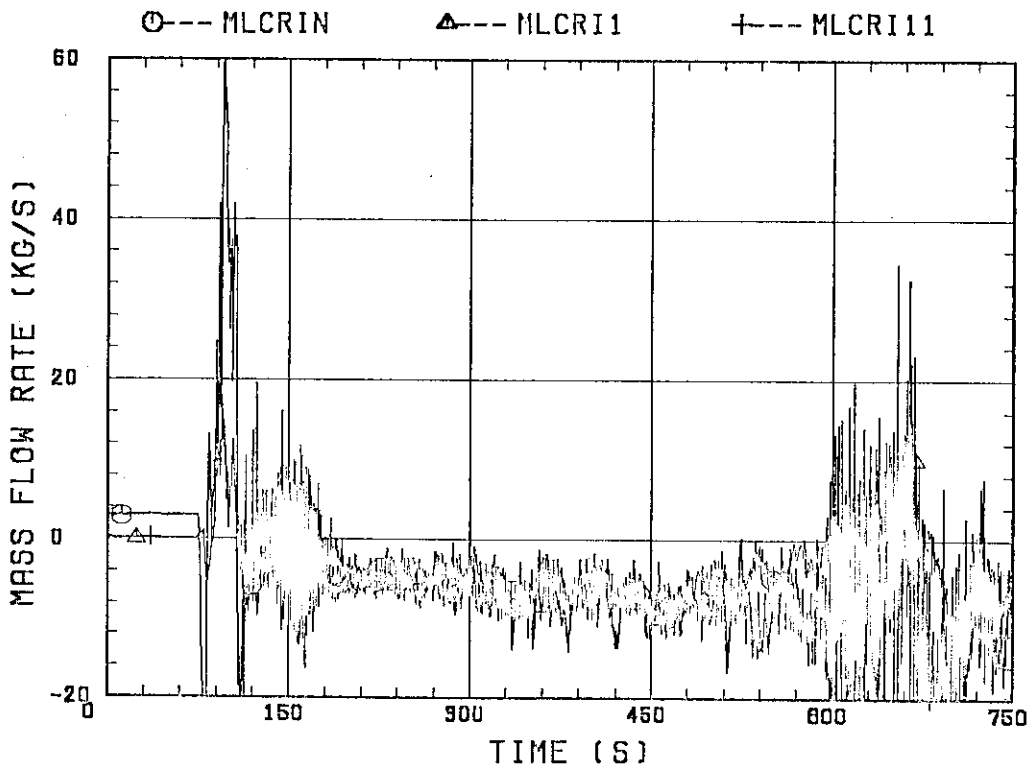

Fig. B.24 Core flooding mass flow rates evaluated with Eqs. (A.1) and (A.2)

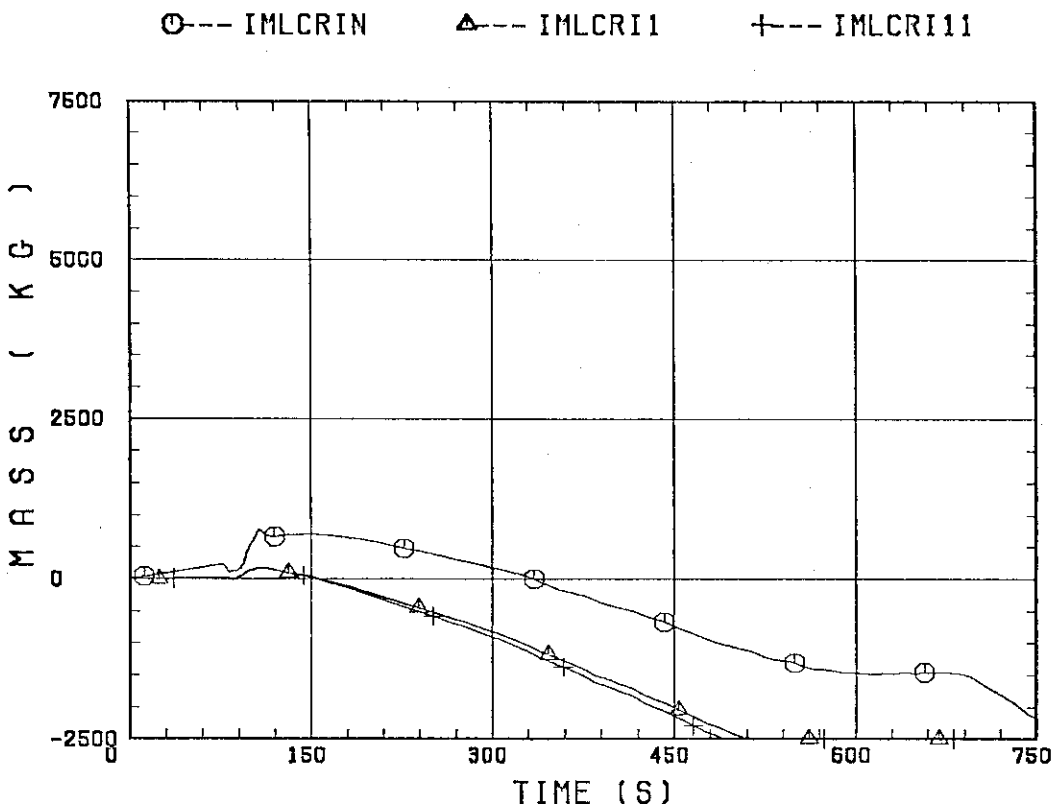

Fig. B.25 Time-integral mass flooded into core evaluated with Eqs. (A.1) and (A.2).

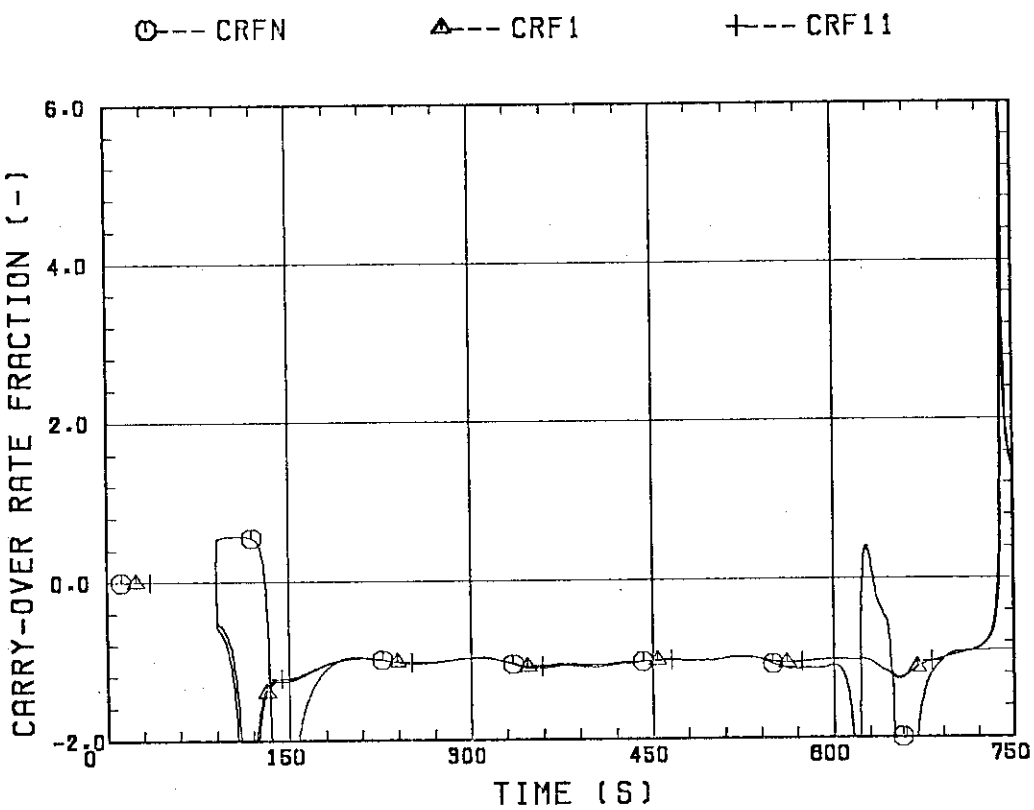

Fig. B.26 Carry-over rate fraction.

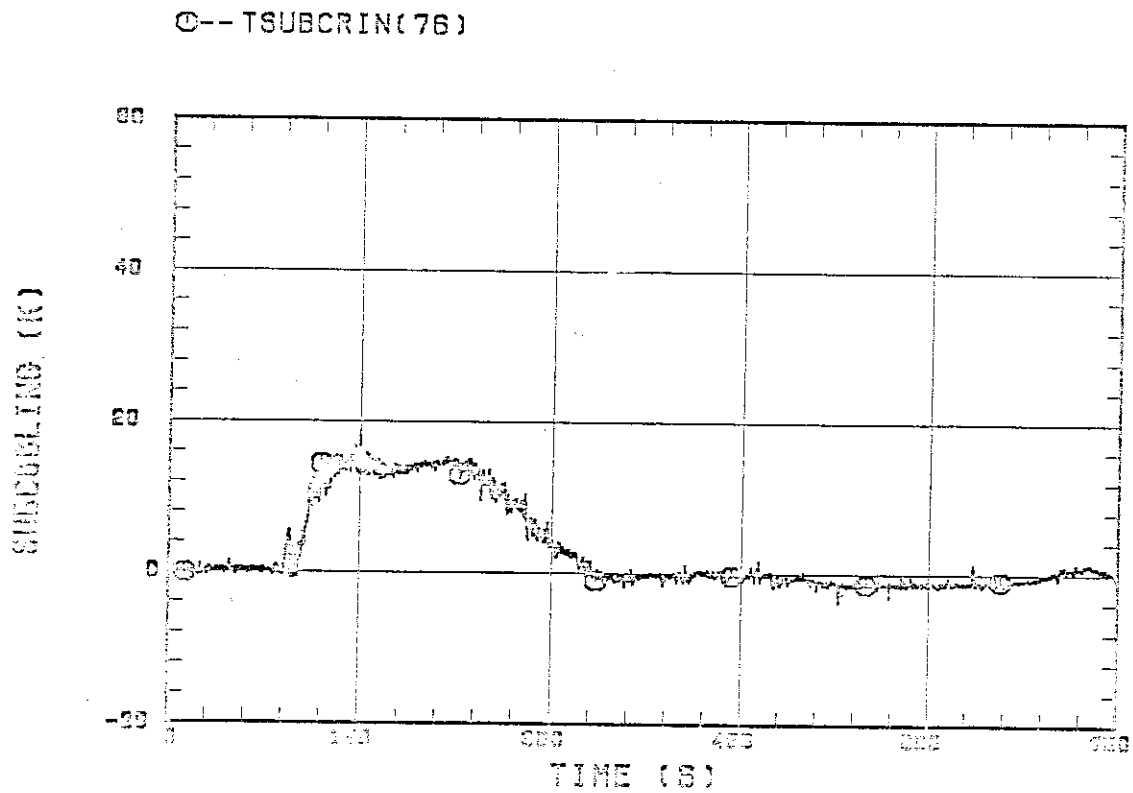

Fig. B.27 Core inlet subcooling.

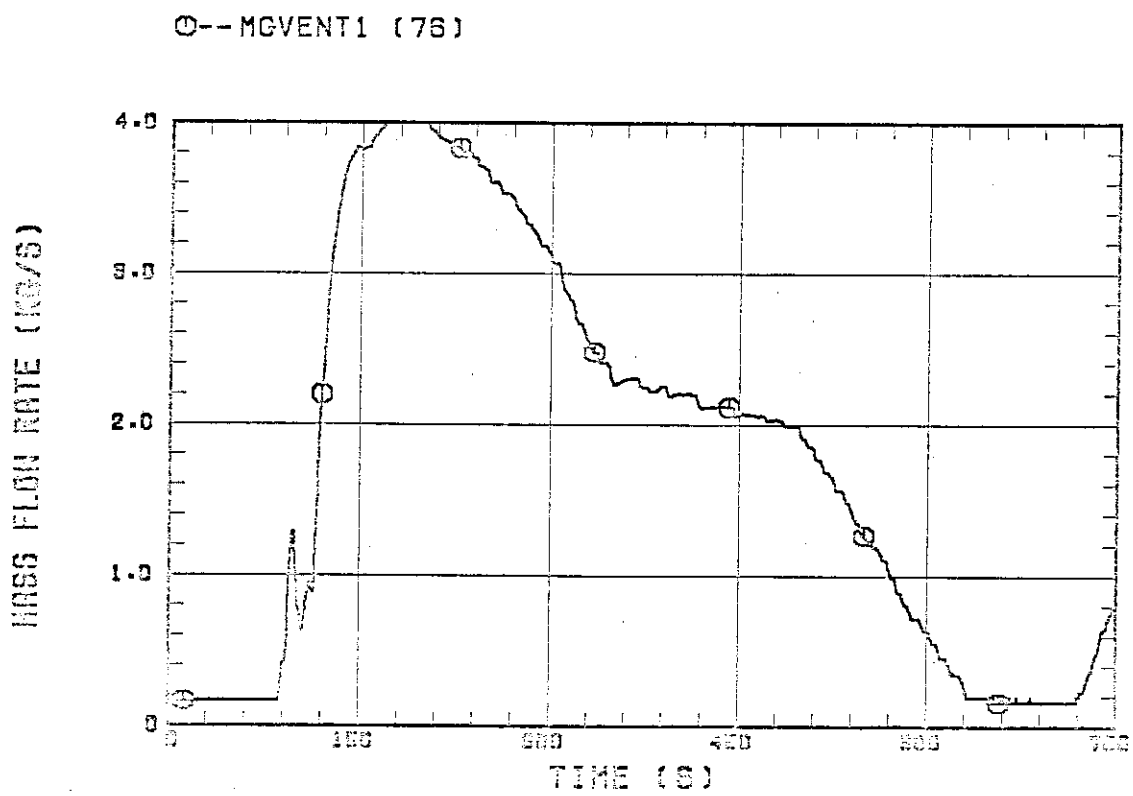

Fig. B.28 Exhausted mass flow rate from containment tank 2.